TABLE OF CONTENTS

Section		Page
3	REACTOR	3-1
3.1	DESIGN BASES	3-1
3.1.1	PERFORMANCE OBJECTIVES	3-1
3.1.2	LIMITS	3-1
3.1.2.1	Nuclear Limits	3-1
3.1.2.2	Reactivity Control Limits	3-2
3.1.2.3	Thermal and Hydraulic Limits	3-2
3.1.2.4	Mechanical Limits	3-3
3.2	REACTOR DESIGN	3-6
3.2.1	GENERAL SUMMARY	3-6
3.2.2	NUCLEAR DESIGN AND EVALUATION	3-6
3.2.2.1	Nuclear Characteristics of the Design	3-6
3.2.2.2	Nuclear Evaluation	3-18
3.2.3	THERMAL AND HYDRAULIC DESIGN AND EVALUATION	3-25
3.2.3.1	Thermal and Hydraulic Characteristics	3-25
3.2.3.2	Thermal and Hydraulic Evaluation	3-33
3.2.4	MECHANICAL DESIGN LAYOUT	3-49
3.2.4.1	Internal Layout	3-49
3.2.4.2	Fuel Asse[illegible]ies	3-54
3.2.4.3	Control System	3-65
3.3	TESTS AND INSPECTIONS	3-~~78~~ 75
3.3.1	NUCLEAR TESTS AND INSPECTION	3-~~78~~ 75
3.3.1.1	Critical Experiments	3-~~78~~ 75
3.3.1.2	Zero Power, Approach to Power, and Power Testing	3-78. 75

~~00 00101~~
145

CONTENTS (Cont'd)

Section		Page
3.3.2	THERMAL AND HYDRAULIC TESTS AND INSPECTION	3-76
3.3.2.1	Reactor Vessel Flow Distribution and Pressure Drop Test	3-76
3.3.2.2	Fuel Assembly Heat Transfer and Fluid Flow Tests	3-76
3.3.2.3	Preoperational Testing and Postoperational Testing	3-77
3.3.3	FUEL ASSEMBLY, CONTROL CLUSTER ASSEMBLY, AND CONTROL ROD DRIVE ASSEMBLY MECHANICAL TESTS AND INSPECTION	3-77
3.3.3.1	Prototype Testing	3-78
3.3.3.2	Model Testing	3-78
3.3.3.3	Component and/or Material Testing	3-78
3.3.3.4	Control Rod Drive Assembly Tests and Inspection	3-~~79~~ 76
3.3.4	INTERNALS TESTS AND INSPECTIONS	3-83
3.4	REFERENCES	3-84

00 00102

14 (b)

LIST OF TABLES

Table No.	Title	Page
3-1	Core Design, Thermal, and Hydraulic Data	3-6
3-2	Nuclear Design Data	3-8
3-3	Excess Reactivity Conditions	3-9
3-4	First Cycle Reactivity Control Distribution	3-10
3-5	Initial Cycle Reactivity Shutdown Analysis	3-12
3-6	Soluble Boron Levels and Worth	3-13
3-7	Exterior Neutron Levels and Spectra	3-16
3-8	Reference Core Parameters	3-23
3-9	First Mode Threshold Dimension and Flatness	3-23
3-10	Threshold Ratio and Power Flatness	3-24
3-11	Coefficients of Variation	3-28
3-12	DNB Results - Maximum Design Condition	3-30
3-13	DNB Results - Most Probable Condition	3-31
3-14	Heat Transfer Test Data	3-39
3-15	Comparison of Heat Transfer Test Data	3-43
3-16	Hot Channel Coolant Conditions	3-44
3-17	Clad Circumferential Stresses	3-58
3-18	LRD Fuel Swelling Irradiation Program	3-63
3-19	Control Rod Drive Design Data	3-~~68~~ 67
3-20	Control Cluster Assembly Design Data	3-~~75~~ 73

FIGURES (Cont'd)

Figure No.	Title
3-44	Fuel Center Temperature for Beginning-of-Life Conditions
3-45	Fuel Center Temperature for End-of-Life Conditions
3-46	Reactor Vessel and Internals General Arrangement
3-47	Reactor Vessel and Internals General Arrangement - Cross Section
3-48	Core Flooding Arrangement
3-49	Fuel Assembly
3-50	Orifice Cluster Assembly
3-51	Control Rod Drive - General Arrangement
3-52	Control Rod Drive - Vertical Section
3-53	(Deleted by 4-29-67 Amendment)
3-54	(Deleted by 4-29-67 Amendment)
3-55	(Deleted by 4-29-67 Amendment)
3-56	(Deleted by 4-29-67 Amendment)
3-57	Drive Mechanism Control Block Diagram
3-58	Limit Signal and Position Indication System
3-59	Reactor Trip Circuit
3-60	Control Cluster Assembly

00 00148

FIGURES (Cont'd)

Figure No.	Title
3-20	Burnout Factor Versus Population for Various Confidence Levels
3-21	Rods in Jeopardy Versus Power
3-22	Ratio of Experimental to Calculated Burnout Heat Flux
3-23	Ratio of Experimental to Calculated Burnout Heat Flux
3-24	Ratio of Experimental to Calculated Burnout Heat Flux
3-25	Ratio of Experimental to Calculated Burnout Heat Flux
3-26	Ratio of Experimental to Calculated Burnout Heat Flux
3-27	Ratio of Experimental to Calculated Burnout Heat Flux
3-28	Ratio of Experimental to Calculated Burnout Heat Flux
3-29	Ratio of Experimental to Calculated Burnout Heat Flux
3-30	Ratio of Experimental to Calculated Burnout Heat Flux
3-31	Ratio of Experimental to Calculated Burnout Heat Flux
3-32	Ratio of Experimental to Calculated Burnout Heat Flux
3-33	Ratio of Experimental to Calculated Burnout Heat Flux
3-34	Ratio of Experimental to Calculated Burnout Heat Flux
3-35	Ratio of Experimental to Calculated Burnout Heat Flux
3-36	Ratio of Experimental to Calculated Burnout Heat Flux
3-37	Ratio of Experimental to Calculated Burnout Heat Flux
3-38	Maximum Hot Channel Exit Quality Versus Reactor Power
3-39	Hottest Design and Nominal Channel Exit Quality Versus Reactor Power (Without Engineering Hot Channel Factors)
3-40	Flow Regime Map at 2185 psig
3-41	Hot Channel DNB Ratio Comparison
3-42	Reactor Coolant Flow Versus Power
3-43	Thermal Conductivity of 95% Dense Sintered UO_2

FIGURES (Cont'd)

Figure No.	Title
3-44	Fuel Center Temperature for Beginning-of-Life Conditions
3-45	Fuel Center Temperature for End-of-Life Conditions
3-46	Reactor Vessel and Internals General Arrangement
3-47	Reactor Vessel and Internals General Arrangement - Cross Section
3-48	Core Flooding Arrangement
3-49	Fuel Assembly
3-50	Orifice Cluster Assembly
3-51	Control Rod Drive
3-52	Position Indicator Transmitter Assembly
3-53	Nutating Disc Actuator
3-54	Spool Piece and Lower Guide Tube Assembly
3-55	Snubber
3-56	Cap and Drive Line Vent Assembly
3-57	Drive Mechanism Control Block Diagram
3-58	Limit Signal and Position Indication System
3-59	Reactor Trip Circuit
3-60	Control Cluster Assembly

00 00150

3 REACTOR

3.1 DESIGN BASES

The reactor is designed to meet the performance objectives specified in 3.1.1 without exceeding the limits of design and operation specified in 3.1.2.

3.1.1 PERFORMANCE OBJECTIVES

The reactor is designed to operate at 2,452 mwt with sufficient design margins to accommodate transient operation and instrument error without damage to the core and without exceeding the pressure at the safety valve settings in the reactor coolant system.

The fuel rod cladding is designed to maintain its integrity for the anticipated core life. The effects of gas release, fuel dimensional changes, and corrosion- or irradiation-induced changes in the mechanical properties of cladding are considered in the design of fuel assemblies.

Reactivity is controlled by control cluster assemblies (CCA) and chemical poison dissolved in the coolant. Sufficient CCA worth is available to shut the reactor down ($k_{eff} \leq 0.99$) in the hot condition at any time during the life cycle with the most reactive CCA stuck in the fully withdrawn position. Redundant equipment is provided to add soluble poison to the reactor coolant to insure a similar shutdown capability when the reactor coolant is cooled to ambient temperatures.

The reactivity worth of CCA's, and the rate at which reactivity can be added, are limited to insure that credible reactivity accidents cannot cause a transient capable of damaging the reactor coolant system or causing significant fuel failure.

3.1.2 LIMITS

3.1.2.1 Nuclear Limits

The core has been designed to the following nuclear limits:

a. Fuel has been designed for an average burnup of 28,200 MWD/MTU and for a maximum burnup of 55,000 MWD/MTU.

b. The power coefficient is negative, and the control system is capable of compensating for reactivity changes resulting from nuclear coefficients, either positive or negative.

c. Control systems will be available to handle core xenon instabilities should they occur during operation without jeopardizing the safety conditions of the system.

d. The core will have sufficient excess reactivity to produce the design power level and lifetime, without exceeding the control capacity or shutdown margin.

e. Controlled reactivity insertion rates have been limited to: 5.8×10^{-5} $\Delta k/k/sec$ for a single regulating CCA group withdrawal, and 7×10^{-6} $\Delta k/k/sec$ for soluble boron removal.

f. Reactor control and maneuvering procedures will not produce peak-to-average power distributions greater than those listed in Table 3-1. The low worth of CCA groups inserted during power operation limits power peaks to acceptable values.

3.1.2.2 Reactivity Control Limits

The control system and the operational procedures will provide adequate control of the core reactivity and power distribution. The following control limits will be met:

a. Sufficient control will be available to produce a shutdown margin of at least 1% $\Delta k/k$.

b. The shutdown margin will be maintained with the CCA of highest worth stuck out of the core.

c. CCA withdrawal limits the reactivity insertion to $5.8 \times 10^{-5} \Delta k/k/sec$ on a single regulating group. Boron dilution is also limited to a reactivity insertion of 7×10^{-6} $\Delta k/k/sec$.

3.1.2.3 Thermal and Hydraulic Limits

The reactor core is designed to meet the following limiting thermal and hydraulic conditions:

a. No central melting at the design overpower (114 per cent).

b. A 99 per cent confidence that at least 99.5 per cent of the fuel rods in the core are in no jeopardy of experiencing a departure from nucleate boiling (DNB) during continuous operation at the design overpower.

c. Essentially 100 per cent confidence that at least 99.96 per cent of the fuel rods in the core are in no jeopardy of experiencing a DNB during continuous operation at rated power.

d. The generation of net steam in the hottest [illegible] channels is permissible, but steam voids will be low enough to prevent flow instabilities.

The design overpower is the highest credible reactor operating power permitted by the safety system. Normal overpower to trip is significantly less than the design overpower. Rated power (2,452 mwt) is the licensed operating power.

3.1.2.4 Mechanical Limits

3.1.2.4.1 Reactor Internals

The reactor internal components are designed to withstand the stresses resulting from startup; steady state operation with one, two, three, or four pumps running; and shutdown conditions. No damage to the reactor internals will occur as a result of loss of pumping power.

Reactor internals will be fabricated from SA-240 (Type 304) material and will be designed within the allowable stress levels permitted by the ASME Code, Section III, Table N-421. Structural integrity and allowable stress levels of all core support assembly welds will be assured by compliance with ASME Code Sections III and IX, radiographic inspection acceptance standards, and welding qualifications.

The reactor internals will be designed as a Class I structure as defined in Appendix 5A of this report. In addition, the internal structural components will be designed to resist the effects of seismic disturbances. The basic design guide for the seismic analysis will be AEC publication TID-7024, "Nuclear Reactors and Earthquakes."

Lateral deflection and torsional rotation of the lower end of the core barrel will be limited to prevent excessive movements resulting from seismic disturbances and thus prevent interference with control cluster assemblies (CCA's). Core drop in the event of failure of the normal supports will be limited so that the CCA's do not disengage from the fuel assembly guide tubes.

The structural internals will be designed to maintain their functional integrity in the event of a major loss-of-coolant accident as described in 3.2.4.1. The dynamic loading resulting from the pressure oscillations because of a loss-of-coolant accident will not prevent CCA insertion.

3.1.2.4.2 Fuel Assemblies

The fuel assemblies are designed to operate satisfactorily to design burnup and to retain adequate integrity at the end of life to permit safe removal from the core.

The assemblies are designed to operate safely during steady state and transient conditions under the combined effects of flow-induced vibration, cladding strain caused by reactor pressure, fission gas pressure, fuel growth, and thermal strain. The cold-worked Zircaloy-4 cladding is designed to be free-standing. Fuel rod assemblies are held in place by mechanical spacers that are designed to maintain dimensional control of the fuel rod spacing throughout the design life, without impairing cladding integrity. Contact loads are limited to prevent fretting.

The spacers are also designed to permit differential thermal expansion of the fuel rods without restraint that would cause distortion of the rods. The fuel assembly upper end fitting and the guide tube in the internals structure are both indexed to the grid plate above the fuel assemblies, thus insuring continuous alignment of the guide channels for the CCA's. The control pin

travel is designed so that the pins are always engaged in the fuel assembly guide tubes, thus insuring that CCA's can always be inserted. The assembly structure is also designed to withstand handling loads, shipping loads, and earthquake loads.

Stress and strain for all anticipated normal and abnormal operating conditions will be limited as follows:

a. Stresses which are not relieved by small deformations of the material will be prevented from leading to failure by not permitting these stresses to exceed the yield strength of the material nor to exceed levels which would use in excess of 75 per cent of the stress rupture life of the material. An example of this type of stress is the circumferential membrane stress in the clad due to internal or external pressure.

b. Stresses which are relieved by small deformations of the material, and the single occurrence of which will not make a significant contribution to the possibility of a failure, will be permitted to exceed the yield strength of the material. Where such stresses exceed the material yield strength, strain limits will be set, based on low cycle fatigue techniques, using no more than 90 per cent of the material fatigue life. Evaluations of cyclic loadings will be based on conservative estimates of the number of cycles to be experienced. An example of this type of stress is the thermal stress resulting from the thermal gradient across the clad thickness.

c. Combinations of the above two types of stresses, in addition to the individual treatment outlined above, will be evaluated on the low-cycle fatigue basis of Item b. Also, clad plastic strain due to diameter increases resulting from thermal ratcheting and/or creep, including the effects of internal gas pressure and fuel swelling, will be limited to about 1 per cent.

d. Minimum clad collapse pressure margins will be required, as listed below:

   (1) 10 per cent margin over system design pressure, on short time collapse, at end void.

   (2) End void must not collapse (must be either freestanding or have adequate support) on a long time basis.

   (3) 10 per cent margin over system operating pressure, on short time collapse, at hot spot average temperature through the clad wall.

   (4) Clad must be freestanding at design pressure on a short time basis at ~725 F hot spot average temperature through the clad wall.

3.1.2.4.3 Control Cluster Assembly (CCA)

The control pin clad is designed to the same criteria as the fuel clad, as applicable. Adequate clearance will be provided between the control pins and the guide tubes, which position them within the fuel assembly, so that control pin overheating will be avoided, and so that unacceptable mechanical interference between the control pin and the guide tube will not occur under all operating conditions, including earthquake.

Overstressing of the CCA components during a trip will be prevented by minimizing the shock loads by snubbing and by providing adequate strength.

3.1.2.4.4 Control Rod Drive Assembly

Each control rod drive assembly is provided with a pressure breakdown seal to prevent leakage of reactor coolant water external to the reactor coolant system. All pressure-containing components are designed to meet the requirements of the ASME Code, Section III, Nuclear Vessels for Class A vessels.

The control rod drive assemblies provide control cluster assembly (CCA) insertion and withdrawal rates consistent with the required reactivity changes for reactor operational load changes. This rate is based on the worths of the various rod groups, which have been established to limit power-peaking flux patterns to design values. The maximum reactivity addition rate is specified to limit the magnitude of a possible nuclear excursion resulting from a control system or operator malfunction. The normal insertion and withdrawal velocity has been established as 25 in./min.

The control rod drive assemblies provide a "trip" of the CCA's which results in a rapid shutdown of the reactor for conditions that cannot be handled by the reactor control system. The trip is based on the results of various reactor emergency analyses, including instrument and control delay times and the amount of reactivity that must be inserted before deceleration of the CCA occurs. The maximum trip time for a 2/3 insertion of a CCA has been established as 1.4 sec.

The control rod drive assemblies can be coupled and uncoupled to their respective CCA's without any withdrawal movement of the CCA's.

Materials selected for the control rod drive assembly are capable of operating within the specified reactor environment for the life of the mechanism without any deleterious effects. Adequate clearance will be provided between the stationary and moving parts of the control rod drive assemblies so that the CCA trip time to full insertion will not be adversely affected by mechanical interference under all operating conditions and seismic disturbances.

Structural integrity and adherence to allowable stress limits of the control rod drive line and related parts during a trip will be achieved by establishing a limit on impact loads through snubbing.

3.2 REACTOR DESIGN

3.2.1 GENERAL SUMMARY

The important core design, thermal, and hydraulic characteristics are tabulated in Table 3-1. The nuclear design characteristics are presented in Table 3-2.

3.2.2 NUCLEAR DESIGN AND EVALUATION

The basic design of the core satisfies the following requirements:

a. Sufficient excess reactivity is provided to achieve the design power level over the specified fuel cycle.

b. Sufficient reactivity control is provided to permit safe reactor operation and shutdown at all times during core lifetime.

3.2.2.1 Nuclear Characteristics of the Design

3.2.2.1.1 Excess Reactivity

The excess reactivities associated with various core conditions are tabulated in Table 3-3. Data are shown for two-Unit fuel sharing. Unit 1 of the two-Unit site will operate for one cycle of 272 full power days. Fuel from Unit 1 will then be loaded into Unit 2, and both Units will be operated on an equilibrium cycle of 310 full power days. The reactivity data shown in Table 3-3 assumes that 50 per cent of the fuel from Unit 1 is shared with Unit 2. The safe operation of the two Units will not be jeopardized by fuel sharing. Design limits will be held with respect to reactivity control and power distribution. Incore instrumentation will be used to back up the analytical selection of the particular fuel assemblies to be shared and thereby insure proper power peaking levels.

Table 3-1

Core Design, Thermal, and Hydraulic Data

Reactor	
Type	Pressurized Water
Rated Heat Output, mwt	2,452
Vessel Coolant Inlet Temperature, F	555
Vessel Coolant Outlet Temperature, F	602.8
Core Outlet Temperature, F	604.3
Operating Pressure, psig	2,185
Core and Fuel Assemblies	
Total Number of Fuel Assemblies in Core	177

Table 3-1 (Cont'd)

Number of Fuel Rods per Fuel Assembly	208
Number of Control Pins per Control Rod Cluster Assembly	16
Number of Incore Instrumentation Positions per Fuel Assembly	1
Fuel Rod Outside Diameter, in.	0.420
Clad Thickness, in.	0.026
Fuel Rod Pitch, in.	0.558
Fuel Assembly Pitch Spacing, in.	8.587
Unit Cell Metal/Water Ratio	0.80
Clad Material	Zircaloy-4 (cold-worked)

Fuel

Material	UO_2
Form	Dished-end, cylindrical pellets
Diameter, in.	0.362
Active Length, in.	144
Density, % of theoretical	95

Heat Transfer and Fluid Flow at Rated Power

Total Heat Transfer Surface in Core, ft^2	48,578
Average Heat Flux, Btu/hr-ft^2	167,620
Maximum Heat Flux, Btu/hr-ft^2	543,000
Average Power Density in Core, kw/l	79.60
Average Thermal Output, kw/ft of fuel rod	5.4
Maximum Thermal Output, kw/ft of fuel rod	17.49
Maximum Clad Surface Temperature, F	654
Average Core Fuel Temperature, F	1,385
Maximum Fuel Central Temperature at Hot Spot, F	4,160
Total Reactor Coolant Flow, lb/hr	131.32×10^6
Core Flow Area (effective for heat transfer), ft^2	47.75
Core Coolant Average Velocity, fps	15.7
Coolant Outlet Temperature at Hot Channel, F	644.4

Power Distribution

Maximum/Average Power Ratio, radial x local ($F_{\Delta h}$ nuclear)	1.85
Maximum/Average Power Ratio, axial (F_z nuclear)	1.70
Overall Power Ratio (F_q nuclear)	3.15

~~00 00110~~

157

Table 3-1 (Cont'd)

Power Generated in Fuel and Cladding, %	97.3
Hot Channel Factors	
Power Peaking Factor (F_Q)	1.017
Flow Area Reduction Factor (F_A)	0.983
Local Heat Flux Factor (F_Q'')	1.030
Hot Spot Maximum/Average Heat Flux Ratio (F_q nuc. and mech.)	3.24
DNB Data	
Design Overpower Ratio	1.14
DNB Ratio at Design Overpower (BAW-168)	1.38
DNB Ratio at Rated Power (BAW-168)	1.60

Table 3-2

Nuclear Design Data

Fuel Element Volume Fractions		
Fuel		0.285
Moderator		0.590
Zircaloy		0.099
Stainless Steel		0.011
Void		0.015
		1.000
Total UO_2, metric tons		91.61
Core Dimensions, in.		
Equivalent Diameter		128.9
Active Height		144.0
Unit Cell H_2O to U Atomic Ratio		
Cold		2.97
Hot		2.13
Full Power Lifetime, days	**Unit 1**	**Unit 2**
First Cycle	272	310
Each Succeeding Cycle	310	310

Table 3-2 (Cont'd)

Fuel Irradiation, MWD/MTU	Unit 1	Unit 2
First Cycle Average	8,260	9,410
Succeeding Cycle Average	9,410	9,410
Feed Enrichments, w/o U-235		
First Cycle	2.24/2.47/2.77 (by initial zone)	2.47(a)
Control Data		
Control Pin Material		Cd-In-Ag
Number of Control Cluster Assemblies		69
Total Rod Worth ($\Delta k/k$), %		10
Control Pin Cladding Material		Type 304 SS

(a) Average feed enrichment.

Single fuel assembly reactivity information is also included in Table 3-3.

Table 3-3

Excess Reactivity Conditions

Effective Multiplication - BOL(a)	Unit 1	Unit 2
Cold, Zero Power	1.312	1.255
Hot, Zero Power	1.258	1.201
Hot, Rated Power	1.242	1.184
Hot, Equilibrium Xe, Rated Power	1.205	1.154
Hot, Equilibrium Xe and Sm, Rated Power(d)	1.167	1.119
Single Fuel Assembly(b)		
Hot	0.77	
Cold(c)	0.87	

(a) BOL - Beginning-of-Life.

(b) Based on highest probable enrichment of 3.5 weight/per cent.

(c) A center-to-center assembly pitch of 21 in. is required for this k_{eff} in cold nonborated water with no xenon or samarium.

(d) Includes burnup until equilibrium samarium is reached.

The minimum critical mass weight, with and without xenon and samarium poisoning, may be specified in a variety of forms, i.e., single assembly, multiple assemblies in various geometric arrays, damaged or crushed assemblies, etc. The unit fuel assembly has been investigated for comparative purposes. A single cold, clean assembly containing a maximum probable enrichment of 3.5 weight/per cent is subcritical. Two assemblies side-by-side are supercritical except when both equilibrium Xe and Sm are present. Three assemblies side-by-side are supercritical with both equilibrium Xe and Sm present.

3.2.2.1.2 Reactivity Control Distribution

Control of excess reactivity for both Unit 1 and Unit 2 is shown in Table 3-4.

Table 3-4

First Cycle Reactivity Control Distribution

Controlled by Soluble Boron - % Δk/k	Unit 1	Unit 2
1. Moderator Temperature Deficit (70 to 520 F)	3.3	3.6
2. Equilibrium Xenon and Samarium	2.5	2.4
3. Fuel Burnup and Fission Product Buildup	16.0	12.3
Total Soluble Boron Worth Required	21.8	18.3
Controlled by Control Cluster Assemblies - % Δk/k		
1. Doppler Deficit (0 to 100% power)	1.0	1.2
2. Transient Xenon	1.4	1.4
3. Equilibrium Xenon	1.0	0.8
4. Moderator Temperature Deficit (0 to 15% power at end-of-life)	0.6	0.6
5. Dilution Control	0.2	0.2
6. Shutdown Margin	1.0	1.0
Total CCA Worth Required	5.2	5.2
Available Cluster Control Assembly Worth - % Δk/k		
1. Total Movable CCA Worth	10	10
2. Stuck CCA Worth (CCA of highest reactivity value)	(-)3	(-)3
Minimum CCA Worth Available	7	7

Boron in solution is used to control the following relatively slow moving reactivity changes:

a. The moderator deficit in going from ambient to operating temperatures. The value shown is for the maximum change which would occur toward the end of the cycle.

b. Equilibrium samarium and a part (approximately 1.5% $\Delta k/k$) of the equilibrium xenon.

c. The excess reactivity required for fuel burnup and fission product buildup throughout cycle life.

Figure 3-1 shows the typical variation in boron concentration with cycle life for Unit 1 and Unit 2.

Control cluster assemblies (CCA's) will be used to control the reactivity changes associated with the following:

a. Power-level changes (Doppler) and the resultant short-term xenon transients are considered here. Sufficient rod worth remains inserted in the core during normal operation to overcome the peak xenon transient following a power reduction. This override capability facilitates the return to normal operating conditions without extended delays. The presence of these rods in the core during operation does not produce power peaks above the design value, and the shutdown margin of the core is not adversely affected. A typical contour drawing of relative power distribution with the xenon override rods inserted is shown in Figure 3-2. All isopower lines are taken relative to the highest power peak. Axial power peak variation, resulting from partial or full insertion of xenon override rods, is described fully in Figures 3-3 and 3-4.

b. The portion of the equilibrium xenon not controlled by soluble boron, approximately 1% $\Delta k/k$, is held by movable CCA's.

c. Between zero and 15 per cent of full power, reactivity compensation by CCA's may be required as a result of the linear increase of reactor coolant temperature from 520 F to the normal operating value.

d. Additional reactivity is held by a group of partially inserted CCA's (25 per cent insertion maximum) to allow periodic rather than continuous soluble boron dilution. The CCA's are inserted to the 25 per cent limit as the boron is diluted. Automatic withdrawal of these CCA's during operation is allowed to the 5 per cent insertion limit where the dilution procedure is again initiated and this group of CCA's is reinserted.

e. A shutdown margin of 1% $\Delta k/k$ to the hot critical condition is also required as part of the reactivity controlled by CCA's.

A total of 5.2% $\Delta k/k$ is required in movable control. Analysis of the 69 CCA's under the reference fuel arrangement predicts a total CCA worth of at least 10% $\Delta k/k$. The stuck-out CCA worth was also evaluated at a value no larger than 3.0% $\Delta k/k$. This evaluation included selection of the highest worth CCA under the first CCA-out condition.

The minimum available CCA worth of 7.0% $\Delta k/k$ is sufficient to meet movable control requirements.

3.2.2.1.3. Reactivity Shutdown Analysis

The ability to shut down the core under both hot and cold conditions is illustrated in Table 3-5. In this tabulation Unit 1 and Unit 2 are evaluated at the beginning-of-life (BOL) and the end-of-life (EOL) for shutdown capability.

Table 3-5

Initial Cycle Reactivity Shutdown Analysis

Reactivity Effects - % Δk/k	Unit 1		Unit 2	
	BOL	EOL	BOL	EOL
1. Maximum Shutdown CCA Requirements				
Doppler (100 to 0% power)	1.0	1.5	1.2	1.5
Equilibrium Xenon[a]	2.5	2.4	2.2	2.1
Moderator Deficit (15 to 0% power)	0.0	0.6	0.0	0.6
Total	3.5	4.5	3.4	4.2
2. Maximum Available CCA Worth[b]	-10.0	-10.0	-10.0	-10.0
Transient Xenon CCA Worth	1.4	1.4	1.4	1.4
3. Minimum Available CCA Worth				
All CCA's In	-8.6	-8.6	-8.6	-8.6
One Stuck CCA[c]	-5.6	-5.6	-5.6	-5.6
4. Minimum Hot Shutdown Margin				
All CCA's In	-5.1	-4.1	-5.2	-4.4
One Stuck CCA	-2.1	-1.1	-2.2	-1.4
5. Hot-to-Cold Reactivity Changes[d]				
All CCA's In	+0.5	+3.5	+1.5	+6.4
One Stuck CCA	+0.1	+2.8	+0.8	+5.8
6. Cold Reactivity Condition[e]				
All CCA's In	-4.6	-0.6	-3.7	+2.0
One Stuck CCA	-2.0	+1.7	-1.4	+4.4

Notes:

(a) Includes 1.5% Δk/k normally held by soluble boron.

(b) Total worth in 69 CCA's.

(c) CCA of highest reactivity value.

(d) Includes rod worth and all temperature changes.

(e) No boron addition.

Table 3-5 (Cont'd)

Reactivity Effects - % Δk/k	Unit 1 BOL	Unit 1 EOL	Unit 2 BOL	Unit 2 EOL
7. Soluble Boron Concentration (ppm) Addition Required for k_{eff} = 0.99 (cold)				
All CCA's In	0	25	0	190
One Stuck CCA	0	175	0	335

Examination of Table 3-5 for Minimum Hot Shutdown Margin (Item 4) shows that, with the highest worth CCA stuck out, the core can be maintained in a subcritical condition. This is true even if the soluble boron concentration is not increased to control the reactivity released by equilibrium xenon decay (see Note a). Normal conditions indicate a minimum hot shutdown margin of 4.1% Δk/k at end-of-life (Unit 1 only).

Under conditions where a cooldown to reactor building ambient temperature is required, concentrated soluble boron will be added to the reactor coolant to produce a shutdown margin of at least 1% Δk/k. The reactivity changes which take place between the hot zero power to cold conditions are tabulated, and the corresponding increases in soluble boron are listed. Beginning-of-life boron levels for several core conditions are listed in Table 3-6 along with boron worth values. Additional soluble boron could be added for situations involving more than a single stuck CCA. The conditions shown with no CCA's illustrate the highest requirements.

Table 3-6

Soluble Boron Levels and Worth

Core Conditions	BOL Boron Levels, ppm Unit 1	Unit 2
1. Cold, k_{eff} = 0.99		
No CCA's In	1,860	1,600
All CCA's In	1,290	1,030
One Stuck CCA	1,460	1,200
2. Hot, Zero Power, k_{eff} = 0.99		
No CCA's In	2,150	1,770
All CCA's In	1,150	770
One Stuck CCA	1,450	1,070
3. Hot, Full Power		
No CCA's In	1,950	1,550
4. Hot, Equilibrium Xe and Sm, Full Power	1,430	1,060

Table 3-6 (Cont'd)

Boron Worths - % Δk/k/ppm	Unit 1	Unit 2
Hot	1/100	1/100
Cold	1/75	1/75

3.2.2.1.4 Reactivity Coefficients

Reactivity coefficients form the basis for analog studies involving normal and abnormal reactor operating conditions. These coefficients have been investigated as part of the analysis of this core and are described below as to function and overall range of values. This information will apply to both Units except as noted.

a. Doppler Coefficient

The Doppler coefficient reflects the change in reactivity as a function of fuel temperature. A rise in fuel temperature results in an increase in the effective absorption cross section of the fuel (the Doppler broadening of the resonance peaks) and a corresponding reduction in neutron production. The range for the Doppler coefficient under operating conditions is expected to be -1.1×10^{-5} to -1.7×10^{-5} $\Delta k/k/F$.

b. Moderator Void Coefficient

The moderator void coefficient relates the change in neutron multiplication to the presence of voids in the moderator. Cores controlled by appreciable amounts of soluble boron may exhibit a small positive coefficient for very small void levels (several per cent void), while higher void levels produce increasingly negative coefficients. The expected range for the void coefficient is $+1.0 \times 10^{-4}$ to -3.0×10^{-3} $\Delta k/k/\%$ void.

c. Moderator Pressure Coefficient

The moderator pressure coefficient relates the change in moderator density, resulting from a reactor coolant pressure change, to the corresponding effect on neutron production. This coefficient is opposite in sign and considerably smaller when compared to the moderator temperature coefficient. A typical range of pressure coefficients over a life cycle would be -1×10^{-6} to $+2 \times 10^{-6}$ $\Delta k/k/psi$.

d. Moderator Temperature Coefficient

The moderator temperature coefficient relates a change in neutron multiplication to the change in reactor coolant temperature. Reactors employing soluble boron as a reactivity control have less negative moderator temperature coefficients than cores controlled solely by movable or fixed CCA's. The major temperature effect on the coolant is a change in density. An increasing coolant temperature

produces a decrease in water density and an equal percentage reduction in boron concentration. The concentration change results in a positive reactivity component by reducing the absorption in the coolant. The magnitude of this component is proportional to the total reactivity held by soluble boron.

The moderator temperature coefficient has been parameterized for the reference core in terms of boron concentration and reactor coolant temperature. The results of the study are shown in Figures 3-5 and 3-6. Figure 3-5 shows the coefficient variation for ambient and operating temperatures as a function of soluble boron concentration. The operating value ranges from approximately $+0.8 \times 10^{-4}$ to -1.7×10^{-4} $\Delta k/k/F$. Figure 3-6 shows the moderator temperature coefficient as a function of temperature for various poison concentrations. The coefficients of Unit 2 will be more negative than Unit 1, since the boron concentration levels are considerably lower.

The positive temperature coefficient during the initial portion of Cycle 1 for each reactor will not constitute an operational problem. The Doppler deficit represents a much larger reactivity effect in the negative direction, and together with the CCA system response will provide adequate control.

e. pH Coefficient

At the present time there is no definite correlation to predict pH reactivity effects between various operating reactors, pH effects versus reactor operating time at power, and changes in effects with various clad, temperature, and water chemistry. Yankee, Saxton, and Con Edison have experienced reactivity changes at the time of pH changes, but there is no clear-cut evidence that pH is the direct influencing variable without considering other items such as clad materials, fuel assembly crud deposition, system average temperature, and prior system water chemistry.

Saxton experiments have indicated a pH reactivity effect of 0.16 per cent reactivity per pH unit change with and without local boiling in the core. Operating reactor data, and results of applying Saxton observations to the reference reactor, are as follows:

(1) The proposed system pH will vary from a cold measured value of approximately 5.5 to a hot calculated value of 7.8 with 1,400 ppm boron and 3 ppm KOH in solution at the beginning-of-life. Lifetime bleed dilution to 20 ppm boron will reduce pH by approximately 0.8 pH units to a hot calculated pH value of 7.0.

(2) Considering the maximum system makeup rate of 70 gpm, the corresponding changes in pH are 0.071 pH units per hour for boron dilution and 0.231 pH units per hour for KOH dilution. Applying pH worth values observed at Saxton of 0.16% $\Delta k/k$ per pH unit, insertion rates are 3.16×10^{-6}% $\Delta k/k$ sec and 1.03×10^{-5}% $\Delta k/k$ sec, respectively. These insertion rates correspond to 1.03 per cent power/hour and 3.4 per cent power/hour respectively, which are easily compensated by the operator or the automatic control system.

3.2.2.1.5 Reactivity Insertion Rates

Figure 7-7 displays the integrated rod worth of four overlapping rod banks as a function of distance withdrawn. The indicated groups are those used in the core during power operation. Using approximately 1.2% $\Delta k/k$ CCA groups and a 25 in./min drive speed in conjunction with the reactivity response given in Figure 7-7 yields a maximum reactivity insertion rate of 5.8×10^{-5} $\Delta k/k$/sec. The maximum reactivity insertion rate for soluble boron removal is 7×10^{-6} $\Delta k/k$ second.

3.2.2.1.6 Power Decay Curves

Figure 3-7 displays the beginning-of-life power decay curves for the two least effective CCA worths as outlined in Table 3-5, Item No. 3.

The power decay is initiated by the trip release of the CCA's with a 300 msec delay from initiation to start of CCA motion. The time required for 2/3 rod insertion is 1.4 sec.

3.2.2.1.7 Neutron Flux Distribution and Spectrum

The neutron flux levels at the core edge and the pressure vessel wall are given in Table 3-7.

Table 3-7

Exterior Neutron Levels and Spectra

Flux Group		Neutron Flux Levels, $n/cm^2/sec$[a]	
		Core Edge	Interior Wall of Pressure Vessel
1	0.821 mev to 10 mev	6.0×10^{13}	3.4×10^{10}
2	1.230 kev to 0.821 mev	9.0×10^{13}	7.5×10^{10}
3	0.414 ev to 1.230 kev	6.2×10^{13}	5.7×10^{10}
4	Less than 0.414 ev	7.1×10^{13}	2.1×10^{10}

(a) These values include the maximum axial peak-to-average power ratio of 1.7.

The calculations were performed using The Babcock & Wilcox Company LIFE code (BAW-293, Section 3.6.3) to generate input data for the transport code, TOPIC.(1) A 4-group edit is obtained from the LIFE output which includes diffusion coefficients; absorption, removal, and fission cross sections; and the zeroth and first moments of the scattering cross section. TOPIC is an S_n code designed to solve the 1-dimensional transport equation in cylindrical coordinates for up to six groups of neutrons. For the radial and azimuthal variables a linear

approximation to the transport equation is used; for the polar angle Gauss quadrature is used. Scattering functions are represented by a Legendre series. The azimuthal angle can be partitioned into 4 to 10 intervals on the half-space between 0 and π. The number of mesh points in the radial direction is restricted by the number of these intervals. For the core exterior flux calculations, four intervals on the azimuthal were used. This allows the maximum number of mesh points (240) in the "r" direction to describe the shield complex. An option is available to use either equal intervals on the azimuthal angle or equal intervals on the cosine of the angle. Equal intervals on the cosine were chosen since this provides more detail in the forward direction of the flux (toward the vessel). Five Gauss quadrature points were used on the cosine of the polar angle in the half-space between 0 and π.

Results from the above method of calculation have been compared with thermal flux measurements through an array of iron and water slabs in the LIDO pool reactor.(2) Although this is not a direct comparison with fast neutron measurements, it does provide a degree of confidence in the method, since the magnitude of the thermal flux in shield regions is governed by fast neutron penetration.

Results of the comparison showed that fluxes predicted by the LIFE-TOPIC calculation were lower, in general, by about a factor of 2. Results of the fast flux calculations are, consequently, increased by a factor of 2 to predict the nvt in the reactor vessel.

The following conservatisms were also incorporated in the calculations:

a. Neutron fluxes outside the core are based on a maximum power density of 41 watts/cc at the outer edge of the core rather than an estimated average of 28 watts/cc over life, resulting in a safety margin of about 45 per cent.

b. A maximum axial power peaking factor of 1.7 was used. This is about 30 per cent greater than the 1.3 expected over life.

Uncertainties in the calculations include the following:

1. The use of only four neutron groups to describe the neutron energy spectrum.

2. Use of the LIFE code to generate the 4-group cross sections. In the LIFE program, the 4-group data in all regions is computed from a fission spectrum rather than a leakage spectrum.

3. Having only four intervals, i.e., $n = 4$ in the S_n calculation, to describe the angular segmentation of the flux.

It is expected that the combination of 1 and 2 above will conservatively predict a high fast neutron flux at the vessel wall because it underestimates the effectiveness of the thermal shield in reducing the fast flux. In penetration through water, the average energy of the neutrons in the group above 1 mev increases above that of a fission spectrum, i.e., the spectrum in this group

hardens. For neutrons above 1 mev, the non-elastic cross section of iron increases rapidly with energy. Therefore, the assumption of a fission spectrum to compute cross sections in the thermal shield, and the use of a few-group model to cover the neutron energy spectrum, would underestimate the neutron energy loss in the thermal shield and the subsequent attenuation by the water between the vessel and thermal shield. The results from 34-group P3MG(3) calculations show that reduction of the flux above 1 mev by the thermal shield is about a factor of 4 greater than that computed from the 4-group calculations.

The effect of 3 above is expected to underestimate the flux at the vessel wall. In calculations at ORNL using the S_n technique, a comparison between an S_4 and an S_{12} calculation was made in penetration through hydrogen. The results for a variety of energies over a penetration range of 140 cm showed the S_4 calculation to be lower than the S_{12} by about a factor of 2 at maximum. Good agreement was obtained between the S_{12} and moments method calculations.

The above uncertainties indicate that the calculation technique should overestimate the fast flux at the reactor vessel wall. However, the comparison with thermal flux data indicates a possible underestimate. Until a better comparison with data can be made, we have assumed that the underestimate is correct and accordingly have increased the flux calculations by a factor of 2 to predict the nvt in the reactor vessel.

3.2.2.2 Nuclear Evaluation

Analytical models and the application of these models are discussed in this section. Core instabilities associated with xenon oscillation are also mentioned, with threshold data evaluated under reference conditions.

3.2.2.2.1 Analytical Models

Reactor design calculations are made with a large number of computer codes. The choice of which code set or sets to use depends on which phase of the design is being analyzed. A list of codes used in core analysis with a brief discussion follows in 3.2.2.2.2.

a. Reactivity Calculations

Calculation of the reactivity of a pressurized water reactor core is performed in one, two, or three dimensions. The geometric choice depends on the type of calculations to be made. In a clean type of calculation where there are no strong localized absorbers of a type differing from the rest of the lattice, 1-dimensional analysis is satisfactory. This type of problem is handled quite well by the B&W 1-dimensional depletion package code LIFE. LIFE is a composite of MUFT (Ref. 4), KATE (Ref. 5), RIP, WANDA (Ref. 6), and a depletion routine. Normally the MUFT portion is used with 34 energy groups, an exact treatment of hydrogen, the Greuling-Goertzel approximation for elements of mass less than 10, and Fermi age for all heavier elements. The KATE portion normally uses a Wigner-Wilkins spectrum. In WANDA, 4 energy groups are utilized. Disadvantage factors for input to the thermal group are calculated with the THERMOS (Ref. 7) code. This code set has been shown to give reliable results for a reactivity calculation of this type. Recent check calculations on critical experiments have a standard deviation of less than 0.5% $\Delta k/k$.

A 1-dimensional analysis of a geometric arrangement, where there are localized strong absorbers such as CCA's, requires a preliminary 2-dimensional analysis. The required properties of the 1-dimensional system are then matched to the 2-dimensional analysis. In this manner, it is possible to analyze the simpler 1-dimensional system in a depletion survey problem with only a small loss in accuracy.

The 1-dimensional calculations are used as preliminary guides for the more detailed 2-dimensional analysis that follows. Values of reactivity coefficients, fuel cycle enrichments, lifetimes, and soluble poison concentrations can be found to improve the initial conditions specified for 2-dimensional analysis.

Two-dimensional reactivity calculations are done with either the PDQ (Ref. 8) or TURBO (Ref. 9) diffusion and/or depletion codes. These codes have mesh limitations on the size of a configuration which can be shown explicitly and are often studied with quarter core symmetry. Symmetry is desirable in the design, and no loss in generality occurs. The geometric description includes each fuel assembly and as much detail as is possible, i.e., usually each unit in the fuel assembly. Analysis of this type permits detailed power distribution studies as well as reactivity analysis. The power distribution in a large PWR core which has zone loading cannot be predicted reliably with 1-dimensional calculations. This is particularly true when local power peaking as a function of power history is of interest. It is necessary to study this type of problem with at least a 2-dimensional code, and in some cases 3-dimensional calculations are necessary.

Use of the 2-dimensional programs requires the generation of group constants as a function of material composition, power history, and geometry. For regions where diffusion theory is valid, MUFT and KATE with THERMOS disadvantage factors are used to generate epithermal and thermal coefficients. This would apply at a distance of a few mean paths from boundaries or discontinuities in the fuel rod lattice. Discontinuities refer to fuel assembly can, water channels, instrumentation ports, and CCA guide assemblies. The interfaces between regions of different enrichment are considered to be boundaries as well as the outer limit of the core.

To generate coefficients for regions where diffusion theory is inappropriate several methods are utilized. The arrangement of structural material, water channels, and adjacent fuel rod rows can be represented well in slab geometry. This problem is analyzed by P3MG (Ref. 3) which is effective in slab geometry. The coefficients so generated are utilized in the epithermal energy range. Coefficients for the thermal energy range are generated by a slab THERMOS calculation. The regions adjacent to an interface of material of different enrichment are also well represented with the P3MG code.

The arrangement of instrumentation ports and control pin guide assemblies lends itself to cylindrical geometry. DTF-IV (Ref. 10) is quite effective in the analysis of this arrangement. Input to DTF-IV is from GAM (Ref. 11) and THERMOS or KATE. Iteration is required between the codes. The flux shape is calculated by DTF-IV and cross

sections by the others. The outer boundary of the core where there is a transition from fuel to reflector and baffle is also represented by the DTF-IV code. The 3-dimensional analysis is accomplished by extending the techniques of 2-dimensional representation.

b. Control Pin Analysis

The analysis of control pins and their guide assemblies requires transport methods similar to techniques mentioned in the previous section. The difference arises in application. Instead of calculating group constants, logarithmic boundary conditions are used. These conditions are derived as a function of material, geometry, and material condition. The material condition part refers to temperature and power history.

The logarithmic boundary conditions are calculated with DTF-IV with input from GAM and THERMOS or KATE. These conditions are then transformed to a PDQ or TURBO representation. This step is necessary because of the differences arising between the transport calculation in cylindrical geometry and the square mesh representation in the 2-dimensional diffusion codes.

This method is at present being verified by comparison with critical experiments containing Ag-In-Cd and boron poison rods. The critical data is reported in References 12, 13, 14, and 15.

c. Determination of Reactivity Coefficients

This type of calculation is different from the reactivity analysis only in application, i.e., a series of reactivity calculations being required. Coefficients are determined for moderator temperature, voiding, and pressure, and for fuel temperature. These are calculated from small perturbations in the required parameter over the range of possible values of the parameter.

The moderator temperature coefficient is determined as a function of soluble poison concentration and moderator temperature, and fuel temperature or Doppler coefficient as a function of fuel temperature. The coefficient for voiding is calculated by varying the moderator concentration or per cent void.

3.2.2.2.2 Codes for Reactor Calculations

This section contains a brief description of codes mentioned in the preceding section.

THERMOS (Ref. 7) - This code solves the integral form of the Boltzmann Transport Equation for the neutron spectrum as a function of position. A diagonalized connection to the isotropic transfer matrix has been incorporated allowing a degree of anisotropic scattering.

MUFT (Ref. 4) - This program solves the P_1 or B_1 multigroup equation for the first two Legendre coefficients of the directional neutron flux, and for the isotropic and anisotropic components of the

slowing down densities due to a cosine-shaped neutron source. Coefficients are generated with MUFT for the epithermal energy range.

KATE (Ref. 5) - The code solves the Wigner-Wilkins differential equation for a homogeneous medium moderated by chemically unbound hydrogen atoms in thermal equilibrium. Coefficients for the thermal energy range are generated by KATE.

RIP - This program averages cross sections over an arbitrary group structure, calculates resonance integrals for a set of resolved peaks, and computes L-factors for input to MUFT, P1MG, and P3MG.

WANDA (Ref. 6) - This code provides numerical solutions of the 1-dimensional few-group neutron diffusion equations.

LIFE - This is a 1-dimensional depletion package code which is a combination of MUFT, KATE, RIP, and WANDA. The combination mechanizes the procedures for using the codes separately.

GAM (Ref. 11) - This code is a multigroup coefficient generation program that solves the P_1 equations and includes anisotropic scattering. Inelastic scattering and resonance parameters are also treated by GAM.

P3MG (Ref. 3) - The code solves the multienergy transport equation in various geometries. The code is primarily used for epithermal coefficient generations.

DTF (Ref. 10) - This code solves the multigroup, 1-dimensional Boltzmann transport equation by the method of discrete ordinates. DTF allows multigroup anisotropic scattering as well as up and down scattering.

PDQ (Ref. 8) - This program solves the 2-dimensional neutron diffusion-depletion problem with up to five groups. It has a flexible representation of time-dependent cross sections by means of fit options.

TURBO (Ref. 9) - This code is similar in application to the PDQ depletion program. It, however, lacks the great flexibility of the PDQ fit options.

CANDLE (Ref. 9) - This code is similar to TURBO, but solves the diffusion equations in one dimension.

TNT (Ref. 9) - This code is similar in application to TURBO, but is a 3-dimensional code extended from DRACO.

3.2.2.2.3 Stability Analysis

The core has been examined for xenon stability. A modal analysis of axial, azimuthal, and radial spatial xenon oscillations for large pressurized water

moderated reactors has been completed.[16] The method used in this analysis is an extension of the 1-group treatment including power coefficient introduced by Randall and St. John. One- and 2-group treatments have been compared, and the conclusion drawn that a 1-group model is satisfactory for large cores. For all three geometries, data were generated as a function of:

a. Core size.

b. Flux level.

c. Degree of flatness in the power distribution.

d. Power coefficient.

e. Reactivity held by saturation xenon.

In addition, slightly dished power distributions were investigated to show that any dishing resulting from high depletion is not sufficient to require corrections to data based on replacing the dished segment with a flat power distribution.

The effect of modal coupling has been examined and shown to be of no consequence for cores similar to the reference reactor design. Values of the critical dimension varied no more than 1 to 2.8 per cent for the same core with and without modal coupling. The lower value was computed with a zero power coefficient and was not conservative without modal coupling. The higher value was computed with the reference power coefficient and was conservative without modal coupling.

Table 3-8 summarizes those parameters for the reference core which affect the xenon stability threshold. The parameters were calculated at two substantially different times in core life. Reference physical dimensions are also shown for comparison purposes in the following discussion.

Table 3-9 shows the threshold dimensions for first mode instability as a function of flux flattening. The percentage of flattening is defined as 100 per cent times the ratio of the flattened power distribution to the total physical dimension under consideration. The parameters of Table 3-8 at two days were used since they are virtually the same as those at 150 days but more conservative. Axial depletion studies show that power distributions are flattened by 0, 63, and 73 per cent at 2, 150, and 354 full power days. A maximum flatness of approximately 80 per cent may be expected for long core life.

An examination of the data in Table 3-9 shows that with the maximum flatness axial oscillations are possible, azimuthal oscillations are unlikely, and radial oscillations will not occur.

Threshold dimensions for second mode oscillations were 50 per cent larger in magnitude than those shown in Table 3-9 for the first mode. Oscillations in the second mode will not occur in the reference core.

Table 3-8

Reference Core Parameters

	Two Full Power Days	150 Full Power Days
M^2, cm^2	57.0	57.0
$\bar{\phi}_{th}$, n/cm^2-sec	3.9×10^{13}	3.8×10^{13}
a_x (reactivity held by saturation xenon), $\Delta k/k$	0.034	0.033
Doppler Coefficient, $\Delta k/k/F$	-1.1×10^{-5}	-1.1×10^{-5}
Moderator Temperature Coefficient	Positive but Small	Negative
a_T (power coeff.), $\Delta k/k$/unit flux	$\approx -2.2 \times 10^{-16}$	$\approx -2.3 \times 10^{-16}$
Equivalent Dimensions, ft		
Height	12.00	
Diameter	10.74	
Radius	5.37	

Table 3-9

First Mode Threshold Dimensions and Flatness

Threshold Dimensions, ft	Flatness, % 0	50	80
Threshold height (axial oscillations)	18.5	14.1	11.8
Threshold diameter (azimuthal oscillation)	20.4	16.5	14.0
Threshold radius (radial oscillation)	16.8	16.7	14.5

Table 3-10 shows the values of H/D versus power flatness for equal likelihood of axial, azimuthal, and radial first harmonic oscillations, i.e., if the core is just at the axial threshold for axial oscillations, it can also be expected that there will be azimuthal and radial oscillations provided the value of H/D in Table 3-10 is satisfied. H/D for this reactor is 1.12.

Table 3-10

Threshold Ratio and Power Flatness

Ratio	Flatness, %				
	0	20	50	80	100
H/D (axial versus azimuthal)	0.91	0.87	0.86	0.86	0.85
H/D (axial versus radial)	0.55	0.49	0.42	0.41	0.41

The modal methods used to examine the xenon oscillation problem made use of core-averaged quantities such as flux, power coefficient, and reactivity held by saturation xenon. In addition, flux distributions were limited to:

a. Geometric distributions.

b. Partially or totally flat.

c. Slightly dished.

In view of these limitations, a study is underway to investigate xenon oscillation using nuclear depletion programs coupled with heat transfer equations. The axial heat transfer equations are included in the B&W LIFE-5 diffusion depletion program and are being used for extensive axial analysis, including control requirements for the suppression of axial oscillations should they occur. Additional analysis will include the study of the first mode azimuthal instability.

The power distribution of Unit 1 during early life is such that no xenon instabilities will occur. The power flattening effect of fuel burnup with time renders the core more susceptible to xenon oscillations.

Assuming that oscillation does occur, adequate notification will be received from incore instrumentation. The long period of the oscillation (approximately 30 hr) provides ample time for system evaluation and the initiation of corrective measures. These corrections would range from CCA adjustments for damping out the oscillation to a temporary reduction in core power level.

3.2.3 THERMAL AND HYDRAULIC DESIGN AND EVALUATION

3.2.3.1 Thermal and Hydraulic Characteristics

3.2.3.1.1 Fuel Assembly Heat Transfer Design

a. Design Criteria

The criterion for heat transfer design is to be safely below Departure from Nucleate Boiling (DNB) at the design overpower (114 per cent of rated power). A detailed description of the analysis is given in 3.2.3.2.2, Statistical Core Design Technique.

The input information for the statistical core design technique and for the evaluation of individual hot channels consists of the following:

(1) Heat transfer critical heat flux equations and data correlations

(2) Nuclear power factors

(3) Engineering hot channel factors

(4) Core flow distribution hot channel factors

(5) Maximum reactor overpower

These inputs have been derived from test data, physical measurements, and calculations as outlined below.

b. Heat Transfer Equation and Data Correlation

The heat transfer relationship used to predict limiting heat transfer conditions is presented in BAW-168.[17] The equation is as follows:

$$q'' = (1.83 - 0.000415\ P) \times 90{,}000 \left[\frac{G}{240} \cdot \left(\frac{S}{L}\right)\right]^{0.3987 + 0.001036\,\Delta T_{esc} - 1.027 \times 10^{-6}(\Delta T_{esc})^2}$$

where:

q'' = critical heat flux as predicted by the best fit form, Btu/hr-ft^2

P = core operating pressure, psia

G = channel mass velocity, lb/hr-ft^2

S = channel equivalent diameter, ft

L = length up the channel to the point of interest, ft

ΔT_{esc} = inlet subcooling (T_{sat} - T_{inlet}), F

T_{sat} = coolant saturation temperature corresponding to P, F

This equation was derived from experimental heat transfer data. An analysis of heat transfer data for this and other relationships is described in detail in 3.2.3.2.3, Correlation of Heat Transfer Data.

Individual channels are analyzed to determine a DNB ratio, i.e., the ratio of the heat flux at which a DNB is predicted to occur to the heat flux in the channel being investigated. This DNB ratio is related to the data correlation as in Figure 3-8. A confidence and population value is associated with every DNB ratio as described in the Statistical Core Design Technique. The plot of DNB versus P shown is for a confidence of 99 per cent.

The DNB and population relationships shown are also the values associated with the single hot channel analysis for the hottest unit cell where a 1.38 DNB ratio corresponds to a 99 per cent confidence that at least 94.5 per cent of the population of all such hot channels are in no jeopardy of experiencing a DNB. This statement is a corollary to the total core statistical statement given in 3.1.2.3, Thermal and Hydraulic Limits. The criterion for evaluating the thermal design margin for individual channels or the total core is the confidence-population relationship. The DNB ratios required to meet the basic criteria or limits are a function of the experimental data and heat transfer correlation used, and vary with the quantity and quality of data.

c. Nuclear Power Factors

The heated surfaces in every flow channel in the core are examined for heat flux limits. The heat input to the fuel rods comprising a coolant channel is determined from a nuclear analysis of the core and fuel assemblies. The results of this analysis are as follows:

(1 The nominal nuclear peaking factors for the worst time in core life are:

$F\Delta h = 1.79$
$Fz = 1.70$
$Fq = 3.04$

(2) The design nuclear peaking factors for the worst time in core life are:

$F\Delta h = 1.85$
$Fz = 1.70$
$Fq = 3.15$

where:

$F\Delta h$ = max/avg total power ratio (radial x local nuclear)

Fz = max/avg axial power ratio (nuclear)

$Fq = F\Delta h \times Fz$ (nuclear total)

The nominal values are the maximum calculated values. The design values are obtained by increasing the maximum calculated total power ratio, $F\Delta h$, from 1.79 to 1.85 to obtain a more conservative design.

The axial nuclear factor, Fz, is illustrated in Figure 3-9. The distribution of power expressed as $P/\overline{P}$ is shown for two conditions of reactor operation. The first condition is an inlet peak with a max/avg value of 1.70 resulting from partial insertion of a CCA group for transient control following a power level change. This condition results in the maximum local heat flux and maximum linear heat rate. The second power shape is a symmetrical cosine which is indicative of the power distribution with xenon override rods withdrawn. The flux peak max/avg value is 1.50 in the center of the active core. Both of these flux shapes have been evaluated for thermal DNB limitations. The limiting condition is the 1.5 cosine power distribution. The inlet peak shape has a larger maximum value. However, the position of the 1.5 cosine peak farther up the channel results in a less favorable flux to enthalpy relationship. This effect has been demonstrated in DNB tests of nonuniform flux shapes.[18] The 1.5 cosine axial shape has been used to determine individual channel DNB limits and make the associated statistical analysis.

The nuclear factor for total radial x local rod power, $F\Delta h$, is calculated for each rod in the core. A distribution curve of the fraction of the core fuel rods operating above various peaking factors is shown in Figure 3-10. Line B shows the distribution of the maximum calculated values of $F\Delta h$ for nominal conditions with a maximum value of 1.79. The distribution of peaking factors for the design condition is obtained by increasing the maximum calculated value for all rods in the core by the ratio of 1.85/1.79 or 1.033 to provide conservative results. Determination of the peaking distribution for the design condition in this manner has the effect of increasing reactor power by about 3 per cent. This assumption is conservative since the distribution with a maximum peak $F\Delta h$ of 1.85 will follow a line similar to Line C where the average power of all rods in the core is represented by an $F\Delta h$ of 1.0. The actual shape of the distribution curve is dependent upon statistical peaking relationships, CCA positions, moderator conditions, and operating history. The shape of the distribution curve will be more accurately described during the detailed core design.

d. Engineering Hot Channel Factors

Power peaking factors obtained from the nuclear analysis are based on mechanically-perfect fuel assemblies. Engineering hot channel factors are used to describe variations in fuel loading, fuel and

clad dimensions, and flow channel geometry from perfect physical quantities and dimensions.

The application of hot channel factors is described in detail in 3.2.3.2.2, Statistical Core Design Technique. The factors are determined statistically from fuel assembly as-built or specified data where F_Q is a heat input factor, $F_{Q''}$ is a local heat flux factor at a hot spot, and F_A is a flow area reduction factor describing the variation in coolant channel flow area. Several subfactors are combined statistically to obtain the final values for F_Q, $F_{Q''}$, and F_A. These subfactors are shown in Table 3-11. A description of the factor, the coefficient of variation, the standard deviation, and the mean value are tabulated.

Table 3-11

Coefficients of Variation

CV No.	Description	σ	$\bar{x}$	CV
1	Flow Area	0.00075	0.17625	0.00426
2	Local Rod Diameter	0.000485	0.420	0.00116
3	Average Rod Diameter (Die-drawn, local and average same)	0.000485	0.420	0.00116
4	Local Fuel Loading			0.00687
	Subdensity	0.00647	0.95	0.00681
	Subfuel area (Diameter effect)	0.000092	0.1029	0.00089
5	Average Fuel Loading			0.00370
	Subdensity	0.00324	0.95	0.00341
	Sublength	0.16181	144	0.00112
	Subfuel area (Diameter effect)	0.000092	0.1029	0.00089
6	Local Enrichment	0.00323	2.24	0.00144
7	Average Enrichment	0.00323	2.24	0.00144

CV Coefficient of Variation, $\sigma/\bar{x}$
σ Standard Deviation of Variable
$\bar{x}$ Mean Value of Variable

(Enrichment values are for worst case normal assay batch; maximum variation occurs for minimum enrichment.)

e. Core Flow Distribution Hot Channel Factors

The physical arrangement of the reactor vessel internals and nozzles results in a nonuniform distribution of coolant flow to the various fuel assemblies. Reactor internal structures above and below the active core are designed to minimize unfavorable flow distribution. A 1/6 scale model test of the reactor and internals is being performed to demonstrate the adequacy of the internal arrangements. The final variations in flow will be determined when the tests are completed. Interim factors for flow distribution effects have been calculated from reactor vessel model test data for previous pressurized water reactor designs.

A flow factor is determined for each fuel assembly location in the core. The factor is expressed as the ratio of fuel assembly flow to average fuel assembly flow. The finite values of the ratio may be greater or less than 1.0 depending upon the position of the assembly being evaluated. The flow in the central fuel assemblies is in general larger than the flow in the outermost assemblies due to the inherent flow characteristics of the reactor vessel.

The flow distribution factor is related to a particular fuel assembly location and the quantity of heat being produced in the assembly. A flow-to-power comparison is made for all of the fuel assemblies. The worst condition expected in the hottest fuel assembly is five per cent less than average flow. Two assumptions for flow distribution have been made in the thermal analysis of the core as follows:

(1) For the maximum design condition and for the analysis of the hottest channel, it has been assumed that all fuel assemblies receive five per cent less than average flow, regardless of assembly power or location.

(2) For the most probable design conditions predicted flow factors have been assigned for each fuel assembly consistent with location and power. The flow factor assumed for the maximum design condition is conservative. Application of vessel flow test data and individual assembl flow factors in the detailed core design will result in improve. statistical statements for the maximum design condition.

f. Maximum Reactor Design Overpower

Core performance is assessed at the maximum design overpower. The selection of the design overpower is based on an analysis of the reactor protective system as described in Section 7. The reactor trip point is 107.5 per cent power; and the maximum overpower, which is 114 per cent, will not be exceeded under any conditions.

g. Maxim. Design Conditions Analysis Summary

The Statistical Core Design Technique described in 3.2.3.2.2 was used to analyze the reactor at the maximum design conditions described previously. The total number of fuel rods in the core that have a

possibility of reaching DNB is shown in Figure 3-11 for 100 to 118 per cent overpower. Point A on Line 1 is the maximum design point for 114 per cent power with the design $F\Delta h$ nuclear of 1.85. Line 2 was calculated using the maximum calculated value for $F\Delta h$ nuclear of 1.79 to show the margin between maximum calculated and design conditions. It is anticipated that detailed core nuclear analyses will permit a lowering of the maximum design value for $F\Delta h$.

The number of fuel rods that may possibly reach a DNB at the maximum design condition with an $F\Delta h$ of 1.85 and at 114 per cent overpower, represented by point A on Figure 3-11, forms the basis for this statistical statement:

> There is a 99 per cent confidence that at least 99.5 per cent of the fuel rods in the core are in no jeopardy of experiencing a departure from nucleate boiling (DNB) during continuous operation at the design overpower of 114 per cent.

Statistical results for the maximum design condition calculation shown by Figure 3-11 may be summarized as follows in Table 3-12.

Table 3-12

DNB Results - Maximum Design Condition
(99% Confidence Level)

Point	Power, % of 2,452 mwt	$F\Delta h$	Possible DNB's	Population Protected, %
A	114	1.85	184	99.50
B	114	1.79	100	99.73
C	100	1.85	17	99.95
D	100	1.79	10	99.98
E	118	1.79	184	99.50

h. Most Probable Design Condition Analysis Summary

The previous maximum design calculation indicates the total number of rods that are in jeopardy when it is conservatively assumed that every rod in the core has the mechanical and heat transfer characteristics of a hot channel as described in 3.2.3.2.2. For example, all channels are analyzed with F_A (flow area factor) less than 1.0, F_Q (heat input factor) greater than 1.0, and with minimum fuel assembly flow. It is physically impossible for all channels to have hot channel characteristics. A more realistic indication of the number of fuel rods in jeopardy may be obtained by the application of the statistical heat transfer data to average rod power and mechanical conditions.

An analysis for the most probable conditions has been made based on the average conditions described in 3.2.3.2.2. The results of this

180

analysis are shown in Figure 3-12. The analysis may be summarized as follows in Table 3-13.

Table 3-13

DNB Results - Most Probable Condition

Point	Power, % of 2,452 mwt	F Δh	Possible DNB's	Population Protected, %
F	100	1.79	2	99.994
G	114	1.79	32	99.913
H	118	1.79	70	99.815

The analysis was made from Point F at 100 per cent power to Point H at 118 per cent power to show the sensitivity of the analysis with power. The worst condition expected is indicated by Point G at 114 per cent power where it is shown that there is a small possibility that 32 fuel rods may be subject to a departure from nucleate boiling (DNB). This result forms the basis for the following statistical statement for the most probable design conditions:

> There is at least a 99 per cent confidence that at least 99.9 per cent of the rods in the core are in no jeopardy of experiencing a DNB, even with continuous operation at the design overpower of 114 per cent.

i. Distribution of the Fraction of Fuel Rods Protected

The distribution of the fraction (P) of fuel rods that have been shown statistically to be in no jeopardy of a DNB has been calculated for the maximum design and most probable design conditions. The computer programs used provide an output of (N) number of rods and (P) fraction of rods that will not experience a DNB grouped for ranges of (P). The results for the most probable design condition are shown in Figure 3-13.

The population protected, (P), and the population in jeopardy, (1-P), are both plotted. The integral of (1-P) and the number of fuel rods gives the number of rods that are in jeopardy for given conditions as shown in Figures 3-11 and 3-12. The number of rods is obtained from the product of the percentage times the total number of rods being considered (36,816). The two distributions shown in Figure 3-13 are for the most probable condition analysis of Points F and G on Figure 3-12. The lower line of Figure 3-13 shows P and (1-P) at the 100 per cent power condition represented by Point F of Figure 3-12. The upper curve shows P and (1-P) at the 114 per cent power condition represented by Point G of Figure 3-12. The integral of N and (1-P) of the upper curve forms the basis for the statistical

statement at the most probable design condition described in paragraph h above.

j. Hot Channel Performance Summary

The hottest unit cell with all surfaces heated has been examined for hot channel factors, DNB ratios, and quality for a range of reactor powers. The cell has been examined for the maximum value of $F\Delta h$ nuclear of 1.85. The hot channel was assumed to be located in a fuel assembly with 95 per cent of the average fuel assembly flow. The heat generated in the fuel is 97.3 per cent of the total nuclear heat. The remaining 2.7 per cent is assumed to be generated in the coolant as it proceeds up the channel within the core and is reflected as an increase in ΔT of the coolant.

Error bands of 65 psi operating pressure and ± 2 F are reflected in the total core and hot channel thermal margin calculations in the direction producing the lowest DNB ratios or highest qualities.

The DNB ratio versus power is shown in Figure 3-14. The DNB ratio in the hot channel at the maximum overpower of 114 per cent is 1.38 which corresponds to a 99 per cent confidence that at least 94.5 per cent of the fuel channels of this type are in no jeopardy of experiencing a DNB. The engineering hot channel factors corresponding to the above confidence-population relationship are described in 3.2.3.2.2 and listed below:

$$F_Q = 1.008$$

$$F_{Q''} = 1.013$$

$$F_A = 0.992$$

The hot channel exit quality for various powers is shown in Figure 3-15. The combined results may be summarized as follows:

Reactor Power, %	DNB Ratio (BAW-168)	Exit Quality, %
100	1.60	0
107.5 (trip setting)	1.47	2.6
114 (maximum power)	1.38	5.4
149	1.00	23.0

3.2.3.1.2 Fuel and Cladding Thermal Conditions

a. Fuel

A digital computer code is used to calculate the fuel temperature. The program uses uniform volumetric heat generation across the fuel diameter, and external coolant conditions and heat transfer coefficients determined for thermal-hydraulic channel solutions. The fuel thermal conductivity is varied in a radial direction as a

function of the temperature variation. Values for fuel conductivity were used as shown in Figure 3-16, a plot of fuel conductivity versus temperature. The heat transfer from the fuel to the clad is calculated with a fuel and clad expansion model proportional to temperatures. The temperature drop is calculated using gas conductivity at the beginning-of-life conditions when the gas conductivity is 0.1 Btu-ft/hr-F-ft^2. The gas conduction model is used in the calculation until the fuel thermal expansion relative to the clad closes the gap to a dimension equivalent to a contact coefficient. The contact coefficient is pressure- and gas conductivity-dependent.

A plot of fuel center temperature versus linear heat rate in kw/ft is shown in Figure 3-17. The linear heat rate at the maximum overpower of 114 per cent is 19.9 kw/ft. The corresponding center fuel temperature is 4,400 F.

The following peaking factors were used in the calculation:

$$F\Delta h = 1.85$$

$$F_z = 1.70$$

$$F_{Q''} = 1.03$$

A conservative value of 1.03 was assumed for the heat flux peaking factor, $F_{Q''}$. The assigned value corresponds to a 99 per cent confidence and 99.99 per cent population-protected relationship as described in the statistical technique.

b. Clad

The assumptions in the preceding paragraph were applied in the calculation of the clad surface temperature at the maximum overpower. Boiling conditions prevail at the hot spot, and the Jens and Lottes relationship(19) for the coolant-to-clad ΔT for boiling was used to determine the clad temperature. The resulting maximum calculated clad temperature is 654 F at a system operating pressure of 2,185 psig.

3.2.3.2 Thermal and Hydraulic Evaluation

3.2.3.2.1 Introduction

Summary results for the characteristics of the reactor design were presented in 3.2.3.1. The Statistical Core Design Technique employed in the design represents a refinement in the methods for evaluating pressurized water reactors. Corresponding single hot channel DNB data were presented to relate the new method with previous criteria. A comprehensive description of the new technique is included in this section to permit a rapid evaluation of the methods used.

The BAW-168 correlation is a B&W design equation. An extensive review of data available in the field was undertaken to derive the correlation and to determine the confidence, population, and DNB relationships

included in this section. A comparison of BAW-168 with other correlations in use is also included.

A detailed evaluation and sensitivity analysis of the design has been made by examining the hottest channel in the reactor for DNB ratio, quality, and fuel temperatures. BAW-168 DNB ratios have been compared with W-3 DNB ratios to facilitate a comparison of the design with PWR reactor core designs previously reviewed.

3.2.3.2.2 Statistical Core Design Technique

The core thermal design is based on a Statistical Core Design Technique developed by B&W. The technique offers many substantial improvements over older methods, particularly in design approach, reliability of the result, and mathematical treatment of the calculation. The method reflects the performance of the entire core in the resultant power rating and provides insight into the reliability of the calculation. This section discusses the technique in order to provide an understanding of its engineering merit.

The statistical core design technique considers all parameters that affect the safe and reliable operation of the reactor core. By considering each fuel rod the method rates the reactor on the basis of the performance of the entire core. The result then will provide a good measure of the core safety and reliability since the method provides a statistical statement for the total core. This statement also reflects the conservatism or design margin in the calculation.

A reactor safe operating power has always been determined by the ability of the coolant to remove heat from the fuel material. The criterion that best measures this ability is the DNB, which involves the individual parameters of heat flux, coolant temperature rise, and flow area, and their intereffects. The DNB criterion is commonly applied through the use of the departure from nucleate boiling ratio (DNBR). This is the minimum ratio of the DNB heat flux (as computed by the DNB correlation) to the surface heat flux. The ratio is a measure of the margin between the operating power and the power at which a DNB might be expected to occur in that channel. The DNBR varies over the channel length, and it is the minimum value of the ratio in the channel of interest that is used.

The calculation of DNB heat flux involves the coolant enthalpy rise and coolant flow rate. The coolant enthalpy rise is a function of both the heat input and the flow rate. It is possible to separate these two effects; the statistical hot channel factors required are a heat input factor, F_Q, and a flow area factor, F_A. In addition, a statistical heat flux factor, F_Q'', is required; the heat flux factor statistically describes the variation in surface heat flux. The DNBR is most limiting when the burnout heat flux is based on minimum flow area (small F_A) and maximum heat input (large F_Q), and when the surface heat flux is large (large F_Q''). The DNB correlation is provided in a best-fit form, i.e., a form that best fits all of the data on which the correlation is based. To afford protection against DNB, the DNB heat flux computed by the best-fit correlation is divided by a DNB factor (B.F.) greater than 1.0 to yield the design DNB surface heat flux. The basic relationship,

$$DNBR = \frac{Q''_{DNB}}{B.F.} \times f(F_A, F_Q) \times \frac{1}{Q''_{surface} \times F_{Q''}},$$

involves as parameters statistical hot channel and DNB factors. The DNB factor (B.F.) above is usually assigned a value of unity when reporting DNB ratios so that the margin at a given condition is shown directly by a DNBR greater than 1.0, i.e., 1.38 in the hot channel.

To find the DNB correlation, selected correlations are compared with DNB data obtained in the B&W burnout loop and with published data. The comparison is facilitated by preparing histograms of the ratio of the experimentally determined DNB heat flux (ϕ_E) to the calculated value of the burnout heat flux (ϕ_C). A typical histogram is shown in Figure 3-18.

A histogram is obtained for each DNB correlation considered. The histograms indicate the ability of the correlations to describe the data. They indicate, qualitatively, the dispersion of the data about the mean value--the smaller the dispersion, the better the correlation. Since thermal and hydraulic data generally are well represented with a Gaussian (normal) distribution (Figure 3-18), mathematical parameters that quantitatively rate the correlation can be easily obtained for the histogram. These same mathematical parameters are the basis for the statistical burnout factor (B.F.).

In analyzing a reactor core, the statistical information required to describe the hot channel subfactors may be obtained from data on the as-built core, from data on similar cores that have been constructed, or from the specified tolerances for the proposed core. Regardless of the source of data, the subfactors can be shown graphically (Figures 3-19 and 3-20).

All the plots have the same characteristic shape whether they are for subfactors, hot channel factors, or burnout factor. The factor increases with either increasing population or confidence. The value used for the statistical hot channel and burnout factor is a function of the percentage of confidence desired in the result, and the portion of all possibilities desired, as well as the amount of data used in determining the statistical factor. A frequently used assumption in statistical analyses is that the data available represent an infinite sample of that data. The implications of this assumption should be noted. For instance, if limited data are available, such an assumption leads to a somewhat optimistic result. The assumption also implies that more information exists for a given sample than is indicated by the data; it implies 100 per cent confidence in the end result. The B&W calculational procedure does not make this assumption, but rather uses the specified sample size to yield a result that is much more meaningful and statistically rigorous. The influence of the amount of data for instance can be illustrated easily as follows: Consider the heat flux factor which has the form

$$F_{Q''} = 1 + K\sigma_{F_{Q''}}$$

where:

$F_{Q"}$ is the statistical hot channel factor for heat flux

K is a statistical multiplying factor

$\sigma_{F_{Q"}}$ is the standard deviation of the heat flux factor, including the effects of all the subfactors

If $\sigma_{F_{Q"}} = 0.05$ for 300 data points, then a K factor of 2.608 is required to protect 99 per cent of the population. The value of the hot channel factor then is

$$F_{Q"} = 1 + (2.608 \times 0.050) = 1.1304$$

and will provide 99 per cent confidence for the calculation. If, instead of using the 300 data points, it is assumed that the data represent an infinite sample, then the K factor for 99 per cent of the population is 2.326. The value of the hot channel factor in this case is

$$F_{Q"} = 1 + (2.326 \times 0.050) = 1.1163$$

which implies 100 per cent confidence in the calculation. The values of the K factor used above are taken from SCR-607.[20] The same basic techniques can be used to handle any situation involving variable confidence, population, and number of points.

Having established statistical hot channel factors and statistical DNB factors, we can proceed with the calculation in the classical manner. The statistical factors are used to determine the minimum fraction of rods protected, or that are in no jeopardy of experiencing a DNB at each nuclear power peaking factor. Since this fraction is known, the maximum fraction in jeopardy is also known. It should be recognized that every rod in the core has an associative DNB ratio that is substantially greater than 1.0, even at the design overpower, and that theoretically no rod can have a statistical population factor of 100 per cent, no matter how large its DNB ratio.

Since both the fraction of rods in jeopardy at any particular nuclear power peaking factor and the number of rods operating at that peaking factor are known, the total number of rods in jeopardy in the whole core can be obtained by simple summation. The calculation is made as a function of power, and the plot of rods in jeopardy versus reactor overpower is obtained (Figure 3-21). The summation of the fraction of rods in jeopardy at each peaking factor summed over all peaking factors can be made in a statistically rigorous manner only if the confidence for all populations is identical. If an infinite sample is not assumed, the confidence varies with population. To form this summation then, a conservative assumption is required. P&W's total core model assumes that the confidence for all rods is equal to that for the least-protected rod, i.e., the minimum possible confidence factor is associated with the entire calculation.

The result of the foregoing technique, based on the maximum design conditions (114 per cent power), is this statistical statement:

There is at least a 99 per cent confidence that at least 99.5 per cent of the rods in the core are in no jeopardy of experiencing a DNB, even with continuous operation at the design overpower.

The maximum design conditions are represented by these assumptions:

a. The maximum design values of $F_{\Delta h}$ (nuclear max/avg total fuel rod heat input) are obtained by increasing the maximum calculated value of $F_{\Delta h}$ by a factor of 1.033 to provide additional design margin.

b. The maximum value for F_z (nuclear max/avg axial fuel rod heat input) is determined for a transient condition following a power level change with partial insertion of a rod group for control.

c. Every coolant channel in the core is assumed to have less than the nominal flow area represented by engineering hot channel area factors, F_A, less than 1.0.

d. Every channel is assumed to receive the minimum flow associated with core flow maldistribution.

e. Every fuel rod in the core is assumed to have a heat input greater than the maximum calculated value. This value is represented by engineering hot channel heat input factors, F_Q and $F_{Q''}$, which are greater than 1.0.

f. Every channel and associated fuel rod has a heat transfer margin above the experimental best-fit limits reflected in DNB ratios greater than 1.0 at maximum overpower conditions.

The statistical core design technique may also be used in a similar manner to evaluate the entire core at the most probable mechanical and nuclear conditions to give an indication of the most probable degree of fuel element jeopardy. The result of the technique based on the most probable design conditions leads to a statistical statement which is a corollary to the maximum design statement:

There is at least a 99 per cent confidence that at least 99.9 per cent of the rods in the core are in no jeopardy of experiencing a DNB, even with continuous operation at the design overpower.

The most probable design conditions are assumed to be the same as the maximum design conditions with these exceptions:

a. Every coolant channel is assumed to have the nominal flow area ($F_A = 1.0$).

b. Every fuel rod is assumed to have (1) the maximum calculated value of heat input, and (2) F_Q and $F_{Q''}$ are assigned values of 1.0.

c. The flow in each coolant channel is based on core flow and power distributions.

d. Every fuel rod is assumed to have a nominal value for $F_{\Delta h}$ nuclear.

The full meaning of the maximum and most probable design statements requires additional comment. As to the 0.5 per cent or 0.1 per cent of the rods not included in the statements, statistically, it can be said that no more than 0.5 per cent or 0.1 per cent of the rods will be in jeopardy, and that in general the number in jeopardy will be fewer than 0.5 per cent or 0.1 per cent. The statements do not mean to specify a given number of DNB's, but only acknowledge the possibility that a given number could occur for the conditions assumed.

In summary, the calculational procedure outlined here represents a substantially improved design technique in two ways:

a. It reflects the performance and safety of the entire core in the resultant power rating by considering the effect of each rod on the power rating.

b. It provides information on the reliability of the calculation, and therefore the core, through the statistical statement.

3.2.3.2.3 Correlation of Heat Transfer Data

The BAW-168 report (Ref. 17) serves as a reference for the "best-fit" form of the design relationship used by B&W. This heat transfer correlation has been found to be the most satisfactory in the representation of both uniform and nonuniform heat flux test data. The BAW-168 correlation is used by comparing the integrated average heat flux along a fuel rod to a DNB heat flux limit predicted by the correlation. For uniform heat flux the integrated average heat flux is equal to the local heat flux. The comparison is carried out over the entire channel length. The point at which the ratio of the DNB heat flux to the integrated average heat flux is a minimum is selected as the DNB point, and that value of the ratio at that point is the DNB ratio (DNBR) for that channel.

This particular discussion deals with the comparison of DNB data to three particular correlations. The correlations selected were: The B&W correlation in the case of BAW-168,[17] a correlation with which the industry is familiar in the case of WAPD-188,[21] and a correlation recently proposed for use in the design of pressurized water reactors in the case of W-3.[22]

The data considered for the purpose of these comparisons were taken from the following sources:

a. WAPD-188 (Ref. 21).

b. AEEW-R213 (Ref. 23).

c. Columbia University Data (Ref. 24, 25, and 26).

168

d. Argonne National Laboratory Data, ANL (Ref. 27).

e. The Babcock & Wilcox Company Data, B&W (Ref. 28).

f. The Babcock & Wilcox Company Euratom Data (Ref. 29).

The comparison of data to the BAW-168 correlation is presented as histograms of the ratio of the experimental DNB heat flux (ϕ_E) to the calculated heat flux (ϕ_C). The data from each source were grouped by pressure and analyzed as a group; batches were then prepared including common pressure groups from all sources. Altogether there are 41 different data groups and batches considered. Histograms for only the BAW-168 correlation are presented to minimize the graphical material. The information required for the generation of histograms of the other two correlations was also prepared.

The comparison of the various correlations to each other is facilitated through the use of tabulations of pertinent statistical parameters. The standard deviation and mean value were obtained from the computed values of (ϕ_E/ϕ_C) for each group or batch. A comparison of standard deviations is somewhat indicative of the ability of the correlation to represent the data.

However, differences in mean values from group to group and correlation to correlation tend to complicate this type comparison. A relatively simple method may be used to compare the correlations for various data; this method uses the coefficient of variation (Ref. 30) which is the ratio of the standard deviation (σ) to the mean $\overline{X}$. The coefficient of variation may be thought of as the standard deviation given in per cent; it essentially normalizes the various standard deviations to a common mean value of 1.0.

Table 3-14 is a tabulation of the data source, heat flux type, and corresponding histogram numbers. The histograms are shown on Figures 3-22 through 3-37.

Table 3-14

Heat Transfer Test Data

Source	Heat Flux Type	Histogram Number	Figure Number
WAPD-188	Uniform	1-9	3-22 3-23 3-24
AEEW-R-213	Uniform	10-14	3-24 3-25 3-26
Columbia	Uniform	15-19	3-26 3-27 3-28
ANL	Uniform	20	3-28

Table 3-14 (Cont'd)

Source	Heat Flux Type	Histogram Number	Figure Number
B&W	Uniform	21	3-29
B&W-Euratom	Uniform	22-24	3-29 3-30
Combined Data (500-720 psia)	Uniform	25	3-30
Combined Data (1,000 psia)	Uniform	26	3-31
Combined Data (1,500 psia)	Uniform	27	3-32
Combined Data (2,000 psia)	Uniform	28	3-33
Combined Data (1,750-2,750 psia)	Uniform	29	3-34
B&W-Euratom Chopped Cosine	Nonuniform	30-32	3-35
B&W-Euratom and B&W Inlet Peak	Nonuniform	33-35	3-35 3-36
Euratom and B&W Outlet Peak	Nonuniform	36-38	3-36 3-37
Combined Nonuniform (1,000 psia)	Nonuniform	39	3-37
Combined Nonuniform (1,500 psia)	Nonuniform	40	3-37
Combined Nonuniform (2,000 psia)	Nonuniform	41	3-37

The histograms graphically demonstrate the distribution of (ϕ_E/ϕ_C) for each data group. The Gaussian type distribution of (ϕ_E/ϕ_C) about the mean for the group is apparent in the large data groups. Some data groups are too small to provide meaningful histograms, but they are presented in order to complete this survey.

The data were used as presented in the source for the calculation of (ϕ_E/ϕ_C); no points were discarded for any reason. A good correlation should be capable of representing DNB data for a full range of all pertinent parameters. The result of the comparison on this basis is demonstrated in Table 3-15. The data source, pressure, histogram figure number, heat flux type, and number of data points in the group are tabulated. For each of the three correlations the following data is indicated:

$\sigma/\overline{\chi}$ The coefficient of variation based on all available data in the group.

n_R The number of data points rejected using Chauvenet's criterion (Ref. 31). This criterion is statistical in nature and is applied to the

values of (ϕ_E/ϕ_C). Data points which fall outside certain limits with respect to the main body of data are rejected.

$(\sigma/\bar{\chi})'$ The coefficient of variation based on the original data sample less those points rejected by Chauvenet's criterion, i.e., based on $n-n_R$ values of (ϕ_E/ϕ_C).

It is unfortunate that Chauvenet's criterion must be applied to the values of (ϕ_E/ϕ_C) rather than to the original data, since application to (ϕ_E/ϕ_C) leads to the rejection of points for either of two reasons:

a. Bad data points.

b. Inability of the correlation to represent a particular data point.

It is not desirable to reject points for the second reason, and yet one might expect to encounter some bad data. The logical choice then is to present data both ways, i.e., with and without Chauvenet's criterion applied. Of the 41 groups and batches analyzed the following is observed from Table 3-15:

Correlation	Groups and Batches of Data With Smallest $\sigma/\bar{\chi}$ Without Chauvenet's Criterion	Groups and Batches of Data With Smallest $\sigma/\bar{\chi}$ With Chauvenet's Criterion
BAW-168	38	36
WAPD-188	2	3
W-3	1	2

Chauvenet's criterion rejected the following numbers of points for each correlation:

	Uniform	Nonuniform	Total
BAW-168 (Groups Only)	32	1	33
BAW-168 (Batches Only)	39	0	39
WAPD-188 (Groups Only)	34	2	36
WAPD-188 (Batches Only)	33	0	33
W-3 (Groups Only)	59	12	71
W-3 (Batches Only)	50	9	59

Several notable peculiarities exist in the tabulation of Table 3-15. The Columbia data 500 psia group contained only five data points of which four were rejected by Chauvenet's criterion leaving one point. A standard deviation cannot be computed for one point; therefore all three values of $(\sigma/\bar{\chi})'$ are shown as not available (N.A.). Neither the BAW-168 nor the WAPD-188 predicted any negative DNB heat fluxe ; the W-3 predicted 93 negative values for uniform data. The fact that only , were rejected for this correlation indicates that the remaining 34 unifor points which were negative (93-59 = 34) were close enough to the body of the data to be considered statistically significant. Table 3-15 may be consolidated somewhat as below by tabulating the

number of groups and batches of data having coefficients of variation within a specified interval for each correlation.

$(\sigma/\overline{\chi})$ Interval	BAW-168	BAW-168'[a]	WAPD-188	WAPD-188'[a]	W-3	W-3'[a]
Negative	0	0	0	0	2	0
0-0.1	6	8	0	0	0	1
0.1-0.2	24	24	13	13	1	5
0.2-0.3	8	8	7	8	3	1
0.3-0.4	1	0	3	4	1	2
0.4-0.5	1	0	5	7	5	6
0.5-0.6	0	0	6	5	3	4
0.6-0.7	0	0	3	2	1	1
0.7-0.8	0	0	2	1	7	8
0.8-0.9	1	0	0	0	1	5
0.9-1.0	0	0	0	0	1	0
Greater than 1.0	0	0	2	0	16	7
Total	41	40	41	40	41	40

[a]Chauvenet's criterion applied.

As is seen from the above tabulation the column for BAW-168 with Chauvenet's criterion applied indicates a grouping of 0.1 to 0.2, and a maximum value of 0.28780 is noted from Table 3-15. For WAPD-188 the spread is greater with a maximum value of 0.74018. For W-3 the spread is still greater, and a maximum value of 1.7483 is noted. The negative values of DNB heat flux predicted by the W-3 correlation are in part responsible for the large spread in $(\sigma/\overline{\chi})$.

The ability of the BAW-168 correlation to fit both uniform and nonuniform heat flux data over a wide range of pertinent variables leads us to believe that it is the best DNB correlation available.

Table 3-15

Comparison of Heat Transfer Test Data

Source	Pressure	Histogram No.	Heat Flux Type	Number of Data Points	BAW-168			WAPD-188			W-3		
					$\sigma/\bar{X}$	n_R	$(\sigma/\bar{X})'$	$\sigma/\bar{X}$	n_R	$(\sigma/\bar{X})'$	$\sigma/\bar{X}$	n_R	$(\sigma/\bar{X})'$
WAPD-188	500	1	Uniform	57	0.22792	0	- -----	0.74018	0	-------	1.6785	2	1.7483
WAPD-188	600	2	Uniform	146	0.24525	1	0.23373	0.60506	5	0.54011	0.89407	3	0.81663
WAPD-188	1000	3	Uniform	164	0.27351	1	0.26755	0.53793	4	0.50000	0.75947	0	-------
WAPD-188	1500	4	Uniform	46	0.13390	3	0.10537	0.30489	0	-------	0.44994	0	-------
WAPD-188	1750	5	Uniform	30	0.076698	0	-------	0.18176	0	-------	0.34816	0	-------
WAPD-188	2000	6	Uniform	371	0.13529	4	0.12480	0.23113	6	0.20482	5.1193	7	0.79051
WAPD-188	2250	7	Uniform	9	0.081572	0	-------	0.15613	0	-------	0.17494	0	-------
WAPD-188	2500	8	Uniform	9	0.081763	0	-------	0.16477	0	-------	0.23851	1	0.19424
WAPD-188	2750	9	Uniform	9	0.057343	0	-------	0.11820	0	-------	0.24127	0	-------
AEEW-R213	560	10	Uniform	148	0.26674	3	0.23709	0.61784	0	-------	2.9296	1	1.4097
AEEW-R213	720	11	Uniform	33	0.18958	0	-------	0.50684	2	0.43312	2.3964	3	1.3510
AEEW-R213	1000	12	Uniform	322	0.20439	3	0.19366	0.50541	0	-------	6.3726	3	1.4589
AEEW-R213	1200	13	Uniform	18	0.15915	0	-------	0.42712	0	-------	0.58600	0	-------
AEEW-R213	1500	14	Uniform	104	0.12956	2	0.079859	0.28924	1	0.27054	0.28314	15	0.090829
Columbia	500	15	Uniform	5	0.13704	4	N.A.	0.12752	4	N.A.	0.91541	4	N.A.
Columbia	720	16	Uniform	29	0.16308	0	-------	0.51437	0	-------	0.58437	0	-------
Columbia	1000	17	Uniform	281	0.80468	6	0.18678	12.009	6	0.43991	0.45519	0	-------
Columbia	1200	18	Uniform	15	0.12211	0	-------	0.29242	0	-------	0.46815	0	-------
Columbia	1500	19	Uniform	80	0.21043	3	0.12241	0.69765	3	0.24029	1.5097	3	0.11183
AEL	2000	20	Uniform	232	0.10271	2	0.092803	0.19348	2	0.17973	3.6745	14	0.52340
B&W	2000	21	Uniform	21	0.058701	0	-------	0.13647	1	0.11792	-24.400	3	1.1838
Euratom	1000	22	Uniform	18	0.13104	0	-------	0.47621	0	-------	0.77404	0	-------
Euratom	1500	23	Uniform	18	0.094606	0	-------	0.30104	0	-------	0.47690	0	-------
Euratom	2000	24	Uniform	14	0.12106	0	-------	0.19650	0	-------	1.6369	0	-------
Combined	500-720	25	Uniform	418	0.31215	5	0.28780	0.72108	10	0.65124	2.7046	2	1.4052
Combined	1000	26	Uniform	785	0.47694	9	0.24909	17.834	8	0.56791	4.1325	3	0.88632
Combined	1500	27	Uniform	144	0.19631	4	0.14211	0.57512	3	0.31718	1.2237	3	0.31754
Combined	2000	28	Uniform	638	0.14976	4	0.14251	0.24186	8	0.21986	5.2840	21	0.81792
Combined	1750-2750	29	Uniform	695	0.18236	17	0.14913	0.24463	4	0.23227	5.1401	21	0.81288
Euratom	1000	30	Chopped Cosine	14	0.17017	0	-------	0.48187	0	-------	0.72772	0	-------
Euratom	1500	31	Chopped Cosine	13	0.2122	0	-------	0.24251	0	-------	0.66671	0	-------
Euratom	2000	32	Chopped Cosine	13	0.13652	0	-------	0.19268	0	-------	-5.7922	3	0.16023
B&W & Euratom	1000	33	Inlet Peak	16	0.19273	0	-------	0.42785	0	-------	0.70580	0	-------
B&W & Euratom	1500	34	Inlet Peak	12	0.13127	1	0.10703	0.18121	0	-------	0.72369	0	-------
B&W & Euratom	2000	35	Inlet Peak	32	0.13755	0	-------	0.17637	0	-------	4.4474	5	0.81144
B&W & Euratom	1000	36	Outlet Peak	12	0.23023	0	-------	0.55501	2	0.14656	0.74323	0	-------
B&W & Euratom	1500	37	Outlet Peak	16	0.16799	0	-------	0.30113	0	-------	0.45609	0	-------
B&W & Euratom	2000	38	Outlet Peak	36	0.13481	0	-------	0.16799	0	-------	1.0478	4	0.10233
Combined	1000	39	Non-Uniform	42	0.20445	0	-------	0.49656	0	-------	0.71082	0	-------
Combined	1500	40	Non-Uniform	31	0.17435	0	-------	0.25368	0	-------	0.58846	0	-------
Combined	2000	41	Non-Uniform	81	0.17846	0	-------	0.17621	0	-------	9.6963	9	0.46885

3.2.3.2.4 Evaluation of the Thermal and Hydraulic Design

a. Hot Channel Coolant Quality and Void Fraction

An evaluation of the hot channel coolant conditions provides additional confidence in the thermal design. Sufficient coolant flow has been provided to insure low quality and void fractions. The quality in the hot channel versus reactor power is shown in Figure 3-38. The sensitivity of channel outlet quality with pressure and power level is shown by the 2,185 and 2,120 psig system pressure conditions examined. These calculations were made for an $F\Delta h$ of 1.85. Additional calculations for a 10 per cent increase in $F\Delta h$ to 2.035 were made at 114 per cent power. The significant results of both calculations are summmarized in Table 3-16. The effects of using an $F\Delta h$ of 1.79 are shown in Figure 3-38.

Table 3-16

Hot Channel Coolant Conditions

Power, %	$F\Delta h$	Exit Quality, %	Exit Void Fraction, %	Operating Pressure, psig
100	1.85	(-)2.4(b)	0.5(a)	2,185
114	1.85	2.8	13.5	2,185
130	1.85	9.4	36.9	2,185
114	2.035	8.7	35.0	2,185
100	1.85	0	3.8(a)	2,120
114	1.85	5.4	25.2	2,120
130	1.85	12.1	45.2	2,120
114	2.035	11.3	43.4	2,120

(a) Subcooled voids.

(b) Negative indication of quality denotes subcooling of 10.2 Btu/lb.

The conditions of Table 3-16 were determined with all of the hot channel factors applied. Additional calculations were made for unit cell channels without engineering hot channel factors to show the coolant conditions more likely to occur in the reactor core. Values for $F\Delta h$ of 1.79 and 1.85 were examined with and without fuel assembly flow distribution hot channel factors at 2,185 psig as shown on Figure 3-39. These results show that the exit qualities from the hottest

00 001194

cells should in general be considerably lower than the maximum design conditions.

b. Core Void Fraction

The core void fractions were calculated at 100 per cent power for the normal operating pressure of 2,185 psig and for the minimum operating pressure of 2,120 psig. The influence of core fuel assembly flow distribution was checked by determining the total voids for both 100 and 95 per cent total core flow for the two pressure conditions.

The results are as follows:

Flow, %	Pressure, psig	Core Void Fraction, %
100	2,185	0.007
100	2,120	0.033
95	2,185	0.041
95	2,120	0.127

The most conservative condition of 95 per cent flow at 2,120 psig results in no more than 0.13 per cent void volume in the core. Conservative maximum design values for $F\Delta h$ nuclear described by Line A of Figure 3-10 were used to make the calculation.

c. Coolant Channel Hydraulic Stability

A flow regime map was constructed to evaluate channel hydraulic stability. The transition from bubbly to annular flow at high mass velocities was determined using Baker's[32] correlation, and the transition from bubbly to slug flow which occurs at low mass velocities was determined with Rose's[33] correlation. The transition from slug flow to annular flow was determined by Haberstroh's[34] correlation. Bergles[35] found that these correlations, which were developed from adiabatic data, are adequate for locating flow regime transitions with heat addition, and that they adequately predict the effects of pressure. Figure 3-40 shows the flow regime map on which have been plotted points representing operating conditions in the hot channel at 114 per cent overpower. To aid in assessing the conservatism of the design, an additional point is plotted at 130 per cent overpower. Inspection shows that both points lie well within the bubbly flow regime. Since the bubbly flow regime is hydraulically stable, no flow instabilities should occur.

d. Hot Channel DNB Comparisons

DNB ratios for the hottest channel have been determined for the BAW-168 and W-3 correlations. The results are shown in Figure 3-41. DNB ratios for both correlations are shown for the 1.50 axial max/avg symmetrical cosine flux shape from 100 to 150 per cent power. The BAW-168 DNB ratio at the maximum design power of 114 per cent is 1.38; the corresponding W-3 value is 1.72. This compares with the suggested

W-3 design value of 1.3. It is interesting to note that the calculated DNB ratio reaches a value of 1.0 at about 150 per cent power with the BAW-168 equation which adequately describes DNB at the high quality condition of 20 per cent. The W-3 calculation is accurate to about 130 per cent power, but because of quality limitations it cannot be used to examine the channel at the 150 per cent power condition.

The sensitivity of DNB ratio with $F\Delta h$ and Fz nuclear was examined from 100 to 114 per cent power. The detailed results are labeled in Figure 3-41. A cosine flux shape with an Fz of 1.80 and an $F\Delta h$ of 1.85 results in a W-3 DNB ratio of 1.45 and a BAW-168 ratio of 1.33. The W-3 value is well above suggested design values, and the BAW-168 value of 1.33 corresponds to a hot channel confidence of 99 per cent that about 93 per cent of the population is in no jeopardy as shown in the Population-DNB ratio plot in 3.2.3.2.2, Statistical Core Design Technique.

The influence of a change in $F\Delta h$ was determined by analyzing the hot channel for an $F\Delta h$ of 2.035. This value is 14 per cent above the maximum calculated value of 1.79 and 10 per cent above the maximum design value of 1.85. The resulting BAW-168 DNB ratio is 1.22 and the W-3 value is 1.26. Both of these values are well above the correlation best-fit values of 1.0 for the severe conditions assumed.

e. Reactor Flow Effects

Another significant variable to be considered in the evaluation of the design is the total system flow. Conservative values for system and reactor pressure drop have been determined to insure that the required system flow is obtained in the as-built plant. The experimental programs previously outlined in Section 1 will confirm the pressure drop and related pump head requirements. It is anticipated that the as-built reactor flow will exceed the design value and will lead to increased power capability.

An evaluation of reactor core flow and power capability was made by determining the maximum steady state power rating versus flow. The analysis was made by evaluating the hot channel at the overpower conditions while maintaining (1) a DNB ratio of 1.38 (BAW-168), and (2) the statistical core design criteria. The results of the analysis are shown in Figure 3-42. The power shown is the 100 per cent rating, and the limiting condition is 114 per cent of the rated power. An examination of the slope of the curve indicates stable characteristics, and a 1 per cent change in flow changes the power capability by only about 1/2 per cent.

f. Reactor Inlet Temperature Effects

The influence of reactor inlet temperature on power capability at a given flow was evaluated in a similar manner. A variation of 1 F in reactor inlet temperature will result in a power capability change of slightly less than $\frac{1}{2}$ percent.

00 00196

g. Fuel Temperature and Fission Gas Release Evaluation

Temperature Determination

A fuel temperature and gas pressure computer code was developed to calculate fuel temperatures, expansion, densification, equiaxed and columnar grain growth, center piping of fuel pellets, fission gas release, and fission gas pressure. Program and data comparisons were made on the basis of the fraction of the fuel diameter within these structural regions:

(1) Outer limit of equiaxed grain growth - 2,700 F
(2) Outer limit of columnar grain growth - 3,200 F
(3) Outer limit of molten fuel (UO_2) - 5,000 F

Data from References 36 through 39 were used to compare calculated and experimental fractions of the rod in grain growth and central melting.

The radial expansion of the fuel pellet is computed from the mean fuel temperature and the average coefficient of linear expansion for the fuel over the temperature range considered. This model combined with the model for calculating the heat transfer coefficient was compared with the model developed by Notley et al (Ref. 40) of AECL. The difference in fuel growth for the two calculation models was less than the experimental scatter of data.

The program uses a polynomial fit relationship for fuel thermal conductivity. Three relationships were used to evaluate the effects of conductivity. A comparison of these conductivity relationships with the reference design CVNA-142(41) is shown in Figure 3-43. The values suggested in GEAP-4624(42) and CVNA-246(43) are very similar up to 3,000 F, and the former values are more conservative above 3,000 F. McGrath(43) concludes that the CVNA-246 values are lower limits for the high temperature conditions. Fuel center temperatures for all three of the conductivity relationships at the peaking factors given in 3.2.3.1.2 have been calculated to evaluate the margin to central melting at the maximum overpower, and to show the sensitivity of the calculation with respect to thermal conductivity. Since the power peaks will be burned off with irradiation, the peaking factors used are conservative at end-of-life.

The temperature drop from the fuel to clad is calculated with a simple gas gap conduction model until thermal expansion of the fuel introduces a contact effect. A contact coefficient is calculated considering contact under pressure and gas gap conduction as suggested by Ross and Stoute.(44)

The results of the analysis with the methods described above are shown in Figures 3-44 and 3-45 for beginning and end-of-life conditions. The beginning and end-of-life gas conductivity values are 0.1 and 0.01 Btu/hr-ft^2-F respectively. The calculated end-of-life center fuel temperatures are higher than the beginning-of-life values because of the reduction in the conductivity of the gas in the gap. The effect is apparent even though a contact condition prevails. The

model does not include the effects of fuel swelling due to irradiation; consequently the ca ·ulated contact pressures are conservatively lower than those expected at end-of-life conditions in the hottest fuel rods.

The B&W model gives very good results when compared to the results of others in the field as is shown in Figure 3-45. In the linear heat range of most interest, i.e., approximately 20 kw/ft, there is only about 300 F difference between the maximum and minimum values calculated. Also the small difference between the B&W curve and the other curves indicates the relative insensitivity of the results to the shape of the conductivity at the elevated temperatures.

The most conservative assumptions, using GEAP-4624 data with relatively little increase in thermal conductivity above 3,000 F, result in central fuel melting at about 22 kw/ft, which is 2 kw/ft higher than the maximum design value of 19.9 kw/ft at 114 per cent power. Further evaluation of the two figures shows that central fuel melting is predicted to occur between 22 and 26 kw/ft depending on the time-in-life and conductivity assumptions.

h. Fission Gas Release

The fission gas release is based on results reported in GEAP-4596,[45] Additional data from GEAP-4314,[46] AECL-603,[47] and CF-60-12-14[48] have been compared with the suggested release rate curve. The release rate curve[45] is representative of the upper limit of release data in the temperature region of most importance. A release rate of 51 per cent is assumed above 3,500 F.

The fission gas release rates may be summarized as follows for end-of-life conditions with maximum burnup.

Conductivity Model	Release Rate, %
CVNA-142	43
CVNA-246	42
GEAP-4624	40

A release rate of 43 per cent is used to determine the fuel clad internal design conditions reported in 3.2.4.2, Fuel Assemblies.

3.2.4 MECHANICAL DESIGN LAYOUT

3.2.4.1 Internal Layout

Reactor internal components include the upper plenum assembly, the core support assembly (consisting of the core support shield, core barrel, lower grid and flow baffle, thermal shield, and surveillance specimen holder tubes), and the incore instrument guide extensions. Figure 3-46 shows the reactor vessel, reactor vessel internals arrangement, and the reactor coolant flow path. Figure 3-47 shows a cross section through the reactor vessel, and Figure 3-48 shows the core flooding arrangement.

Reactor internal components do not include fuel assemblies, control cluster assemblies (CCA's), surveillance specimen assemblies, or incore instrumentation. Fuel assemblies are described in 3.2.4.2, control cluster and drive assemblies in 3.2.4.3, surveillance specimen assemblies in 4.4.3, and incore instrumentation in 7.3.3.

The reactor internals are designed to support the core, maintain fuel alignment, limit fuel assembly movement, and maintain CCA guide tube alignment between fuel assemblies and control rod drive assemblies. They also direct the flow of reactor coolant, provide gamma and neutron shielding, provide guides for incore instrumentation between the reactor vessel lower head and the fuel assemblies, and support the surveillance specimen assemblies in the annulus between the thermal shield and the reactor vessel wall.

All reactor internal components can be removed from the reactor vessel to allow inspection of the reactor internals and the reactor vessel internal surface.

A shop fitup and checkout of all internal components in an as-built reactor vessel mockup will insure proper alignment of mating parts prior to shipment. Dummy fuel assemblies and control cluster assemblies will be used to check fuel assembly clearances and CCA free movement.

In anticipation of lateral deflection of the lower end of the core support assembly as a result of horizontal seismic loadings, integral weld-attached, deflection-limiting spacer blocks have been placed on the reactor vessel inside wall. In addition, these blocks limit the rotation of the lower end of the core support assembly which could conceivably result from flow-induced torsional loadings. The blocks allow free vertical movement of the lower end of the internals for thermal expansion throughout all ranges of reactor operating conditions, but in the unlikely event of a flange, circumferential weld, or bolted joint failure, the blocks will limit the possible core drop to 1/2 in. or less. The final elevation plane of these blocks will be established on the same elevation as the vessel support skirt attachment to minimize dynamic loading effects on the vessel shell or bottom head. Preliminary calculations indicate the impact loading on the stop blocks for a 1/4 in. core drop would be approximately 5 g's total. Block location and geometry will be evaluated and determined to transfer this loading through the vessel support skirt to the reactor building concrete. A significant reduction of the above impact loading can be achieved through proper stop block design and detailed analysis.

A 1/2 in. core drop will not allow the lower end of the CCA poison pins to disengage from their respective fuel assembly guide tubes if the CCA's are in the full-out position, as approximately 6-1/2 in. of pin length would remain in the fuel assembly guide tubes. A core drop of 1/2 in. will not result in a significant reactivity change. The core cannot rotate and bind the drive lines because rotation of the core support assembly is prevented by the stop blocks.

The failure of the core support shield and core barrel upper flanges, or related flanges and other circumferential joints, is not considered credible on the basis of the conservative design criteria and large safety factors employed in the internals design. The final internals design will be capable of withstanding various combinations of forces and loadings resulting from the static weight of internals (179,000 lb total), core with control rod drive line (303,000 lb total), dynamic load from trip (10 g's gives 207,000 lb), seismic (0.05 g vertical gives 24,000 lb), coolant flow hydraulic loading (230,000 lb), and other related loadings. The algebraic sum of this simplified loading case is 483,000 lb. This results in a tensile stress of about 700 psi in the core support shell, which is approximately 4 per cent of the material yield strength. Final internals component weights, seismic analysis, dynamic loadings from flow-induced vibration, detailed stress analysis with consideration for thermal stress during all transients, and resolution of fabrication details such as shell rolling tolerances and weld joint preparation details will increase the stress levels listed above. As a final design criterion, the core support components will meet the stress requirements of the ASME Code, Section III. The structural integrity of all core support weld joints in the internals shells will be insured by compliance with the radiographic inspection requirements in the above code. The seismic analysis will include detailed calculations to determine the maximum structural response of the reactor vessel and internals. This analysis will be performed as described in 3.1.2.4.1.

In the event of a major loss-of-coolant accident, such as a 36 in. diameter coolant pipe break near the reactor vessel outlet, the fuel assembly and vessel internals would be subjected to dynamic loadings resulting from an oscillating (approximately sinusoidal) differential pressure across the core. A preliminary analysis of this postulated accident indicates that the fuel assemblies would move upward less than 3/8 in. Some deflection of the internals structures would occur, but internals component failure will not occur. The occurrence of a loss-of-coolant accident and resulting loadings will be evaluated during the detailed design period for the fuel assemblies and related internals structural components.

The deflections and movements described above would not prevent CCA insertion because the control poison pins are guided by split tubes throughout their travel, and the guide tube to fuel assembly alignment cannot change regardless of related component deflections. CCA trip could conceivably be delayed momentarily as a result of the oscillating pressure differential. However, the CCA travel time to full insertion would remain relatively unaffected as transient pressure oscillations are dampened out in approximately 0.5 sec. On this basis, the CCA trip time to 2/3 insertion will be approximately 1.55 sec instead of the specified 1.40 sec. Also, this possible initial minor delay in trip initiation would not contribute to the severity of the loss-of-coolant accident because at the initiation of CCA trip, the core would be subcritical from voids.

Material for the reactor internals bolting will be subjected to rigid quality control requirements to insure structural integrity. The bolts will be dye penetrant-inspected for surface flaw indications after all fabrication operations have been completed. Torque values will be specified for the final assembly to develop full-bolting capability. All fasteners will be lock-welded to insure assembly integrity.

3.2.4.1.1 Upper Plenum Assembly

The upper plenum assembly is located directly above the reactor core and is removed as a single component prior to refueling. It consists of upper and center grid assemblies, CCA guide tubes, a flanged plenum cylinder, ~~openings for passage of water for core flooding,~~ and openings for reactor coolant outlet flow. The upper grid is a series of parallel flat bars intersecting to form square lattices and is welded to the plenum cylinder top flange. Rectangular flanges on the CCA guide tubes are bolted and lock-welded to the upper grid bars. CCA guide tubes provide CCA guidance and protect the CCA from the effects of coolant cross-flow.

Each CCA guide tube consists of an outer tube housing and sixteen slotted tubes which are properly oriented and brazed to a series of castings. As the tubes are slotted for their full length, the brazement provides continuous guidance for the CCA full stroke travel. Design clearances in the guide tube will accommodate some degree of misalignment between the CCA guide tubes and the fuel assemblies. Final design clearances will be established by tolerance studies and the results of control rod drive assembly prototype tests.

The center grid assembly consists of parallel flat bars intersecting to form square lattices at the top and bottom of the center grid assembly. The bars are attached to a flange which is bolted to the plenum cylinder lower flange. The center grid assembly locates the lower end of the individual CCA guide tube relative to the upper end of the corresponding fuel assembly.

Locating slots in the upper plenum assembly top flange engage the reactor vessel top flange locating devices to align the upper plenum assembly with the reactor vessel, reactor vessel top head control drive penetrations, and the core support shield. The bottom of the upper plenum assembly is guided and aligned by locating blocks attached to the inside of the core support shield.

3.2.4.1.2 Core Support Assembly

The core support assembly consists of the core support shield, core barrel, lower grid and flow baffle, thermal shield, and surveillance specimen holder tubes.

Static loads from the assembled components and fuel assemblies, and dynamic loads from CCA trip, hydraulic flow, thermal expansion, seismic disturbances, and loss-of-coolant accident considerations, are all carried by the core support assembly.

Each of the core support assembly components is described as follows:

201

a. Core Support Shield

The core support shield is a large flanged cylinder which mates with the reactor vessel opening. The top flange rests on a circumferential ledge in the reactor vessel top closure flange. The core support shield lower flange is bolted to the core barrel. The cylinder wall has two nozzle openings for reactor coolant outlet flow. ~~Two core flooding chambers, each containing a nozzle opening, are welded to the cylinder wall of the core support shield.~~ Locating blocks on the inside of the cylinder wall near the bottom guide and align the upper plenum chamber relative to the core support shield.

The reactor vessel outlet nozzles ~~and the core flooding nozzles~~ are sealed to the mating components of the core support shield by the differential thermal expansion between the carbon steel reactor vessel and the stainless steel core support shield. The nozzle seal surfaces are finished and fitted to a predetermined cold gap providing clearance during core support assembly installation and removal. At reactor operating temperature the mating metal surfaces are in contact to make a seal without exceeding allowable stresses in either the reactor vessel or internals.

b. Core Barrel

The core barrel supports the fuel assemblies and lower grid and flow baffle, and directs the reactor coolant flow through the vessel.

The core barrel consists of a flanged cylinder, a series of internal horizontal spacers bolted to the cylinder, and a series of vertical plates bolted to the inner surfaces of the horizontal spacers to form an inner wall enclosing the fuel assemblies. The core barrel construction will be similar to the reactor internals component developed by B&W for the Indian Point Station Unit No. 1.

Coolant flow is downward along the outside of the core barrel cylinder, and upward through the fuel assemblies contained in the core barrel. A small portion of the coolant flows upward through the space between the core barrel outer cylinder and the inner plate wall.

Coolant pressure in this space is maintained slightly lower than the core coolant pressure, thus avoiding tension loads on the bolts which attach the plates to the horizontal spacers. The vertical plate inner wall will be carefully fitted together to reduce reactor coolant leakage to an acceptable rate.

The upper flange of the core barrel outer cylinder is bolted to the mating lower flange of the core support shield, and the lower flange is bolted to the mating flange of the lower grid and flow baffle.

All bolts will be inspected and installed as described in 3.2.4.1, and will be lock-welded after final assembly.

Spacer bars and support lugs are welded to the core barrel outer cylinder to position and support the thermal shield.

00 ~~00133~~ 202

c. Lower Grid and Flow Baffle

The lower grid provides alignment and support for the fuel assemblies and aligns the incore instrument guide extensions with the fuel assembly incore instrument tubes. The lower grid consists of two flat plate and bar lattice structures separated by short tubular columns surrounded by a flanged cylinder. The top flange is bolted to the lower flange of the core barrel.

The flow baffle is a dished plate with an external flange which is bolted to the bottom flange of the lower grid. The flow baffle is perforated to distribute the reactor coolant entering the bottom of the core.

d. Thermal Shield

A cylindrical stainless steel thermal shield is installed in the annulus between the core barrel outer cylinder and the reactor vessel inner wall. The thermal shield reduces the neutron and gamma internal heat generation in the reactor vessel wall, thereby reducing the resulting thermal stresses.

The thermal shield is supported on, and bolted to, lugs welded to the core barrel outer cylinder to minimize the possibility of thermal shield vibration. The support lugs are designed to prevent the bolts being loaded in shear. Bolts are lock-welded after final assembly.

e. Surveillance Specimen Holder Tubes

Surveillance specimen holder tubes are installed on the core support assembly outer wall to contain the surveillance specimen assemblies. The tubes extend from the top flange of the core support shield to the lower end of the thermal shield. The tubes will be rigidly attached to prevent flow-induced vibration. Slip joints at the lower end of the core support shield will allow the core support shield to be removed from the core support assembly without destructively removing the surveillance specimen holder tubes.

3.2.4.1.3 Incore Instrument Guide Extensions

The incore instrument guide extensions guide the incore instrument assemblies between the instrument penetrations in the reactor vessel bottom head and the instrument tubes in the fuel assemblies.

A spring-loaded ball joint at the lower end of the instrument guide extensions provides for minor misalignment between the reactor vessel instrument penetrations and the fuel assembly instrument tubes. A perforated shroud tube concentric with the instrument guide tube adds rigidity to the assembly and reduces the effect of coolant flow forces. Fifty-one incore instrument guide extensions are provided. The incore instrument guide extensions are designed with a slip joint so they will not be affected by the core drop described in 3.2.4.1.

3.2.4.2 Fuel Assemblies

3.2.4.2.1 Description

a. General Description

The fuel for the reactor is sintered pellets of low enrichment uranium dioxide clad in Zircaloy-4 tubing. The clad, fuel pellets, end supports, holddown spring, and end caps form a "Fuel Rod Assembly". Two hundred and eight fuel rod assemblies are mechanically joined in a 15 x 15 array to form a "Fuel Assembly". The fuel assembly is shown in Figure 3-49. The center position in the assembly is reserved for instrumentation. The remaining 16 positions in the array are provided with "Guide Tubes" for use as control pin locations. The complete core consists of 177 fuel assemblies. All assemblies are identical in mechanical construction, i.e., all are designed to accept the control cluster assemblies (CCA). However, only 69 are provided with CCA's to control the reactivity of the core under operating conditions. In those 108 fuel assemblies which do not contain a CCA during a given core cycle, the guide tubes are partially filled at the top by an "Orifice Cluster Assembly" (Figure 3-50) in order to minimize bypass coolant flow. These orifice cluster assemblies also tend to equalize coolant flow between fuel assemblies with CCA's and those with orifice clusters.

Fuel assembly components, materials, and dimensions are listed below:

Item	Material	Dimensions, in.
Fuel	UO_2 Sintered Pellets	0.362 diam.
Fuel Clad	Zircaloy-4	0.420 OD x 0.368 ID x 152-7/8 long
Fuel Rod Pitch		0.558
Fuel Assembly Pitch		8.587
Active Fuel Length		144
Overall Length		165
Control Pin Guide Tube	Zircaloy-4	0.530 OD x 0.015 wall
Incore Instrument Tubes	Zircaloy-4	0.530 OD x 0.075 wall
Spacer Grid Assemblies	Stainless Steel, Tp-304	Spaced at 21 in.
Structural Can Panel	Stainless Steel, Tp-304	0.031 thick
End Fitting	Stainless Steel, Tp-304	

b. Fuel

The fuel is in the form of sintered and ground pellets of uranium dioxide. The pellets are dished on each end face to minimize the difference in axial thermal expansion between the fuel and cladding. The density of the fuel is 95 per cent of theoretical.

Average design burnup of the fuel is 28,200 MWD/MTU. Peak burnup is 55,000 MWD/MTU. At the peak burnup, the fuel growth is calculated to be 9-1/2 volume per cent by the method given in Reference 49. This growth is accommodated by pellet porosity, by the radial clearance provided between the pellets and the cladding, and by a small amount of plastic strain in the cladding.

Each fuel column is located, at the bottom, by a thin-wall stainless steel pedestal and is held in place during handling by a spring at the top. The spring allows axial differential thermal expansion between fuel and cladding, and axial fuel growth. The bottom pedestal is also collapsible, thus providing a secondary buffer to prevent excess cladding axial strain.

Fission gas release from the fuel is accommodated by voids within the fuel, by the radial gap between the pellets and cladding, and by void space at the top and bottom ends of the fuel rod.

c. Fuel Assembly Structure

(1) General

The fuel assembly, shown in Figure 3-49, is of the canned type. Eight spacer grid assemblies and four perforated panels form the basic structure. The panels are welded together at the corners for the entire length. The spacer grid assemblies are welded to the panels, and the lower and upper end fitting assemblies are welded to the panels to complete the structure. The upper end fitting assembly is not attached until the fuel rods, guide tubes, and instrument tube have been installed. At each spacer grid assembly each fuel rod is supported on four sides by integral leaf-type springs. These springs are designed to provide a radial load on the fuel rod sufficient to restrain it so that flow-induced vibrational amplitudes are minimal. However, to avoid undesirable bowing of the fuel rods, the spring loads are designed small enough to permit the relative axial motion required to accommodate the differential thermal expansion between the Zircaloy fuel rod and the stainless steel structure.

(2) Spacer Grid Assembly

These assemblies are comprised of ferrules made of square tubing. The ferrule has a portion of each side formed into spring sections which have hydrodynamically shaped "dimples" that contact the fuel rods. The ferrules are joined together by brazing to form the spacer grid assemblies. The grid assemblies, which

provide the desired pitch spacing between fuel rods, are spot-welded at intervals to the perforated stainless steel can panels.

(3) Lower End Fitting Assembly

The lower end fitting assembly is constructed from Type 304 stainless steel members which when joined together form a box structure. Four deep cross members serve as the positioning surfaces for the fuel assembly when it is inserted into the lower core support structure. The assembly includes a grid structure which provides a support base for fuel rods, while maintaining a maximum inlet flow area for the coolant.

(4) Upper End Fitting Assembly

The upper end fitting assembly is similar to the lower end fitting assembly. It positions the upper end of the fuel assembly and provides coupling between the fuel assembly and the handling equipment. A hollow post, welded in the center of the assembly, is designed to provide an uncoupling means for the CCA-to-drive connection, and to retain the orifice cluster assembly. In order to identify a fuel assembly under water, a serial number is milled into a flat, chrome-plated surface which is welded to the box frame.

(5) Guide Tubes

The guide tubes are Zircaloy tubes which serve to guide the control pins within the fuel assembly during operation. The tubes are restrained axially by the upper and lower end fitting assemblies in the fuel assembly, and are restrained radially by the spacer grids in the same manner as the fuel rods.

3.2.4.2.2 Evaluation

a. Fuel Rod Assembly

(1) General

The basis for the design of the fuel rod assembly is discussed in 3.1.2.4. Materials testing and actual operation in reactor service with Zircaloy cladding has demonstrated that Zircaloy-4 material has ample corrosion resistance and sufficient mechanical properties to maintain the integrity and serviceability required for design burnup.

(2) Clad Stress

Stress analysis for cladding is based on several conservative assumptions that make the actual margins of safety greater than calculated. For example, it is assumed that the clad with the thinnest wall and the greatest ovality permitted by the specification is operating in the region of the core where performance requirements are the most severe. Fission gas release rates,

00 00206

fuel growth, and changes in mechanical properties with irradiation are based on a conservative evaluation of currently available data. Thus, it is unlikely that significant failure of the cladding will result during operation.

The actual clad stresses are considerably below the yield strength. Circumferential stresses due to external pressure, calculated using those combinations of clad dimensions, ovality, and eccentricity which produce the highest stresses, are shown in Table 3-17. The maximum stress of 33,000 psi compression, at the design pressure of 2,500 psi, is the sum of 22,000 psi compressive membrane stress plus 11,000 psi compressive bending stress due to ovality at the clad OD in the expansion void, and at the beginning-of-life. The maximum stress in the heat-producing zone is 32,000 psi at design pressure, 27,000 psi at operating pressure. At this stress, the material may creep sufficiently to allow an increase in ovality until further creep is restrained by support from the fuel. Contact loads on the order of 20 lb/in. of length are sufficient to counteract the bending stress. Creep collapse tests have indicated a long time collapse resistance in excess of the requirement to prevent collapse in the end void. As the fuel rod internal pressure builds up with time, these stresses are reduced.

Late in life, the fuel rod internal pressure exceeds the system pressure, up to a maximum difference of 1,110 psi. The resultant circumferential pressure stress of 9,000 psi is about 1/4 of the yield strength, and therefore is not a potential source of short time burst. The possibility of stress-rupture burst has been investigated, using finite-difference methods to estimate the long time effects of the increasing pressure on the clad. The predicted pressure-time relationship produced stresses which are less than 1/3 of the stress levels which would produce stress rupture at the end-of-life. Outpile stress-rupture data were used, but the greater than 3:1 margin on stress is more than enough to account for decreased stress-rupture strength due to irradiation.

Clad circumferential stresses are listed in Table 3-17.

The free gas content of the fuel rod is calculated by considering (1) initial helium fill gas, (2) initial water vapor and atmospheric gases adsorbed on the fuel, and (3) fission product gases. The water vapor present initially is expected to dissociate over the life of the fuel and enter into hydriding and oxidizing reactions. The gas remaining at the end-of-life, when the maximum internal pressures exist, consists of the atmospheric gases and helium present initially plus the released fission gases.

The fission gas production is evaluated for a range of neutron fluxes and the fissionable material present over the life of the fuel.[50] A design value for gas production of 0.29 atoms of gas per fission has been determined.

Table 3-17

Clad Circumferential Stresses

Operating Condition	Calc. Stress, psi	Yield Stress, psi	Ultimate Tensile Stress, psi
1. BOL[a] - Operating at Design Pressure			
Total Stress (membrane + bending) Due to 2,500 psig System Design Pressure Minus 100 psig Fuel Rod Internal Pressure			
Average Clad Temperature - Approximately 625 F (expansion void)	-33,000	46,000	
2. EOL - Maximum Overpower			
System Pressure - 2,185 psig			
Fuel Rod Internal Pressure - 3,300 psig			
Average Temperature Through Clad Thickness at Hot Spot - Approximately 725 F			
Pressure Stress Only[b]	9,000		
- Including 4,000 psi Thermal Stress	13,000	36,000	38,000
3. EOL - Shutdown			
Immediately After Shutdown			
System Pressure - 2,200 psig			
Fuel Rod Internal Pressure - 1,750 psig			
Average Clad Temperature - Approximately 575 F	-4,000	45,000	48,000
3 Hours Later			
(50 F/hr Pressurizer Cooldown Rate)			
Fuel Rod Internal Pressure - 1,050 psig			
System Pressure - 680 psig			
Average Clad Temperature - Approximately 425 F	3,300	52,000	55,000

(a) Cladding is being ordered with 45,000 psi minimum yield strength and 10 per cent minimum elongation, both at 650 F. Minimum room temperature strengths will be approximately 75,000 psi yield strength (0.2 per cent offset), and 85,000 psi ultimate tensile strength.

(b) Clad stresses due to fuel swelling are discussed further below.

00 00208

The total production of fission gas in the hottest fuel rod assembly is based on the hot rod average burnup of 38,000 MWD/MTU. The corresponding maximum burnup at the hot fuel rod midpoint is 55,000 MWD/MTU.

The fission gas release is based on temperature versus release fraction experimental data.[45] Fuel temperatures are calculated for small radial and axial increments. The total fission gas release is calculated by integrating the incremental releases.

The maximum release and gas pressure buildups are determined by evaluating the following factors for the most conservative conditions:

(a) Gas conductivity at the end-of-life with fission gas present.

(b) Influence of the pellet-to-clad radial gap and contact heat transfer coefficient on fuel temperature and release rate.

(c) Unrestrained radial and axial thermal growth of the fuel pellets relative to the clad.

(d) Hot rod local peaking factors.

(e) Radial distribution of fission gas production in the fuel pellets.

(f) Fuel temperatures at reactor design overpower.

The fuel temperatures used to determine fission gas release and internal gas pressure have been calculated at the reactor overpower condition. Fuel temperatures, total free gas volume, fission gas release, and internal gas pressure have been evaluated for a range of initial diametral clearances. This evaluation shows that the highest internal pressure results when the maximum diametral gap is assumed because of the resulting high average fuel temperature. The release rate increases rapidly with an increase in fuel temperature, and unrestrained axial growth reduces the relatively cold gas end plenum volumes. A conservative ideal thermal expansion model is used to calculate fuel temperatures as a function of initial cold diametral clearance. Considerably lower resistance to heat transfer between the fuel and clad is anticipated at the end-of-life due to fuel fracture, swelling, and densification. The resulting maximum fission gas release rate is 43 per cent.

(3) Collapse Margins

Short time collapse tests have demonstrated a clad collapsing pressure in excess of 4,000 psi, at expansion void maximum temperature. Collapse pressure margin is approximately 1.7. Extrapolation to hot spot average clad temperature ($\approx$ 725 F)

indicates a collapse pressure of 3,500 psi and a margin of 1.4, which also greatly exceeds requirement. Outpile creep collapse tests have demonstrated that the clad meets the long time (creep collapse) requirement.

(4) Fuel Swelling

Fuel rod average and hot spot operating conditions and design parameters at 100 per cent power, pertinent to fuel swelling considerations, are listed below.

	Average	Maximum
Heat Flux, Btu/ft^2-hr	167,620	543,000
Linear Heat Rate, kw/ft	5.4	17.5
Fuel Temperature, F	1,385	4,160
Burnup (MWD/MTU) at Equilibrium	28,200	55,000

	Nominal Values
Pellet OD, in.	0.362
Pellet Density, % of Theoretical	95
Pellet-Clad Diametral Gap at Assy., in.	0.004 - 0.008
Clad Material	Cold-Worked Zr-4
Clad Thickness, in.	0.026

The capability of Zircaloy-clad UO_2 fuel in solid rod form to perform satisfactorily in PWR service has been amply demonstrated through operation of the CVTF and Shippingport cores, and through results of their supplementary development programs, up to approximately 40,000 MWD/MTU.

As outlined below, existing experimental information supports the various individual design parameters and operating conditions up to and perhaps beyond the maximum burnup of 55,000 MWD/MTU, but not in a single experiment. However, the LRD irradiation test program, currently in progress, does combine the items of concern in a single experiment, and the results are expected to be available for final design confirmation by the end of 1966.

(5) Application of Experimental Data to Design Adequacy of the Clad-Fuel Initial Gap to Accommodate Clad-Fuel Differential Thermal Expansion

Experimental Work

00 00210

Six rabbit capsules, each containing three, 5 in. fuel length, Zr-2 clad rods, were irradiated in the Westinghouse Test Reactor[41] at power levels up to 24 kw/ft. The 94 per cent theoretical density (T.D.) UO_2 pellets (0.430 OD) had initial clad-fuel diametral gaps of 6, 12, and 25 mils. No dimensional changes were observed. Central melting occurred at 24 kw/ft only in those rods which had the 25 mil initial gap.

Two additional capsules were tested.[51] The specimens were similar to those described above except for length and initial gap. Initial gaps of 2, 6, and 12 mils were used in each capsule. In the A-2 capsule, three 38 in. long rods were irradiated to 3,450 MWD/MTU at 19 kw/ft maximum. In the A-4 capsule, four 6 in. long rods were irradiated to 6,250 MWD/MTU at 22.2 kw/ft maximum. No central melting occurred in any rod, but diameter increases up to 3 mils in the A-2 capsule and up to 1.5 mils in the A-4 capsule were found in rods which had the 2 mil initial gap.

Application

In addition to demonstrating the adequacy of Zircaloy-clad UO_2 pellet rods to operate successfully at the power levels of interest (and without central melting), these experiments demonstrate that the design initial clad fuel gap of 4 to 8 mils is adequate to prevent unacceptable clad diameter increases due to differential thermal expansion between the clad and the fuel. A maximum local diametral increase of less than 0.001 in. is indicated for fuel rods having the minimum initial gap, operating at the maximum overpower condition.

(6) Adequacy of the Available Voids to Accommodate Differential Expansion of Clad and Fuel, Including the Effects of Fuel Swelling

Experimental Work

Zircaloy-clad, UO_2 pellet-type rods have performed successfully in the Shippingport reactor up to approximately 40,000 MWD/MTU.

Bettis Atomic Power Laboratory[49] has irradiated plate-type UO_2 fuel (96-98 per cent T.D.) up to 127,000 MWD/MTU, and at fuel center temperatures between 1,300 and 3,800 F. This work indicates fuel swelling rates of 0.16% $\Delta V/10^{20}$ f/cc until fuel internal voids are filled, then 0.7% $\Delta V/10^{20}$ f/cc after internal voids are filled. This point of "breakaway" appears to be independent of temperature over the range studied, and dependent on clad restraint and the void volume available for collection of fission products. The additional clad restraint and greater fuel plasticity (from higher fuel temperatures) of rod-type elements tend to reduce these swelling effects by providing greater resistance to radial swelling, and lower resistance to longitudinal swelling than was present in the plate-type test specimens.

This is confirmed in part by the work of Frost, Bradbury, and Griffiths of Harwell[52] in which 1/4 in. diameter UO_2 pellets, clad in 0.020 in. stainless steel with a 2 mil diametral gap, were irradiated to 53,300 MWD/MTU at a fuel center temperature of 3,180 F without significant dimensional change.

In other testing[53] 0.150 in. OD, 82-96 per cent T.D. oxide pellets (20 per cent Pu, 80 per cent U), clad with 0.016 in. stainless steel with 6-8 mil diametral gaps, have been irradiated to 77,000 MWD/MTU at fuel temperatures high enough to approach central melting without apparent detrimental results. Comparable results were obtained on rods swaged to 75 per cent T.D. and irradiated to 100,000 MWD/MTU.

Application

Based on the BAPL experimental data, swelling of the fuel rods is estimated as outlined below

Fuel is assumed to swell uniformly in all directions. Clad-pellet differential thermal expansion is calculated to be about 0.004 in. at the maximum linear heat rate, so that all of the minimum initial gap of 0.004 in. is filled up by thermal expansion. If the initial gap exceeds the minimum, the additional gap volume is assumed available to accommodate swelling. This additional void volume may initially tend to be filled by pellet thermal expansion because of the low contact pressure and resultant low contact coefficient, but as the fuel swells, the contact pressure must increase if the clad is to be stretched. Where fuel cracking tends to fill the radial gap, it is assumed that the crack voids are available to absorb swelling.

The external effect of fuel swelling is assumed to occur at $0.16\% \Delta V/10^{20}$ f/cc until the 5 per cent initial void in the 95 per cent T.D. pellets is filled at about 9×10^{20} f/cc. From that time on, swelling is assumed to take place at $0.7\% \Delta V/10^{20}$ f/cc until the maximum burnup of 13.6×10^{20} f/cc (55,000 MWD/MTU) is reached. Total fuel volume increase is 4-1/2 per cent which results in a 1-1/2 per cent diameter increase in a rod with the 0.004 in. minimum initial gap. Clad stress is estimated at 20,000 psi, so that the elastic strain is about 0.[illegible] per cent. Net plastic strain is 1.3 per cent. Similar calculations indicate that fuel rods with maximum burnup and the nominal clad-fuel gap (0.006 in. at assembly) will have clad plastic strains of about 0.6 per cent at the end-of-life. Based on outpile data, stress rupture should not be a problem at these strains.

Qualitative information from LSBR[54] suggests that swelling rates for this design may exceed those indicated by the BAPL data, because of the higher fuel temperatures. However, the A.E.R.E. tests[52] and the General Electric tests[53] do not support more than a small increase in post-"breakaway" swelling rates at temperatures of interest.

00 00212

Fuel Swelling Studies - LRD Irradiation Program[55]

Dimensional stability of UO_2 under inpile conditions simulating large reactor environments is under investigation. This study is currently being carried out under USAEC Contract AT(30-1)-3269, "Large Closed-Cycle Water Reactor Research and Development Program".

Parameters which contribute to swelling are burnup, heat rating, fuel density and grain size, and clad restraint. These are systematically being studied by irradiating a series of capsules containing fuel rods. These experiments were assigned by the AEC to ETR/MTR. Test variables are shown in Table 3-18.

Table 3-18

LRD Fuel Swelling Irradiation Program

Capsule[a] WAPD-49	Enrichment, %	Initial Goal Heat Rating[b] kw/ft	watts/cm	Fuel Density, % T.D.	Burnup, MWD/MTU
A	18.7	12	394	94 and 97	38,000
B	18.7	12	394	94 and 97	38,000
C	18.7	12	394	90, 94, and 97	38,000
D	16.0	18	591	90 and 97	47,000
E	13.5	18	591	94 and 97	47,000
F	13.5	18	591	90, 94, and 97	47,000
G	16.0	18	591	90 and 97	47,000
H	17.0	24	788	94 and 97	56,000
I	18.7	24	788	94 and 97	56,000
J	20.0	24	788	94 and 97	56,000
K	20.0	24	788	90 and 94	56,000
L	20.0	24	788	94 and 97	56,000

(a) Four rods/capsule.

(b) Fuel center temperatures vary from 1,570 to 4,110 F.

Effect of Zircaloy Creep

The effect of Zircaloy creep on the amount of fuel rod growth due to fuel swelling has been investigated. Clad creep has the effect of producing a nearly constant total pressure on the clad ID, by permitting the clad diameter to increase as the fuel diameter increases. Based on out-of-pile data,(56) 1 per cent creep will result in 10,000 hr (corresponding approximately to the end-of-life diametral swelling rate) from a stress of about 22,000 psi at the ≈ 720 F average temperature through the clad at the hot spot. At the start of this high swelling period (roughly the last 1/3 of the core life), the reactor coolant system pressure would more or less be balanced by the rod internal pressure, so that the total pressure to produce the clad stress of 22,000 psi would have to come from the fuel. Contact pressure would be 2,400 psi. At the end-of-life, the rod internal pressure exceeds the system pressure by about 1,100 psi, so that the clad-fuel contact pressure would drop to 1,300 psi. Assuming that irradiation produces a 3:1 increase in creep rates, the clad stress for 1 per cent strain in 10,000 hr would drop to about 15,000 psi. Contact pressures would be 1,800 psi at the beginning of the high swelling period, 700 psi at the end-of-life. Since the contact pressure was assumed to be 825 psi in calculating the contact coefficient used to determine the fuel pellet thermal expansion, there is only a short period at the very end-of-life (assuming the 3:1 increase in creep rates due to irradiation) when the pellet is slightly hotter than calculated. The effect of this would be a slight increase in pellet thermal expansion, and therefore in clad strain. Considering the improbability that irradiation will actually increase creep rates by 3:1, no change is anticipated.

b. Overall Assembly

(1) Assurance of Control Cluster Assembly Free Motion

The 0.058 in. diametral clearance between the guide tube and the control pin is provided to cool the control pin and to insure adequate freedom to insert the control pin. As indicated below, studies have shown that fuel rods will not bow sufficiently to touch the guide tube. Thus, the guide tube will not undergo deformation caused by fuel rod bowing effects. Initial lack of straightness of fuel rod and guide tube, plus other adverse tolerance conditions, conceivably could reduce the 0.083 in. nominal gap between fuel rod and guide tube to a minimum of about 0.045 in., including amplification of bowing due to axial friction loads from the spacer grid. The maximum expected flux gradient across a fuel rod of 1.176 will produce a temperature difference of 12 F, which will result in a thermal bow of less than 0.002 in. Under these conditions for the fuel rod to touch the guide tube, the thermal gradient across the fuel rod diameter would have to be on the order of 300 F.

00 00214

The effect of a DNB occurring on the side of a fuel rod adjacent to a guide tube would result in a large temperature difference. In this case, however, investigation has shown that the clad temperature would be so high that insufficient strength would be available to generate a force of sufficient magnitude to cause a significant deflection of the guide tube. In addition, the guide tube would experience an opposing gradient that would resist fuel rod bowing, and its internal cooling would maintain temperatures much lower than the fuel rod, thus retaining the guide tube strength.

(2) Vibration

The semiempirical expression developed by Burgreen[57] was used to calculate the flow-induced vibratory amplitudes for the fuel assembly and fuel rod. The calculated amplitude for the fuel assembly is 0.010 in., and less than 0.005 in. for the fuel rod. The fuel rod vibratory amplitude correlates with the measured amplitude obtained from a test on a 3 x 3 fuel rod assembly. In order to substantiate what is believed to be a conservatively calculated amplitude for the fuel assembly, a direct measurement will be obtained for a full size prototype fuel assembly during testing of the assembly in the Control Rod Drive Line Facility (CRDL) at the B&W Research Center, Alliance, Ohio.

(3) Demonstration

In addition to the specific items discussed above, the overall mechanical performance of the fuel assembly and its individual components is being demonstrated in an extensive experimental program in the CRDL.

3.2.4.3 Control System

3.2.4.3.1 Control Rod Drive System Design Criteria

The control rod drive system shall be designed to meet the following performance criteria:

a. Single Failure

No single failure shall inhibit the protective action of the control rod drive system. The effect of a single failure shall be limited to one rod drive assembly.

b. Uncontrolled Withdrawal

No single failure or chain of failures shall cause uncontrolled withdrawal of any drive.

c. Equipment Removal

The disconnection of plug-in type connectors, modules, and subassemblies from the protective circuits shall be annunciated or cause a reactor trip.

d. Control Cluster Assembly (CCA) Trip

The trip command shall have priority over all other commands. Trip action shall be positive and nonreversible. Trip circuitry shall provide the final protective action and shall be direct-acting, incur minimum delay, and shall not require external power. Circuit interrupting devices shall not prevent reactor trip. Fuses, where used, shall be provided with blown indicators. Circuit breaker position information shall also be indicated.

e. CCA Insertion

Insert command shall have priority over withdraw command. The drive actuator will be capable of overcoming a "stuck rod" condition equivalent to a 400 lb weight.

f. Withdrawal

The control system allows only two CCA groups out of four regulating CCA groups to withdraw at any time subject to the conditions described in 7.2.2.1.2.

g. Position Indication

Continuous position indication, as well as upper and lower position limit indication, shall be provided for each control rod drive assembly. The accuracy of the position indicators shall be consistent with the tolerance set by reactor safety analysis.

h. System Monitoring

The drive controls shall include provisions for monitoring conditions which are important to safety and reliability. These include such things as detecting power supply troubles and detecting motor or mechanism abnormal conditions.

i. Drive Speed

The drive controls shall provide for single uniform speed of the mechanism. The drive controls, or mechanism and motor combination, shall have an inherent speed-limiting feature. The speed of the mechanism shall be 25 in./min plus or minus 10 per cent of the predetermined value for both insert and withdraw motion. The withdraw speed shall be limited so as not to exceed 25 per cent overspeed in the event of speed control fault.

j. Mechanical Stops

The drive mechanisms shall be provided with positive, mechanical stops at both ends of the stroke or travel. The stops shall be capable of receiving the full operating force of the mechanisms without failure.

3.2.4.3.2 Control Rod Drive Assembly

The control rod drive assemblies provide for controlled withdrawal or insertion of the cluster control assemblies (CCA) out of or into the reactor core to establish and hold the power level required. The drive assemblies are also capable of rapid insertion or trip for emergency reactor conditions. The control rod drive assemblies are buffer seal, rack and pinion-type drives under development by Diamond Power Specialty Corporation. The control rod drive assembly data are listed in Table 3-19.

Table 3-19

Control Rod Drive Design Data

Item	Data
Number of Drives	69
Type	Buffer Seal, Rack and Pinion
Location	Top-Mounted
Direction of Trip	Down
Velocity of Normal Withdrawal and Insertion	25 in./min
Maximum Trip Time for 2/3 Insertion	1.4 sec
Length of Stroke	139 in.
Design Pressure	2500 psig
Design Temperature	650 F

A control rod drive assembly consists of a rack housing, snubber bottoming spring assembly, rack, rack pinion, coupling assembly, drive shaft housing, miter gear set, drive shaft assembly, buffer seal assembly, magnetic clutch, gear reducer, drive motor, position indication transmitters and limit switch system. The spool piece joins the drive assembly to the reactor closure head nozzle as shown in Figure 3-51.

The drive motor supplies torque through the magnetic clutch to the drive shaft-gear system to provide vertical positioning of the rack.

The control rod drive assembly is shown on Figures 3-51 and 3-52. Sub-assemblies of the control rod drive are described as follows:

a. Rack Housing Subassembly

The rack housing subassembly houses the hydraulic snubber, the bottoming spring assembly, the rack, rack pinion assembly and a rack guide bushing. The lower guide tube is attached to the lower end of the rack housing, and the cap and drive line vent assembly is mounted on the upper end of the rack housing.

The hydraulic snubber decelerates the moving elements of the drive at the end of travel by controlled orificing of reactor coolant water. The bottoming spring assembly absorbs the bottoming impact in a stack of spring washers. The rack is guided by an upper shoe attached to the upper end of the rack, a rack guide bushing located at the pinion, and a lower guide tube bushing located at the lower end of the lower guide tube. The rack pinion is carried by two ball bearings.

The valve on the cap and drive line vent assembly is used to bleed air or gases from the rack housing during reactor start-up. The removal of this assembly provides the access for CCA coupling and uncoupling and for securing the racks in the retracted position when the reactor closure head or individual drives are to be removed.

b. Drive Shaft Housing Subassembly

The drive shaft housing subassembly houses the miter gear set, the drive shafts and their supporting ball bearings. The drive shaft assembly is made up of two shaft assemblies with an intermediate bearing to raise the critical speed of the assembly.

This subassembly is attached to the rack housing subassembly by four through-bolts.

All gasketed joints are of the double Conoseal-type with a pressure testing tap between the seals.

c. Buffer Seal Assembly

A pressure breakdown-type seal is employed to seal the drive shaft penetration in the primary pressure container. Seal system water is injected between the eighth and ninth stages of a 9-stage seal to provide a controlled leakage of approximately 3 gal/hr into the reactor coolant system and 12 gal/hr to the letdown storage tank. The seal water is cooled below 120 F, demineralized and specially filtered before injection into the seal. A conventional rotary seal is employed to prevent seal water from entering the drive package.

d. Drive Package

The drive package is a synchronous type containing a synchronous motor, a self-locking worm gear reducer, a magnetic clutch, position indication transmitters and a limit switch system. In conjunction with the magnetic clutch is a unidirectional mechanical clutch which will allow the motor to drive the rods down following a trip. The motor has inherent braking

so no separate brake is required. The self-locking worm gear reducer prevents torque feedback to the motor.

e. Position and Limit Switch Transmitters

The position transmitters and limit switches are located between the buffer seal and the magnetic clutch and supply redundant position signals and limit switch contacts.

There are three separate devices included in the position and limit switch transmitter assembly. A potentiometer generates an analog position signal; a linear variable differential transformer (LVDT) generates both an analog position signal and limit contacts; and the limit switch mechanism provides limit contacts. Refer to Figure 3-58.

The potentiometer is geared directly to the drive shaft and gives a continuous dc signal proportional to the CCA position. The LVDT transmitter has a core that is moved by means of a ball screw mechanism geared to the drive shaft. A demodulator located within the control cabinet contains the necessary electronic circuitry to generate the analog dc signal. This demodulator also has relays with adjustable set points for position contacts. The limit switch assembly consists of switches operated by linear cams that are moved by a ball screw assembly. This is also geared directly to the drive shaft.

By using these three transmitters, it is possible to get both redundant position and redundant limit signals.

3.2.4.3.3 Control Rod Drive Assembly Control System

The control system for the rod drive mechanism is designed to energize and position the drive, indicate the control cluster assembly (CCA) position in the core, and indicate malfunctions in the system.

As shown on Figure 3-57, the control system consists of:

Power supplies and monitors.

Clock (CCA speed standard).

Drive mechanism grouping panel.

Individual CCA control logic.

Position indicator system.

Travel limit system.

Automatic sequence logic.

Trip system.

The rod mechanism control system provides the reactor operators with the flexibility of CCA grouping, manual or automatic group operation, automatic CCA group sequencing, and information of CCA position in the core.

A total of 12 CCA groups is available through facilities of a drive mechanism grouping panel which enables up to 12 CCA's to be assigned to each group. Individual position indicators are provided for all 69 CCA's and are visible to the operator. The operating control panel includes four group position indicators. Associated with each of these four indicators is a switch which selects CCA position data from a single CCA in each group. Three of the indicators are assigned to groups A, B, and C. The other is assigned to groups D through L. In addition, individual CCA selection is achieved through these switches for single CCA trim by manual switch action. CCA groups are programmed such that the power peaking values listed in Table 3-1 are never exceeded.

Automatic sequencing (group overlap) of groups A through D is provided and is available for automatic or manual operator CCA motion requirements. It allows a limited overlap of operation of any two groups in a fixed sequence, but no more than two. Inputs from CCA position and travel limits feed this system.

Automatic and manual control is provided. In "automatic," the selected drive mechanism group receives an automatic command signal from the reactor control system. In "manual," provision is made for operation of any individual CCA or group of CCA's. Manual or automatic operation of four CCA groups in a preset sequence is provided as described above. Grouping is determined at the drive mechanism grouping panel prior to reactor operation.

The drive gate is part of the individual CCA control logic circuitry which performs the function of selection and gating. It receives inputs from the clock,

the IN and OUT control busses, motion "Enable," and travel limits. The drive gate sends pulses to the translator upon receiving (1) clock pulses, (2) "Enable" input, and (3) an IN or OUT control signal. End travel limits and the driver monitor provide inputs to stop CCA motion.

Output signals of the drive gate feed into the translator. This unit produces the proper signals for the drive motor. Direction is determined by the IN and OUT commands, and speed is determined by the fixed clock frequency.

The position indication and travel limit systems consist of three different types of transmitters and produce two independent analog position signals and two independent limit signals. One of the devices, the LVDT, produces both position and limit signals. Either source of signals can be used for the position and for the limit signals.

Position output jacks are provided for a precision meter and for computer monitoring. Calibration of the potentiometer and the LVDT is accomplished by initial adjustments prior to installing the power package and also by making adjustments within the control cabinet. The limit switches are adjusted prior to installation of the drive package.

A fault detection circuit monitors signals to provide extra protection against unwanted withdrawal and insertion motion. See Figure 3-57.

Trip is initiated by de-energizing two series circuit breakers in each of two power sources (Figure 3-59). Each loss-of-voltage trip coil is fed by a separate two-out-of-four relay circuit powered by four inputs from the reactor protective system. Failure of any two inputs causes trip. The manual trip pushbutton opens all trip circuit breakers. Test pushbuttons are provided to test each circuit breaker action.

3.2.4.3.4 Control Rod Drive System Evaluation

a. Design Criteria

The System will be designed, tested, and analyzed for compliance with the design criteria. A preliminary safety analysis has been made on the control rod drive motor control subsystem for failures of logic functions. It was concluded that no single failure in any CCA control would prevent CCA insertion, nor cause inadvertent CCA withdrawal of another CCA or CCA group.

b. Materials Selection

Materials are selected to be compatible with, and operate in, the reactor coolant. Certified mill test reports containing chemical analysis and test data of all materials exposed to the reactor system fluid shall be provided and maintained for the control rod

drives. Certificates of compliance for other materials and components shall also be provided.

c. Relation to Design Temperature

All parts of the control rod drive assembly are designed to operate at 650 F, although it is expected that all parts will operate considerably cooler. Some tests have been completed, and additional tests are planned, to closely determine the operating temperature gradients throughout the drive mechanism during all phases of operation. These tests will also provide an indication of the amount of convection that takes place within the water space of the mechanism. It is expected that the more significant temperature changes will be caused by displacement of reactor coolant in and out of the mechanism water space as the drive line is raised and lowered.

d. Design Life

The expected life of the control rod drive control system is:

(1) Structural portions, such as flanges and pressure housings, have an expected life of 40 years.

(2) Moving parts, such as rack, pinions, and other gears, have an expected life of 20 years.

(3) Electronic control circuitry has an expected life of 20 years.

3.2.4.3.5 Control Cluster Assembly (CCA)

Each control cluster assembly is made up of 16 control pin assemblies which are coupled to a single Type 304 stainless steel spider cluster assembly (Figure 3-60). Each control pin assembly consists of an absorber section of silver-

indium-cadmium poison clad with cold-worked, Type 304 stainless steel tubing and Type 304 stainless steel upper and lower end pieces. The end pieces are welded to the clad to form a water and pressure-tight container for the poison. The control pin assemblies are loosely coupled to the spider cluster assembly in order to permit maximum conformity with the channels provided by the guide tubes. The CCA is inserted through the upper end fitting assembly of the fuel assembly, each control pin assembly being guided by an incore guide tube. Guide tubes are also provided in the upper plenum assembly above the core, so that full length guidance of the control pin assemblies is provided throughout the stroke. With the reactor assembled, the CCA cannot be withdrawn far enough to cause disengagement of the control pin assemblies from these incore guide tube assemblies. Pertinent design data are shown in Table 3-20.

Table 3-20

Control Cluster Assembly Design Data

Item	Data
Number of Cluster Assemblies	69
Number of Control Pins per Cluster Assembly	16
Outside Diameter of Control Pin, in.	0.440
Cladding Thickness, in.	0.019
Cladding Material	Type 304 SS, cold-worked
Poison Material	80% Ag, 15% In, 5% Cd
Length of Poison Section, in.	134
Stroke of Control Pin, in.	139

This type of CCA has been developed under the USAEC Large Reactor Development Program and offers the following significant advantages:

a. More uniform distribution of absorber throughout the core volume.

b. Shorter reactor vessel and shorter internals due to the elimination of control rod followers.

c. Lower reactor building requirements due to the reduction of reactor coolant inventory.

d. Better core power distribution for a given CCA worth.

A CCA prototype similar to the B&W design has been extensively tested(58) at reactor temperature, pressure, and flow conditions under the LRD program.

The silver-indium-cadmium poison material is enclosed in stainless steel tubes to provide structural strength to the control pin assemblies. These pins are designed to withstand all operating loads including those resulting from hydraulic forces, thermal gradients, and reactor trip deceleration.

The cladding of the poison section also prevents corrosion and eliminates possible silver contamination of the reactor coolant.

The ability of the poison clad to resist collapse due to the system pressure has been demonstrated by an extensive collapse test program on cold-worked stainless steel rods. The actual collapse margins are higher than the requirements.

Internal pressure and poison swelling are not expected to cause stressing or stretching of the clad because the Ag-In-Cd alloy poison does not yield a gaseous product under irradiation.

Because of their great length and unavoidable lack of straightness, some slight mechanical interference between control pins and guide tubes must be expected. However, the parts involved, especially the control pins, are so flexible that only very small friction drags will result. Similarly, thermal distortions of the control pins are expected to be small because of the low heat generation and adequate cooling. Consequently, it is not anticipated that the control pin assemblies will encounter significant frictional resistance to their motion in the guide tubes.

Overall performance of the CCA will be demonstrated in the B&W Control Rod Drive Line Facility (CRDL).

3.3 TESTS AND INSPECTIONS

3.3.1 NUCLEAR TESTS AND INSPECTION

3.3.1.1 Critical Experiments

An experimental program is presently underway to verify the control cluster assembly (CCA) design as to reactivity worth, and hence the safety aspect of the CCA. Detailed testing is underway to establish the worth of a CCA and a group of CCA's under various conditions similar to the reference core. These parameters include CCA arrangement, fuel enrichments, fuel element metal-to-water ratios, CCA materials, and soluble boron concentration in the moderator.

A part of the CCA test program includes the study of local power peaking both between fuel assemblies and around the water holes left by withdrawn CCA's. Additional data on the worth of soluble boron under various fuel assembly and water hole arrangements will also be produced by this program.

Zero power tests will be made to establish the worth of soluble boron and the CCA's at the reactor site for both cold and hot conditions. CCA group worths will be determined for all operating patterns to insure that the various limits placed on a single CCA or CCA pattern worth are not exceeded, and that there is sufficient reactivity always fully withdrawn to provide reactor shutdown with the most worthy CCA stuck out.

3.3.1.2 Zero Power, Approach to Power, and Power Testing

Boron worth and CCA worth (including stuck CCA worth) will be determined by physics tests at the beginning of each core cycle. It is expected that recalibration of boron worth and CCA worth will be performed at least once during each core cycle. Calculated values of boron worth and CCA worth will be adjusted as necessary to the test values. The boron worth and CCA worth at a given time in core life will be based on CCA position indication and calculated data as adjusted by experimental data.

Periodic laboratory analysis of the reactor coolant is performed to determine the boron concentration. The reactivity held in boron is then calculated from the concentration and the reactivity worth of boron.

The method of maintaining the hot shutdown margin (hence stuck CCA margin) is related to operational characteristics (load patterns) and to the power peaking restrictions upon CCA patterns at power. The CCA pattern restrictions will be such that sufficient reactivity is always fully withdrawn to provide adequate shutdown with the stuck CCA margin. Power peaking as related to CCA patterns and shutdown margin will be monitored by reactivity calculations, and interlocks will be provided to prevent CCA patterns which produce excessive power peaking and/or reduction of shutdown margin.

Operation under all power conditions will be monitored by incore instrumentation, and the resulting data analyzed and compared with multidimensional calculations in a continuing effort to provide sufficient support for further power escalations.

3.3.2 THERMAL AND HYDRAULIC TESTS AND INSPECTION

3.3.2.1 Reactor Vessel Flow Distribution and Pressure Drop Test

A 1/6 scale model of the reactor vessel and internals will be tested to achieve the following objectives:

a. To measure the flow distribution to each fuel assembly of the reactor core and to develop, if necessary, devices required to produce the desired flow distribution.

b. To measure fluid mixing between the vessel inlet nozzle and the core inlet, and between the inlet and outlet of the core.

c. To measure the overall pressure drop between the vessel inlet and outlet nozzles, and the pressure drop between various points in the reactor vessel flow circuit.

The reactor vessel, thermal shield, flow baffle, core barrel, and upper plenum assembly are made of clear plastic to allow use of visual flow study techniques. All parts of the model except the core are geometrically similar to those in the prototype reactor. However, the simulated core was designed to maintain dynamic similarity between the model and prototype.

Each of the 177 simulated fuel assemblies contains a calibrated flow nozzle at its inlet and outlet. The test loop is capable of supplying cold water (80 F) to three inlet nozzles and hot water (180 F) to the fourth. Temperature measurements will be taken in the inlet and outlet nozzles of the reactor model and at the inlet and outlet of each of the fuel assemblies. Static pressure taps will be located at suitable points along the flow path through the vessel. This instrumentation will provide the data necessary to accomplish the objectives set forth for the tests.

3.3.2.2 Fuel Assembly Heat Transfer and Fluid Flow Tests

B&W is conducting a continuous research and development program for fuel assembly heat transfer and fluid flow applicable to the design of the Duke Power Company reactors. Single channel tubular and annular test sections and multiple rod assemblies have been tested at the B&W Research Center.

3.3.2.2.1 Single Channel Heat Transfer Tests

A large quantity of uniform flux, single channel, critical heat flux data has been obtained. References to uniform flux data are given in BAW-168 and 3.2.3.1.2 of this report. The effect on the critical heat flux caused by nonuniform axial power generation in a tubular test section at 2,000 psi pressure was investigated as early as 1961.[28] This program was extended to include pressures of 1,000, 1,500, and 2,000 psi and mass velocities up to 2.5×10^6 lb/hr-ft^2.[59] The effect on the critical heat flux caused by differences in the radial and axial power distribution in an annular test section was recently investigated at reactor design conditions.[60] Data were obtained at pressures of 1,000, 1,500, 2,000, and 2,200 psi and at mass velocities up to 2.5×10^6 lb/hr-ft^2.

3.3.2.2.2 Multiple Rod Fuel Assembly Heat Transfer Tests

Critical heat flux data are being obtained from 4 ft and 6 ft long, 9-rod fuel assemblies, in a 3 x 3 square array. The operating conditions include pressures up to 2,400 psi and mass velocities up to 3.0×10^6 lb/hr-ft^2. The simulated fuel rod diameter and pitch are identical with the reactor core. The data obtained to date have verified the design procedure. Data will be obtained from a longer, 9-rod fuel assembly to provide additional confidence in the present thermal design and to lead to increased reactor power capability.

3.3.2.2.3 Fuel Assembly Flow Distribution and Pressure Drop Tests

Flow visualization and pressure drop data have been obtained from a 10 times full scale model of a single rod in a square flow channel. These data have been used to refine the spacer ferrule designs with respect to mixing turbulence and pressure drop.

Flow distribution in a square, 4-rod test assembly has been measured. A salt solution injection technique was used to determine the average flow rates in the simulated reactor assembly corner cells, wall cells, and unit cells. Interchannel mixing was obtained for the same assembly. These data have been used to confirm the flow distribution and mixing relationships employed in the core thermal and hydraulic design. Additional mixing, flow distribution, and pressure drop data will be obtained to improve the core power capability. The following fuel assembly geometries will be tested to provide additional data:

a. A 3 x 3 array identical to that for which critical heat flux data have been obtained to provide additional interchannel mixing data.

b. A 4 x 6 array divided in half by a perforated plate simulating adjacent fuel assemblies to provide data on mixing between assemblies.

c. A full scale 15 x 15 rod fuel assembly. This test is to provide additional flow distribution, mixing, and pressure drop information applicable to a complete assembly.

3.3.2.3 Preoperational Testing and Postoperational Testing

Thermocouples are included as part of the incore instrumentation assembly and will enable postoperational temperature measurements to be made at the entrance and exit of all 51 instrumented fuel assemblies. The results of these tests will be compared to the results of the model tests which were used to design calculations.

3.3.3 FUEL ASSEMBLY, CONTROL CLUSTER ASSEMBLY, AND CONTROL ROD DRIVE ASSEMBLY MECHANICAL TESTS AND INSPECTION

To demonstrate the mechanical adequacy and safety of the fuel assembly, control cluster assembly (CCA), and the control rod drive assembly, a number of functional tests have been performed, are in progress, or are in final stages of preparation.

3.3.3.1 Prototype Testing

A full scale prototype fuel assembly, CCA, and control rod drive assembly is presently being tested in the Control Rod Drive Line (CRDL) Facility located at the B&W Research Center, Alliance, Ohio. This full size loop is capable of simulating reactor environmental conditions of pressure, temperature, and coolant flow. To verify the mechanical design, operating compatibility, and characteristics of the entire control rod drive assembly-fuel assembly system, the drive assembly will be stroked and tripped in excess of expected operating life requirements. A portion of the testing will be performed with maximum misalignment conditions. Equipment is available to record and verify data such as fuel assembly pressure drop, vibration characteristics, hydraulic forces, etc., and to demonstrate control drive operation and verify scram times. All prototype components will be examined periodically for signs of material fretting, wear, and vibration/fatigue to insure that the mechanical design of the equipment meets reactor operating requirements.

After the prototype fuel assembly has been tested under simulated reactor operating conditions, it will be installed in the full size low pressure loop to verify specific fuel assembly design data. These data include pressure drop, coolant interchannel mixing, and coolant velocity profiles.

3.3.3.2 Model Testing

Many functional improvements have been incorporated in the design of the prototype fuel assembly as a result of model tests run to date. For example, the spacer grid to fuel rod contact area was fabricated to 10 times reactor size, and tested in a loop simulating coolant flow Reynolds numbers of interest. Thus, visually, the shape of the fuel rod support areas was optimized with respect to minimizing the severity of flow vortices. Also, a 9-rod (3 x 3) actual size model was fabricated (using production fuel assembly materials) and tested at 640 F, 2,200 psi, and 13 fps coolant flow. Principal objectives of this test were to evaluate fuel rod cladding to spacer grid contact wear, and/or fretting corrosion resulting from flow-induced vibration. A wide range of contact loads (including small clearances) was present in this specimen. No significant wear or other flow-induced damage was observed after 210 days of loop operation.

3.3.3.3 Component and/or Material Testing

3.3.3.3.1 Fuel Rod Cladding

Extensive short time collapse testing was performed on Zircaloy-4 tube specimens as part of the B&W overall creep-collapse testing program. Initial test specimens were 0.436 in. OD with wall thicknesses of 0.020 in., 0.024 in., and 0.028 in. Ten specimens of each thickness, 8 in. long, were individually tested at 680 F at slowly increasing pressure until collapse occurred. Collapse pressures for the 0.020 in. wall thickness specimens ranged from 1,800 to 2,200 psig, the 0.024 in. specimens ranged from 2,800 to 3,200 psig, and the 0.028 in. specimens ranged from 4,500 to 4,900 psig. The material yield strength of these specimens ranged from 65,000 to 72,000 psi at room temperature, and was 35,800 psi at 680 F. Additional Zircaloy-4 short time collapse specimens were prepared with a material yield stress of 78,000 psi at room temperature and 48,500 psi at 615 F. Fifteen specimens having an OD of 0.410 in. and an ID of 0.365 in. (0.0225 in. nominal wall thickness) were tested at 615 F at increasing

pressure until collapse occurred. Collapse pressures ranged from 4,470 to 4,960 psig.

Creep-collapse testing was performed on the 0.436 in. OD specimens. Twelve specimens of 0.024 in. wall thickness, and 30 specimens of 0.028 in. wall thickness, were tested in a single autoclave at 680 F and 2,050 psig. During this test, two 0.024 in. wall thickness specimens collapsed during the first 30 days, and two collapsed between 30 and 60 days. None of the 0.028 in. wall thickness specimens had collapsed after 60 days. Creep-collapse testing was then performed on thirty 0.410 in. OD by 0.365 in. ID (0.0225 in. nominal wall) specimens for 60 days at 615 F and 2,140 psig. None of these specimens collapsed, nor was there any significant increase in ovality after 60 days.

Results of the 60 day creep-collapse testing on the 0.410 in. OD specimens showed no indication of incipient collapse. The 60 day period for creep-collapse testing is used since it exceeds the point of primary creep of the material, yet is sufficiently long to enter the stage when fuel rod pressure begins to build up during reactor operation, i.e., past the point of maximum differential pressure that the clad would be subjected to in the reactor.

In order to help optimize the final clad thickness, additional clad-collapse testing is scheduled for 1967 using specimens fabricated to the reference design fuel clad dimensions, material specifications, and operating conditions.

3.3.3.3.2 Fuel Assembly Structural Components

The mechanical design of the prototype can panel assembly is the result of an extensive can panel design and structural evaluation program. The full size, simulated loop functional testing as noted in 3.3.3.1 is expected to verify can panel design criteria. Prototype static and dynamic load testing is underway to verify can panel structural adequacy for vibration, handling, operation and seismic loads.

In the mechanical design of the spacer grids particular attention is given to the ferrule-to-fuel-rod contact points. Sufficient load must be applied to position the fuel rods and to minimize fuel rod vibration, yet allow axial thermal differential expansion, and not produce fretting wear in the fuel rod cladding. Static load and functional testing of the prototype grids will demonstrate their adequacy to perform within the design requirements.

3.3.3.4 Control Rod Drive Assembly Tests and Inspection

3.3.3.4.1 Mechanism Developmental Tests

The prototype buffer seal actuator is under development at the B&W Research Center.

Wear characteristics of critical components such as sleeve bearings, pinion and rack teeth, snubber piston and sleeve, etc, during tests to date indicate that material compatibility and structural design of these components will be adequate for the life of the mechanism.

Subsequent to completion of the actuator development program, the complete prototype control rod drive assembly will be subjected to environmental testing under simulated reactor conditions (except radiation) in the Control Rod Drive Line (CRDL) Facility at Alliance. Environmental tests will include, but not necessarily be limited to, the following:

Operational Tests

Operating speeds.

Temperature profiles.

Trip times for full and partially withdrawn control cluster assemblies (CCA) for various flow-induced pressure drops across the CCA.

Life Tests

(With internals assembled to maximum misalignment permitted by drawing dimensions and tolerances)

2,500 Partial stroke (75 per cent) cycles.

2,500 Full stroke cycles.

25 Partial stroke (40 per cent) trip cycles.

175 Partial stroke (75 per cent) trip cycles.

200 Full stroke trip cycles.

Misalignment Tests

100 Full strokes and 100 full stroke trips with internals tolerances altered to 1.5 times maximum allowable misalignment.

Coupling Tests

Complete check of coupling operations after testing.

The above cycles meet the total test requirements of 5,000 full strokes and 500 trips. Complete disassembly and inspection of the assembly will be accomplished at various B&W facilities after completion of environmental tests.

3.3.3.4.2 Control Rod Drive Assembly Developmental Tests

A control rod drive assembly motor control unit has been built in breadboard form. Following the testing of this breadboard version, prototype circuits

for plug-in modules will be designed and tested. Testing will consist of bench testing, life testing, and determining effects of simulated failures. The simulated failure testing will be designed to verify the safety analysis.

The rod drive control system package will be tested in conjunction with the rod drive motor control package to insure proper operation. Simulated failure testing will also be performed on the combined system to insure that protective requirements are being met.

The position indicator and limit switch subsystem has been built in prototype form and life-tested mechanically under expected environmental conditions. Further testing, both mechanically and electrically, will be done under expected environmental conditions at the B&W Research Center. Characteristics to be determined will include accuracy, repeatability, linearity, short term stability, and long term stability.

3.3.3.4.3 Production Tests

The finished control rod drive assembly will be proof-tested as a complete system, i.e., mechanisms, motor control, and system control working as a system. This proof testing will be above and beyond any developmental testing which is performed in the product development stages.

Mechanism production tests will include the following:

a. Ambient Tests

Coupling tests.

Operating speeds.

Position indication.

Trip tests.

b. Operational Tests

Operating speeds.

Position indication.

Partial and full stroke cycles.

Partial and full stroke trip cycles.

Control system assembly production tests will be performed as described in the following paragraphs.

The finished hardware will be systematically operated through all of its operating modes, checked over the full range of all set points, and checked for proper operation of all patch plugs. This will check completeness and proper functioning of wiring and components.

~~00 00148~~ 231

The operating modes to be checked will include such things as automatic operation, manual group operation, trim or single CCA operation, position indication of all CCA's, travel limit on all CCA's, trip circuit operations, IN command, OUT command, etc.

The trip circuit or circuits will be tested by repeated operation. The overall trip time will be measured.

The accuracy and repeatability of the position indication and limit switch systems will be tested.

Power supply tests will be performed to determine the upper and lower operating voltage and to prove immunity to switching transients.

Fault conditions will be simulated to prove that no unsafe action results from defective components, circuits, or wiring. Ability to detect unsafe fault conditions at the operating console will be determined. Typical of faults which will be simulated are:

a. Defective limit switch or circuit.

b. Improper CCA group patch.

c. Defective patch plugs.

d. Defective group sequencer.

e. Defective clock.

f. Defective automatic control signal.

g. Defective command line.

h. Defective fuses.

i. Defective single CCA control circuit or switch.

j. Defective power supply.

k. Defective motor translator.

l. Defective motor cable.

m. Defective position transmitter.

The finished hardware will be visually inspected for quality of workmanship. This inspection will include an examination of the enclosure, cable entrances, dust-tightness, maintenance features, drawers and cable retractors, fasteners, stiffeners, module mounts, wire harnesses, and other similar details.

3.3.4 INTERNALS TESTS AND INSPECTIONS

The internals upper and lower plenum hydraulic design will be evaluated and guided by the results from the 1/6 scale model flow test which is described in detail in 3.3.2.1. These test results will indicate areas of gross flow maldistribution and allow verification of vessel flow-pressure drop computations. In addition, the test results will provide measured pressure pulses at specific locations as an aid in assessing the vibration response characteristics of the internals components.

The effects of internals misalignment will be evaluated on the basis of the test results from the CRDL tests described in 3.3.3.4. These test results, when correlated with the internals guide tube final design, will insure that the CCA will have the capability for a reactor trip or fast insertion under all modes of reactor operation in the reactor coolant environment. These tests will not include the effects of neutron flux exposure.

After completion of shop fabrication, all internals components will be shop-fitted and assembled to final design requirements. The assembled internals components will be installed in a mockup of the as-built reactor vessel for final shop fitting and alignment of the internals for the mating fit with the reactor vessel. Dummy fuel and CCA's will be used to check out and insure that ample clearances exist between the fuel and internals structures guide tubes to allow free movement of the CCA throughout its full stroke length in various core locations. Fuel assembly mating fit will be checked at all core locations. The dummy fuel and CCA's will be identical to the production components, except that they will be manufactured to the most adverse tolerance space envelope; and even though the assembly weights will be representative of the production units, the dummy components will not contain fissionable or poison materials.

Internals shop fabrication quality control tests, inspection, procedures, and methods will be similar to the pressure vessel tests as described in detail in 4.1.4.

With regard to the internals surveillance specimen holder tubes, the material irradiation surveillance program is described in 4.4.3.

All internal components can be removed from the reactor vessel to allow inspection of all vessel interior surfaces (see 4.4.1). Inspection of internals components surfaces can be performed when the internals are removed to the canal storage location.

3.4 REFERENCES

(1) Putnam, G. E., TOPIC - A Fortran Program for Calculating Transport of Particles in Cylinders, IDO-16968, April 1964.

(2) Avery, A. F., The Prediction of Neutron Attenuation in Iron-Water Shields, AEEW-R125, April 1962.

(3) Bohl, H., Jr., et al., P3MG1, A One-Dimensional Multigroup P-3 Program for the Philco-2000 Computer, WAPD-TM-272.

(4) Bohl, H., Jr. and Hemphill, A. P., MUFT-5, A Fast Neutron Spectrum Program for the Philco-2000, WAPD-TM-218.

(5) Armster, H. J. and Callaghan, J. C., KATE-1, A Program for Calculating Wigner-Wilkins and Maxwellian-Averaged Thermal Constants on the Philco-2000, WAPD-TM-232.

(6) Marlowe, O. J. and Suggs, M. C., WANDA-5, A One-Dimensional Neutron Diffusion Equation Program for the Philco-2000 Computer, WAPD-TM-241.

(7) Honeck, H. C., THERMOS, A Thermalization Transport Theory Code for Reactor Lattices, BNL-5826.

(8) Cadwell, W. R., Buerger, P. F., and Pfeifer, C. J., The PDQ-5 and PDQ-6 Programs for the Solution of the Two-Dimensional Neutron Diffusion-Depletion Problem, WAPD-TM-477.

(9) Marlowe, O. J., Nuclear Reactor Depletion Programs for the Philco-2000 Computer, WAPD-TM-221.

(10) Lathrop, K. D., DTF-IV, A FORTRAN-IV Program for Solving the Multigroup Transport Equation With Anisotropic Scattering, LA-3373.

(11) Joanou, G. D. and Dudek, J. S., GAM-1: A Consistent P_1 Multigroup Code for the Calculation of Fast Neutron Spectra and Multigroup Constants, GA-1850.

(12) Baldwin, M. N., Physics Verification Experiments, CORE I, ρ_{28} and Initial Conversion Ratio Measurements, BAW-TM-454.

(13) Clark, R. H. and Pitts, T. G., Physics Verification Experiments, Core I, BAW-TM-455.

(14) Clark, R. H. and Pitts, T. G., Physics Verification Experiments, Cores II and III, BAW-TM-458.

(15) Clark, R. H., Batch, M. L., and Pitts, T. G., Lumped Burnable Poison Program - Final Report, BAW-3492-1.

(16) Neuhold, R. J., Xenon Oscillation, BAW-305, 1966.

00 ~~00150~~ 234

(17) Wilson, R. H. and Ferrell, J. K., Correlation of Critical Heat Flux for Boiling Water in Forced Circulation at Elevated Pressures, The Babcock & Wilcox Company Report BAW-168, November 1961.

(18) U.S.-Euratom Joint R&D Program, Burnout Flow Inside Round Tubes With Non-uniform Heat Fluxes, The Babcock & Wilcox Company, BAW-3238-9, May 1966.

(19) Jens, W. H. and Lottes, P. A., Analysis of Heat Transfer Burnout, Pressure Drop, and Density Data for High Pressure Water, ANL-4627, May 1951.

(20) Owen, D. B., Factors for One-Sided Tolerance Limits and for Variable Sampling Plans, SCR-607, March 1963.

(21) DeBortoli, R. A., et al., Forced Convection Heat Transfer Burnout Studies for Water in Rectangular Channels and Round Tubes at Pressures Above 500 psia, WAPD-188, Bettis Plant, Pittsburgh, Pennsylvania, 1958.

(22) USAEC Docket 50-244, Exhibit D-3, entitled "Rochester Gas and Electric Corporation, Brookwood Nuclear Station Unit No. 1", (Third Supplement to: Preliminary Facility Description and Safety Analysis Report, February 28, 1966).

(23) Lee, D. H. and Obertelli, J. D., An Experimental Investigation of Forced Convection Burnout in High Pressure Water. Part 1, Round Tubes With Uniform Flux Distribution, AEEW-R-213, August 1963.

(24) Matzner, B. and Griffel, J., Bimonthly Progress Report (BPR-XIII-11 and 12-63), Task XIII of Contract AT(30-3)-187, Basic Experimental Studies of Boiling Fluid Flow and Heat Transfer at Elevated Pressures, for November and December 1963, January 27, 1964.

(25) Matzner, B. and Griffel, J., Monthly Progress Report (MPR-XIII-6-63), Task XIII of Contract AT(30-3)-187, Basic Experimental Studies of Boiling Fluid Flow and Heat Transfer at Elevated Pressures, for June 1963, June 28, 1963.

(26) Matzner, B., Monthly Progress Report (MPR-XIII-5-63), Task XIII of Contract AT(30-3)-187, Basic Experimental Studies of Boiling Fluid Flow and Heat Transfer at Elevated Pressures, for May 1963, May 31, 1963.

(27) Internal Memo, Weatherhead, R. J. to Lottes, P. A., Critical Heat Flux (Burnout) in Small Diameter Tubes at 2000 psia, December 29, 1958.

(28) Swenson, H. W., Carver, J. R., and Kakarala, C. R., The Influence of Axial Heat Flux Distribution on the Departure From Nucleate Boiling in a Water Cooled Tube, ASME Paper 62-WA-297.

(29) Nonuniform Heat Generation Experimental Program, Quarterly Progress Report No. 7, January - March 1965, BAW-3238-7, Joint U.S.-Euratom R&D Program, AEC Contract No. ATC(30-1)-3238.

(30) Hald, A., Statistical Theory With Engineering Applications, John Wiley & Sons, Inc., New York, 1955.

~~00 00151~~ 235

(31) Worthing, A. G. and Geffner, J., Treatment of Experimental Data, John Wiley & Sons, Inc., New York, 1943.

(32) Baker, O., Simultaneous Flow of Oil and Gas, Oil and Gas Journal, Vol. 53, pp 185 - 195, 1954.

(33) Rose, S. C., Jr., and Griffith, P., Flow Properties of Bubbly Mixtures, ASME Paper No. 65-HT-38, 1965.

(34) Haberstroh, R. D. and Griffith, P., The Transition From the Annular to the Slug Flow Regime in Two-Phase Flow, MIT TR 5003-28, Department of Mechanical Engineering MIT, June 1964.

(35) Bergles, A. E. and Suo, M., Investigation of Boiling Water Flow Regimes at High Pressure, NYO-3304-8, February 1, 1966.

(36) Notley, M. J. F., The Thermal Conductivity of Columnar Grains in Irradiated UO_2 Fuel Elements, AECL-1822, July 1963.

(37) Lyons, M. F., et al., UO_2 Fuel Rod Operation With Gross Central Melting, GEAP-4264, October 1963.

(38) Notley, M. J. F., et al., Zircaloy-Sheathed UO_2 Fuel Elements Irradiated at Values of Integral $\int k d\theta$ between 30 and 83 w/cm, AECL-1676, December 1962.

(39) Bain, A. S., Melting of UO_2 During Irradiations of Short Duration, AECL-2289, August 1965.

(40) Notley, M. J. F., et al., The Longitudinal and Diametral Expansions of UO_2 Fuel Elements, AECL-2143, November 1964.

(41) Duncan, R. N., Rabbit Capsule Irradiation of UO_2, CVNA-142, June 1962.

(42) Lyons, M. F., et al., UO_2 Pellet Thermal Conductivity From Irradiations With Central Melting, GEAP-4624, July 1964.

(43) McGrath, R. G., Carolinas-Virginia Nuclear Power Associates, Inc., Research and Development Program, Quarterly Progress Report for the Period April-May-June 1965, CVNA-246.

(44) Ross, A. M. and Stoute, R. L., Heat Transfer Coefficients Between UO_2 and Zircaloy-2, AECL-1552, June 1962.

(45) Hoffman, J. P. and Coplin, D. H., The Release of Fission Gases From Uranium Dioxide Pellet Fuel Operated at High Temperatures, GEAP-4596, September 1964.

(46) Spolaris, C. N. and Megerth, F. H., Residual and Fission Gas Release From Uranium Dioxide, GEAP-4314, July 1963.

(47) Robertson, J. A. L., et al., Behavior of Uranium Dioxide as a Reactor Fuel, AECL-603, 1958.

~~00 00152~~ 236

(48) Parker, G. W., et al., Fission Product Release From UO_2 by High Temperature Diffusion and Melting in Helium and Air, CF-60-12-14, ORNL, February 1961.

(49) Daniel, R. C., et al., Effects of High Burnup on Zircaloy-Clad, Bulk UO_2, Plate Fuel Element Samples, WAPD-263, September 1962.

(50) Blomeke, J. O. and Todd, Mary F., Uranium Fission Product Production as a Function of Thermal Neutron Flux, Irradiation Time, and Decay Time, ORNL-2127, Part 1, Vol. 1 and 2.

(51) Duncan, R. N., CVTR Fuel Capsule Irradiations, CVNA-153, August 1962.

(52) Frost, Bradbury, and Griffiths (AERE Harwell), Irradiation Effects in Fissile Oxides and Carbides at Low and High Burnup Levels, Proceedings of IAEA Symposium on Radiation Damage in Solids and Reactor Materials, Venice, Italy, May 1962.

(53) Gerhart, J. M., The Post-Irradiation Examination of a PuO_2-UO_2 Fast Reactor Fuel, GEAP-3833.

(54) Atomic Energy Clearing House, Vol. 12, No. 3, p 11.

(55) Large Closed-Cycle Water Reactor Research and Development Program Progress Report for the Period, January 1 to March 31, 1964, Westinghouse Electric Corporation, Pittsburgh, Pa., 1964, WCAP-3269-2. Also WCAP-3269-3 for period from April 1 to June 30, 1964.

(56) Physical and Mechanical Properties of Zircaloy-2 and -4, WCAP-3269-41, Figure 18.

(57) Burgreer, D., Byrnes, J. J., and Benforado, D. M., Vibration of Rods Induced by Water in Parallel Flow, Trans. ASME 80, p 991, 1958.

(58) Large Closed-Cycle Water Reactor R&D Program, Progress Report for the Period January 1 to March 31, 1965, WCAP-3269-12.

(59) Burnout for Flow Inside Round Tubes With Nonuniform Heat Fluxes, BAW-3238-9, May 1966.

(60) Nonuniform Heat Generation Experimental Program, BAW-3238-13, July 1966.

~~00-00153~~ 237

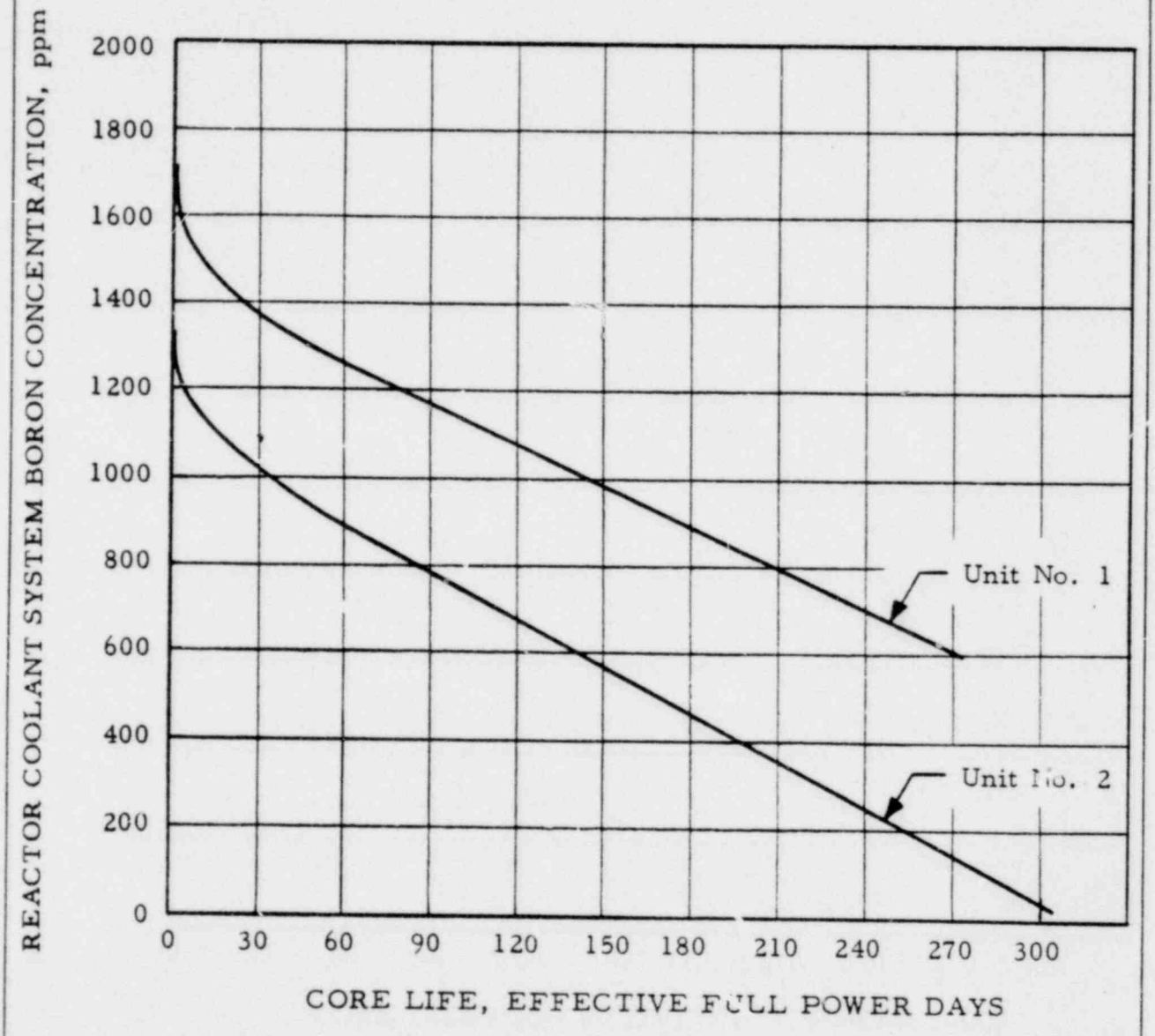

BORON CONCENTRATION VERSUS CORE LIFE

OCONEE NUCLEAR STATION

FIGURE 3-1

00 00154 238

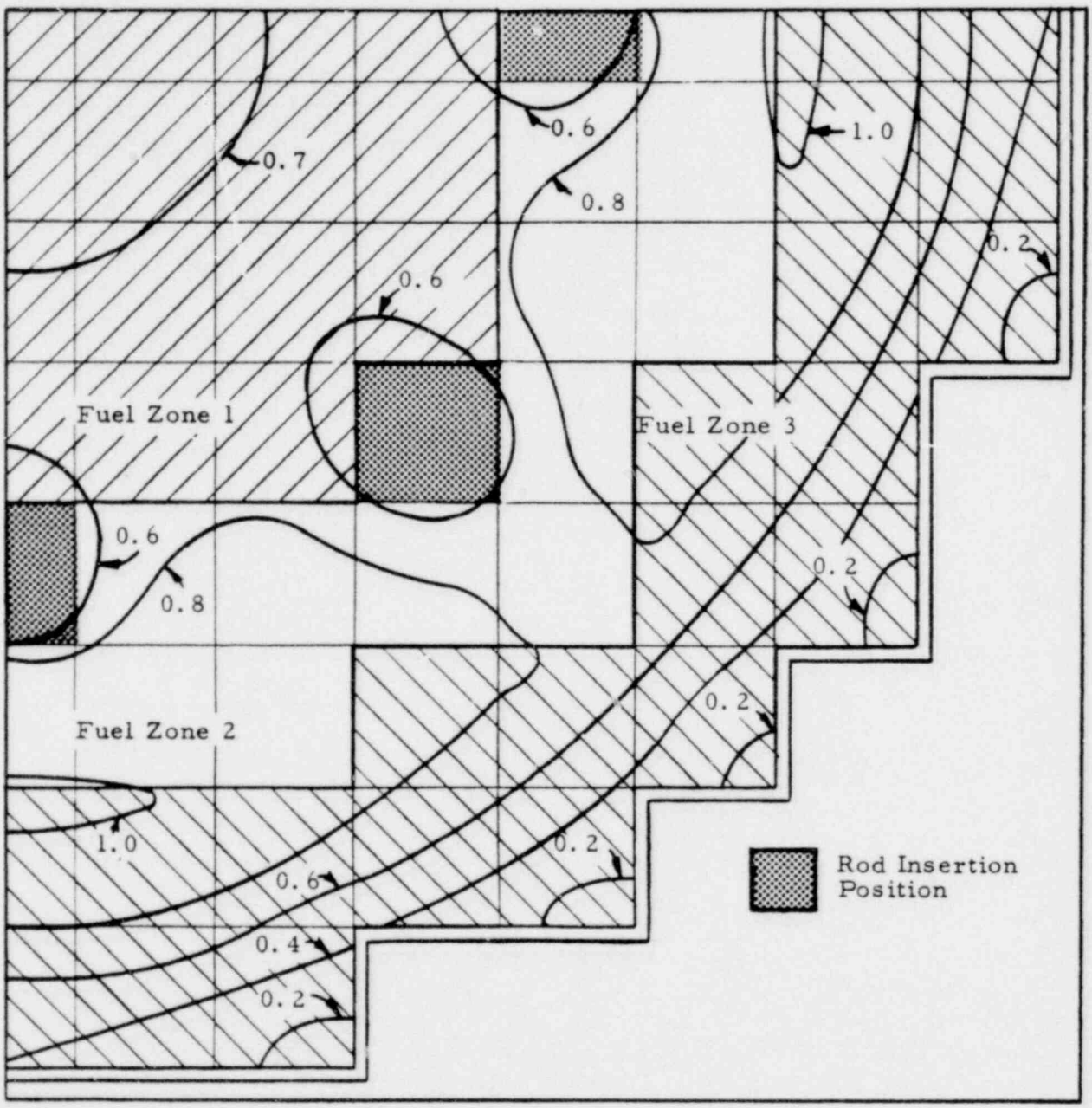

TYPICAL QUARTER CORE POWER DISTRIBUTION
XENON OVERRIDE RODS INSERTED
(CONTOURS TAKEN RELATIVE TO PEAK)

OCONEE NUCLEAR STATION
FIGURE 3-2

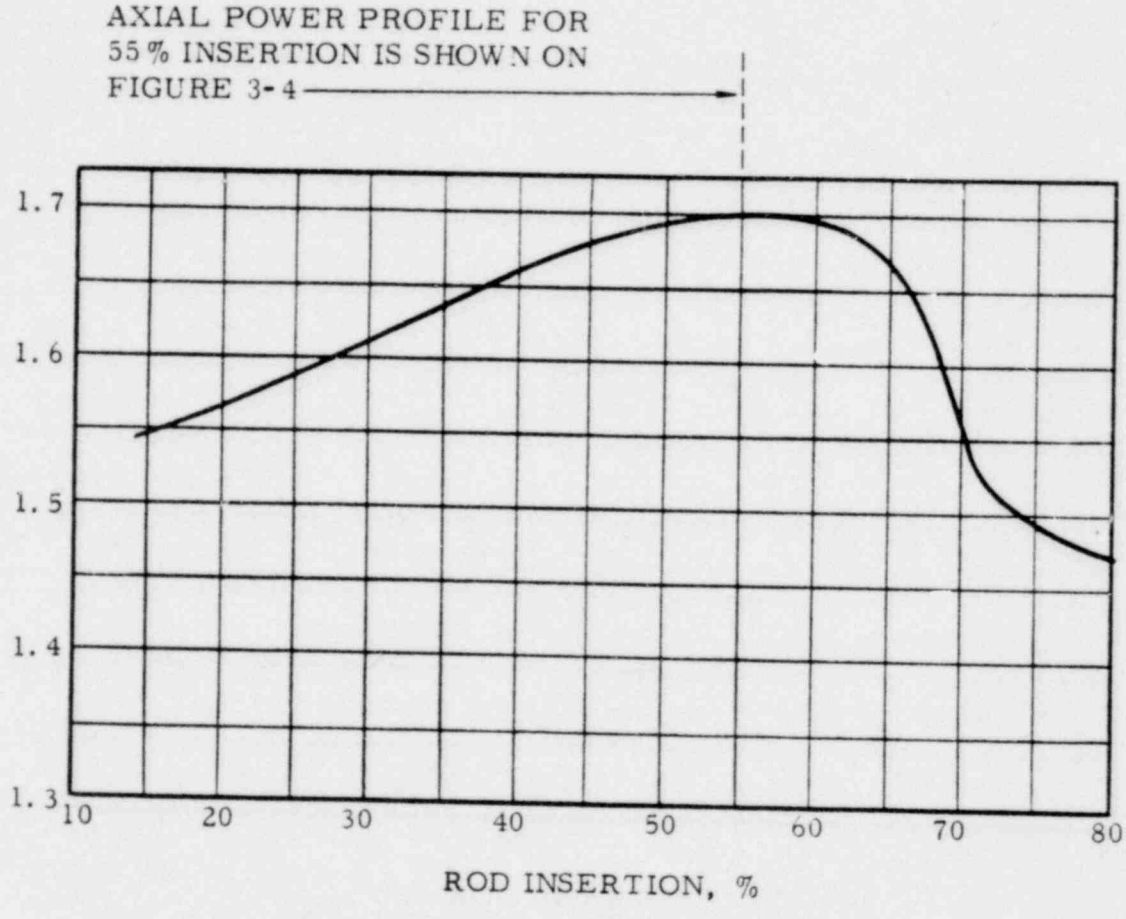

AXIAL PEAK TO AVERAGE POWER
VERSUS XENON OVERRIDE ROD INSERTION

OCONEE NUCLEAR STATION
FIGURE 3-3

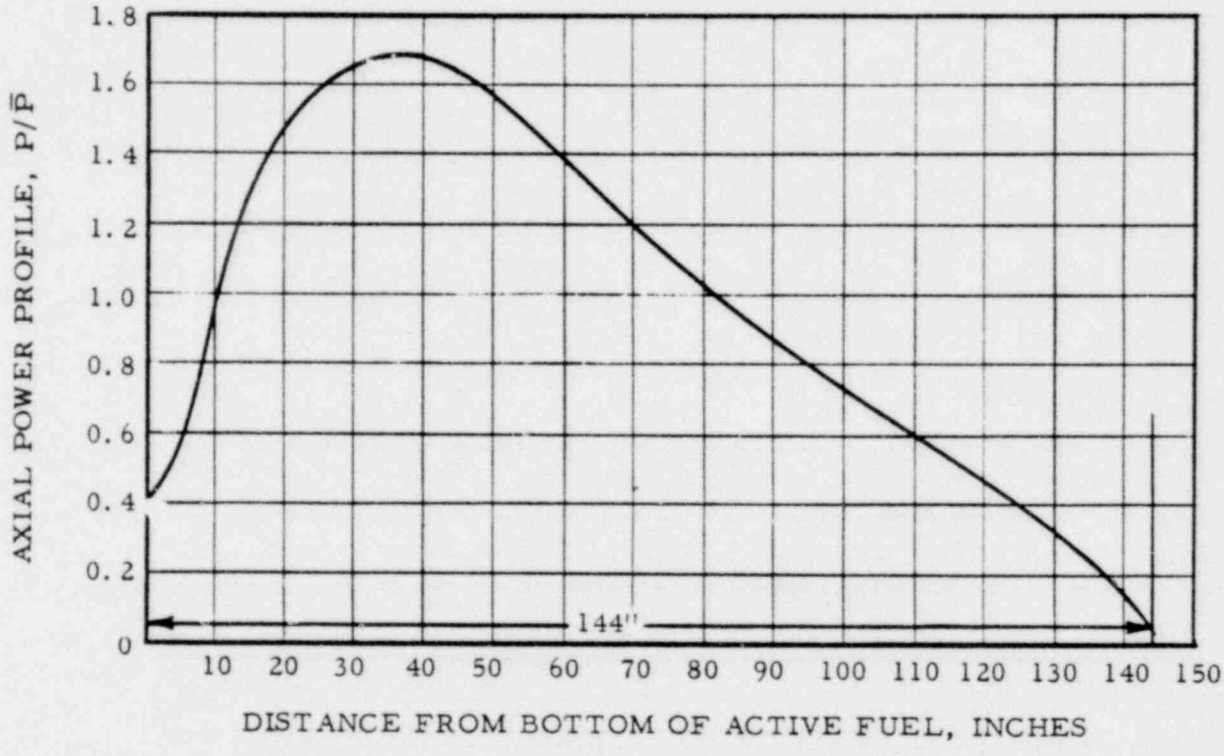

AXIAL POWER PROFILE
XENON OVERRIDE RODS 55 PER CENT INSERTED

OCONEE NUCLEAR STATION
FIGURE 3-4

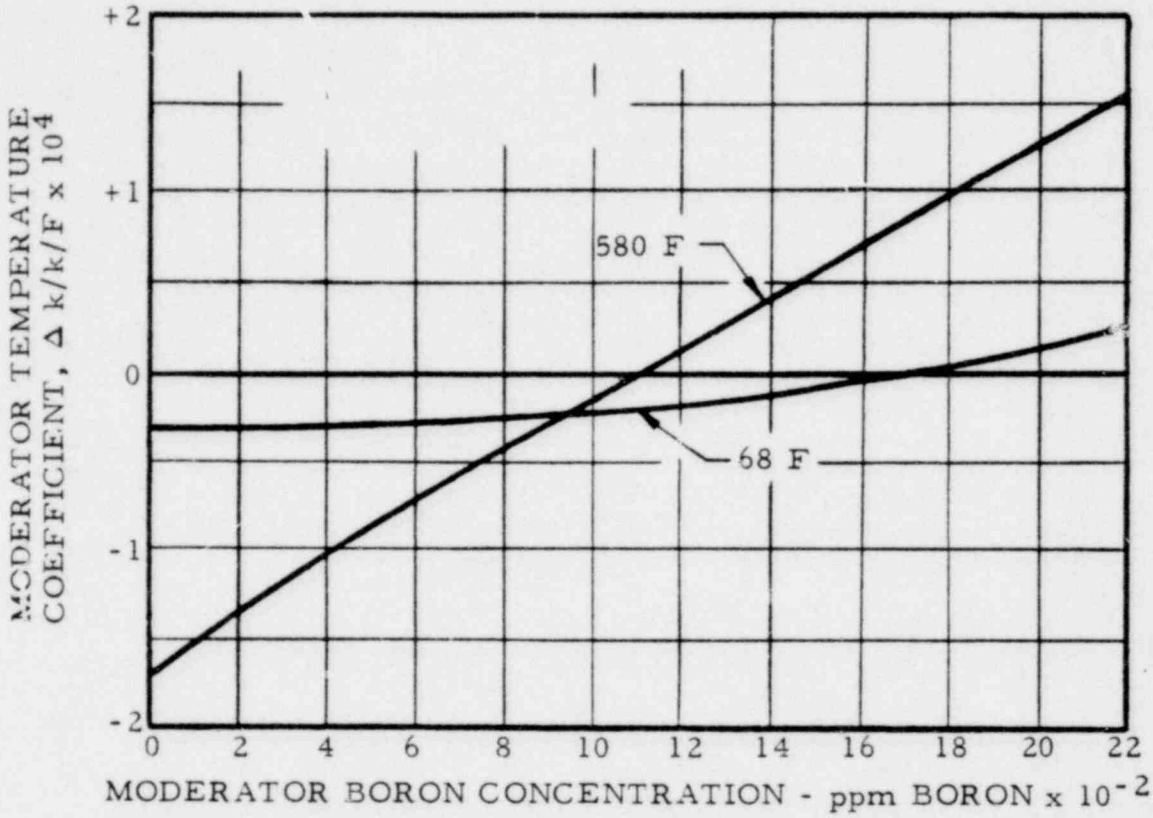

MODERATOR TEMPERATURE COEFFICIENTS
VERSUS BORON CONCENTRATION

OCONEE NUCLEAR STATION
FIGURE 3-5

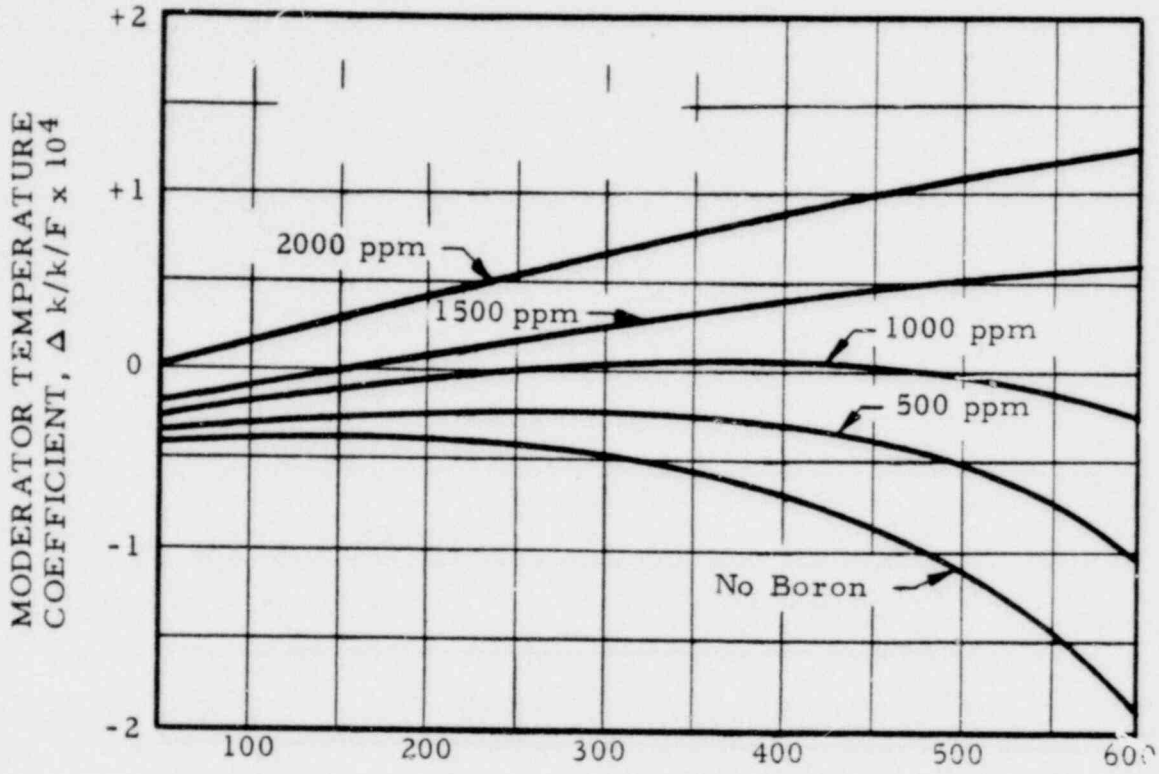

MODERATOR TEMPERATURE COEFFICIENTS VERSUS
MODERATOR TEMPERATURE AND VARIOUS BORON LEVELS

OCONEE NUCLEAR STATION
FIGURE 3-6

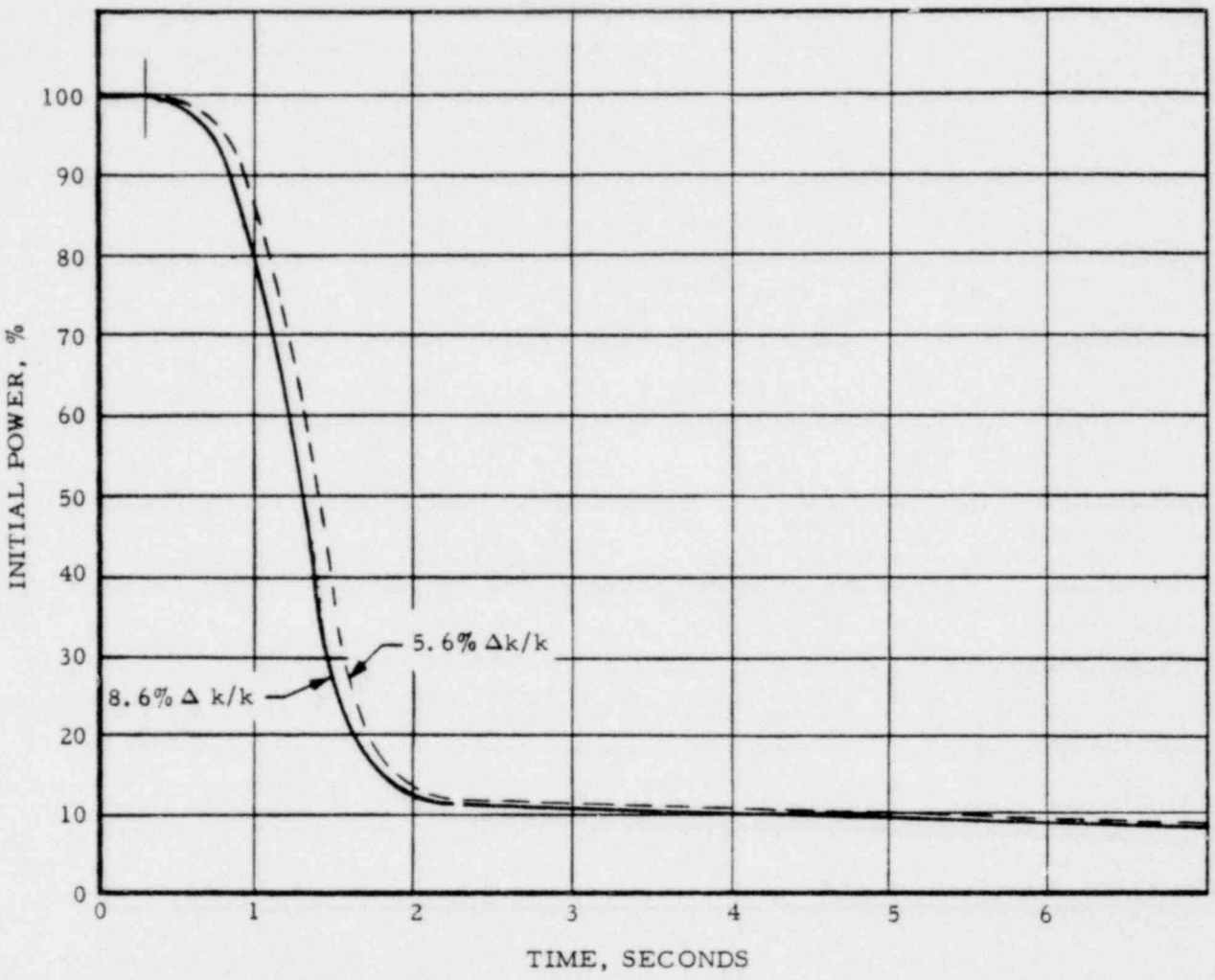

PER CENT INITIAL POWER VERSUS TIME FOLLOWING TRIP

DUKE POWER COMPANY

OCONEE NUCLEAR STATION

FIGURE 3-7

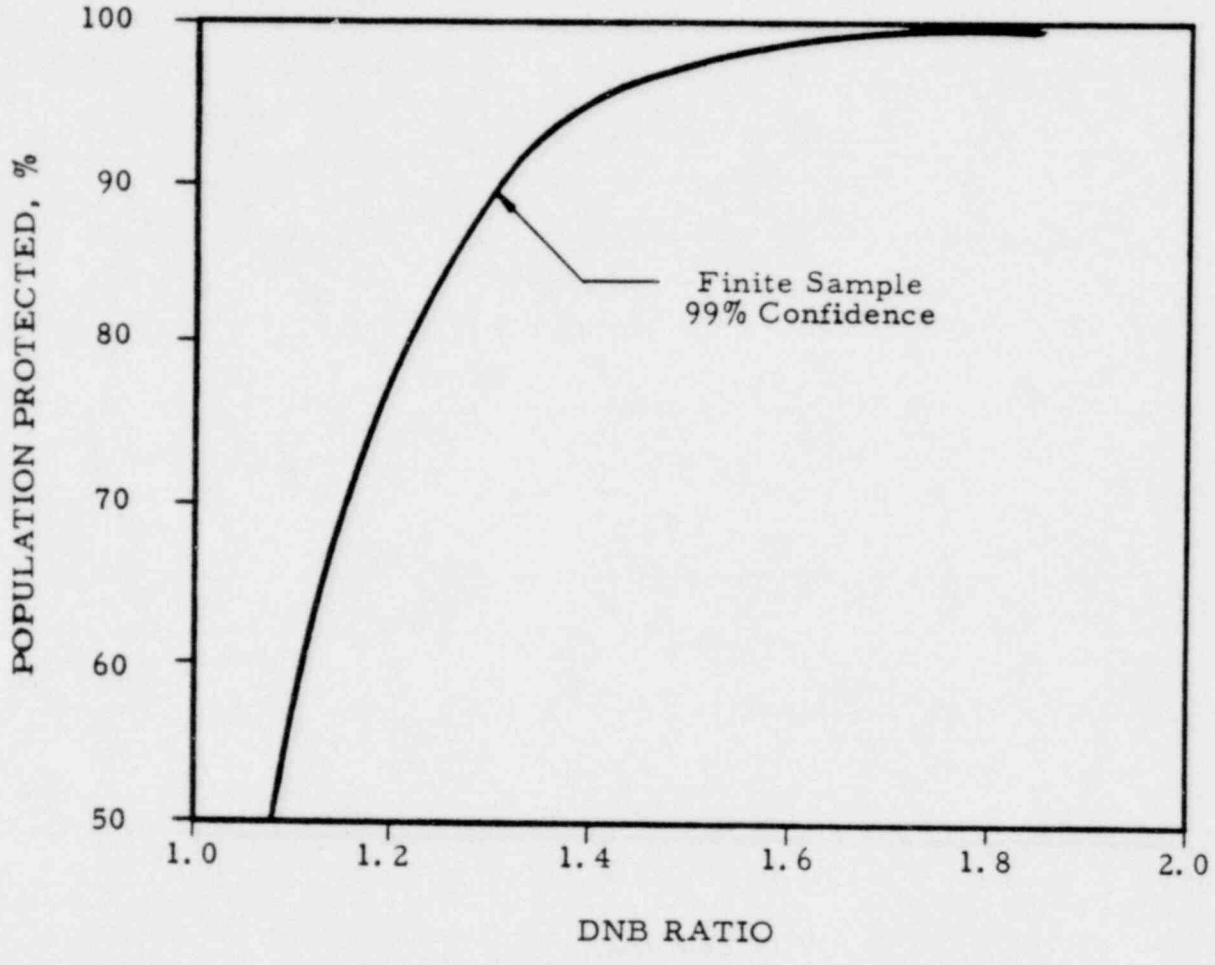

POPULATION INCLUDED IN THE STATISTICAL STATEMENT VERSUS DNB RATIO

OCONEE NUCLEAR STATION

FIGURE 3-8

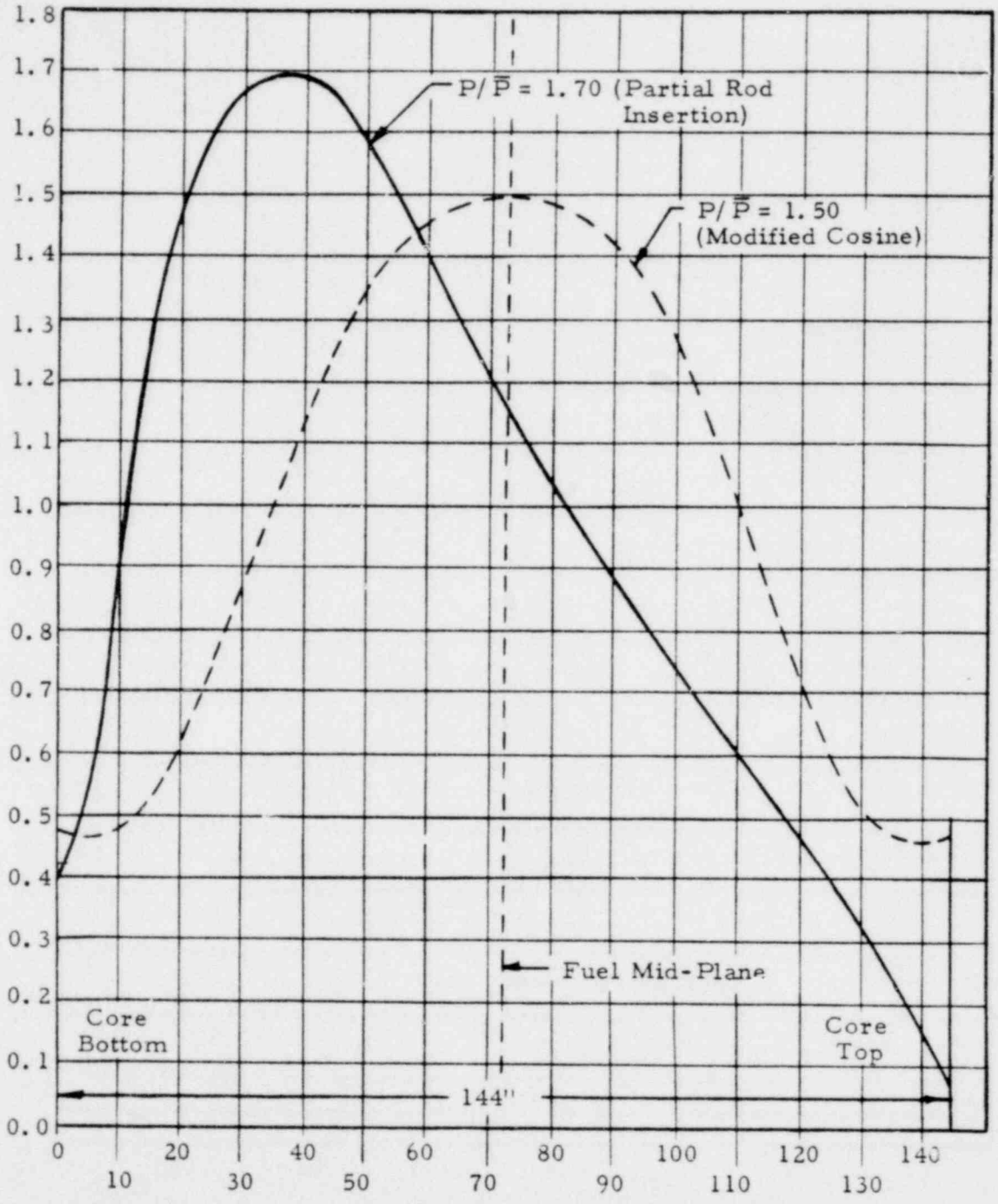

POWER SHAPE REFLECTING INCREASED
AXIAL POWER PEAK FOR 144 INCH CORE

OCONEE NUCLEAR STATION

FIGURE 3-9

00 00158246

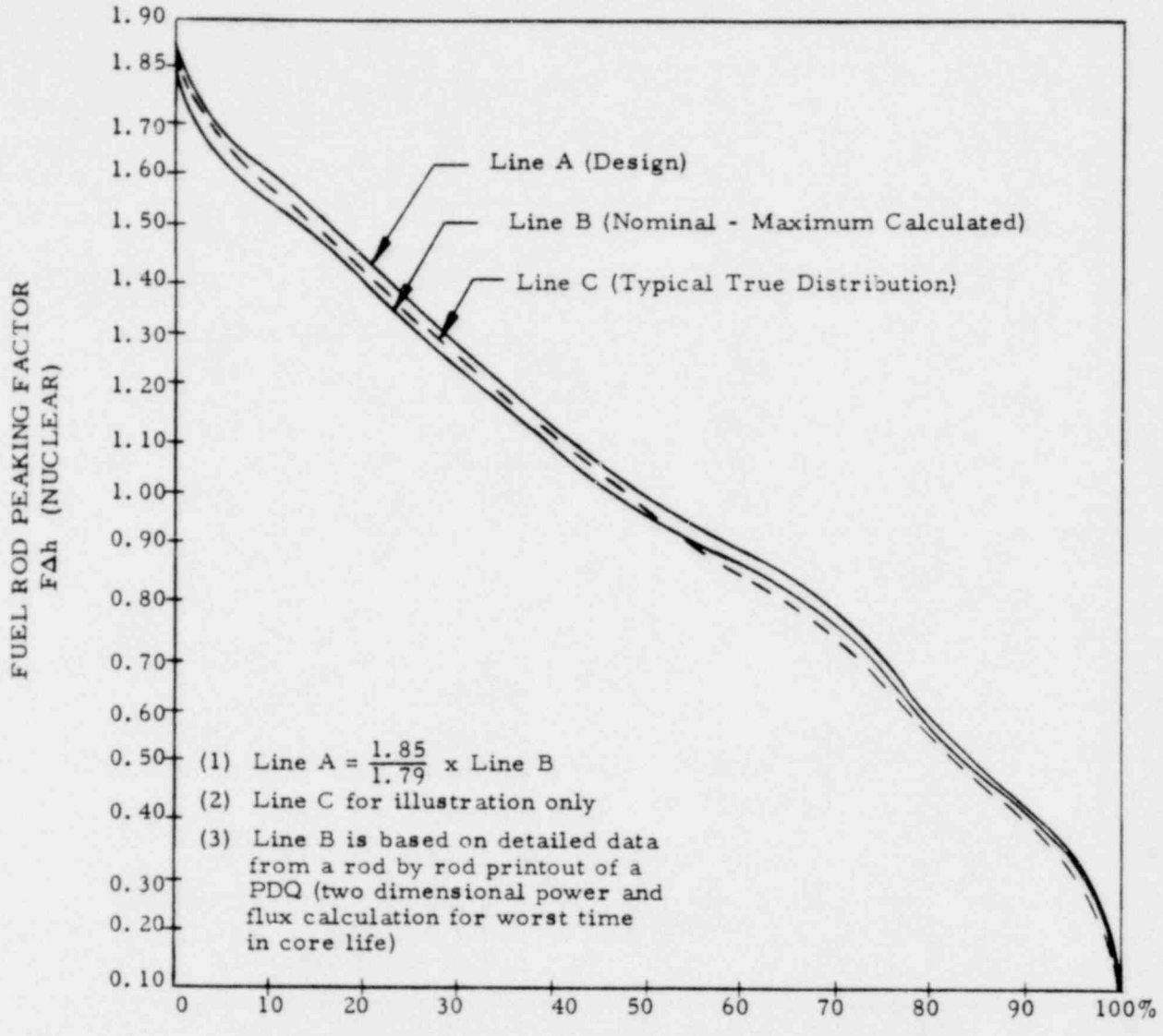

DISTRIBUTION OF FUEL ROD PEAKING

OCONEE NUCLEAR STATION

FIGURE 3-10

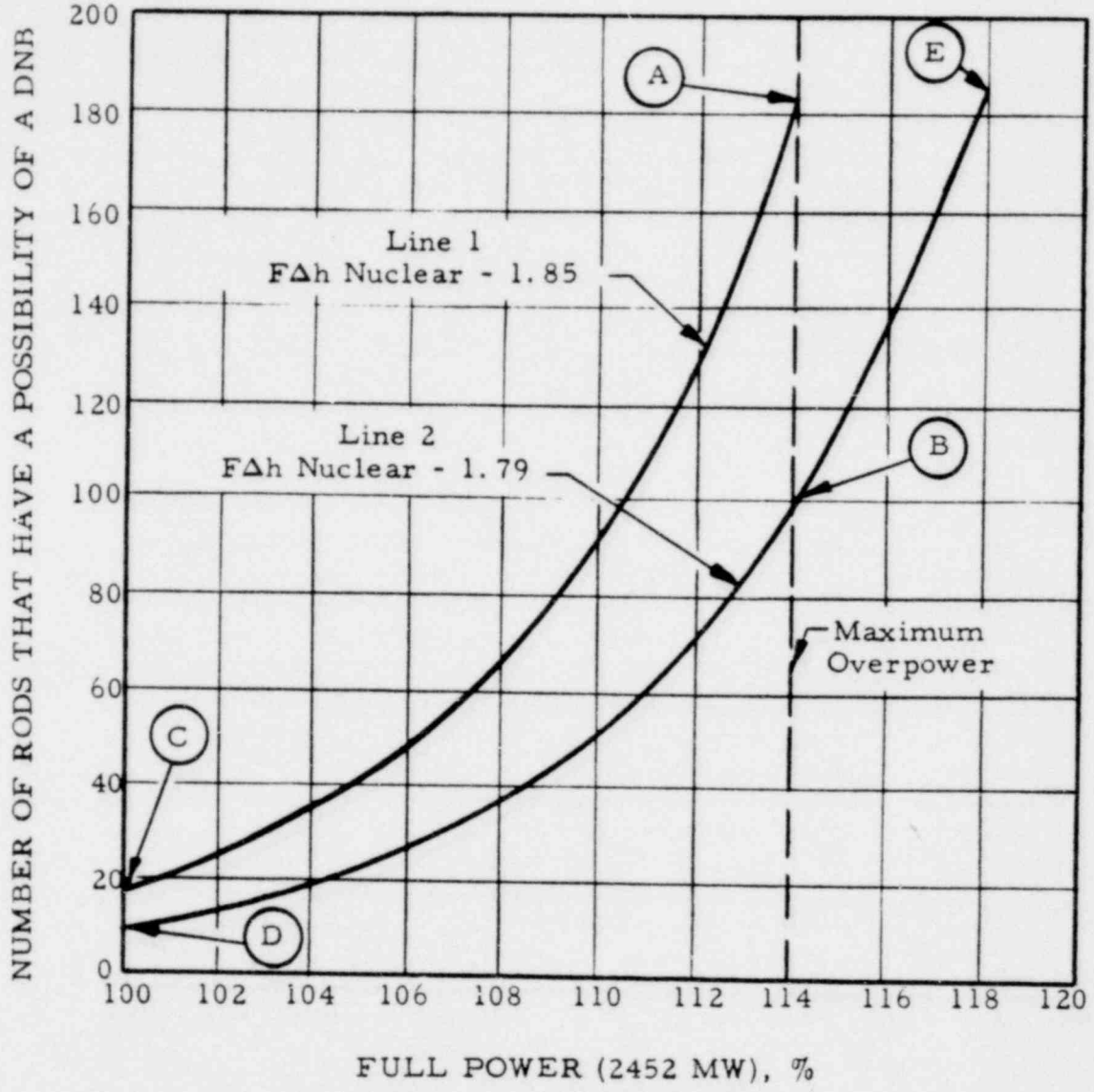

POSSIBLE FUEL ROD DNB'S FOR MAXIMUM
DESIGN CONDITIONS - 36,816 ROD CORE

OCONEE NUCLEAR STATION
FIGURE 3-11

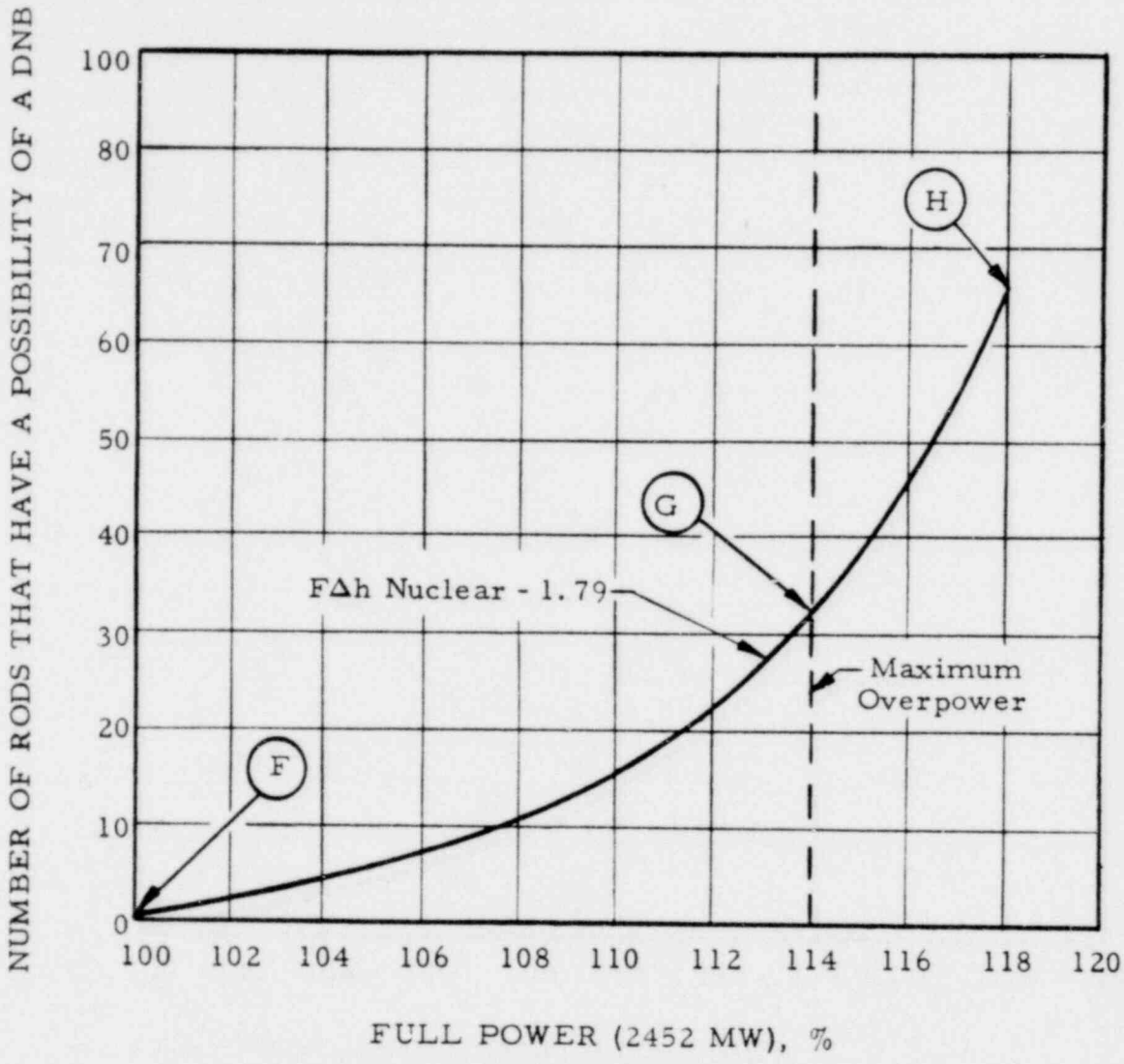

POSSIBLE FUEL ROD DNB'S FOR MOST PROBABLE CONDITIONS - 36,816 ROD CORE

OCONEE NUCLEAR STATION
FIGURE 3-12

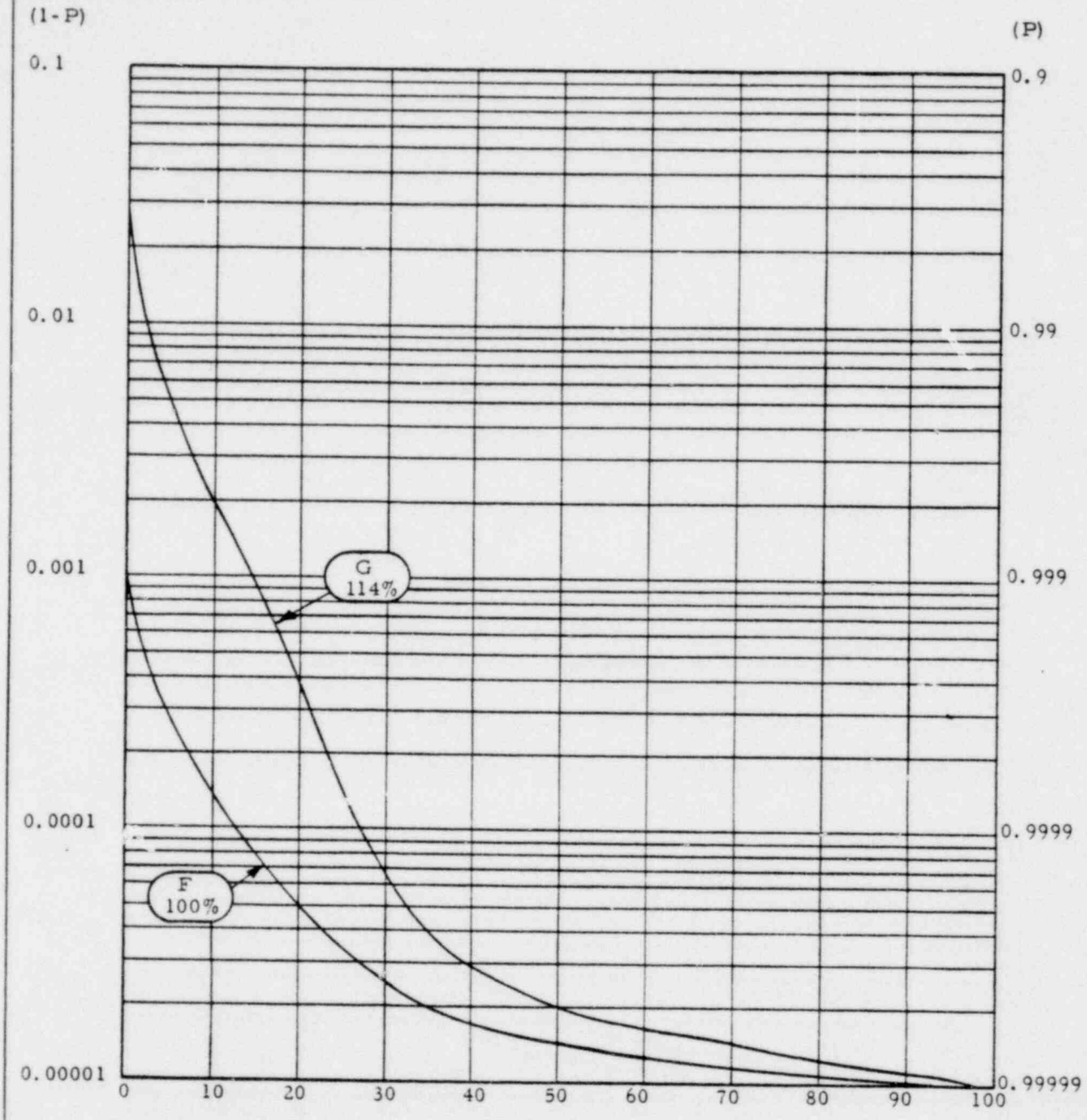

DISTRIBUTION OF POPULATION
PROTECTED P AND 1-P VERSUS NUMBER
RODS FOR MOST PROBABLE CONDITIONS

OCONEE NUCLEAR STATION
FIGURE 3-13

~~00 00160~~ 250

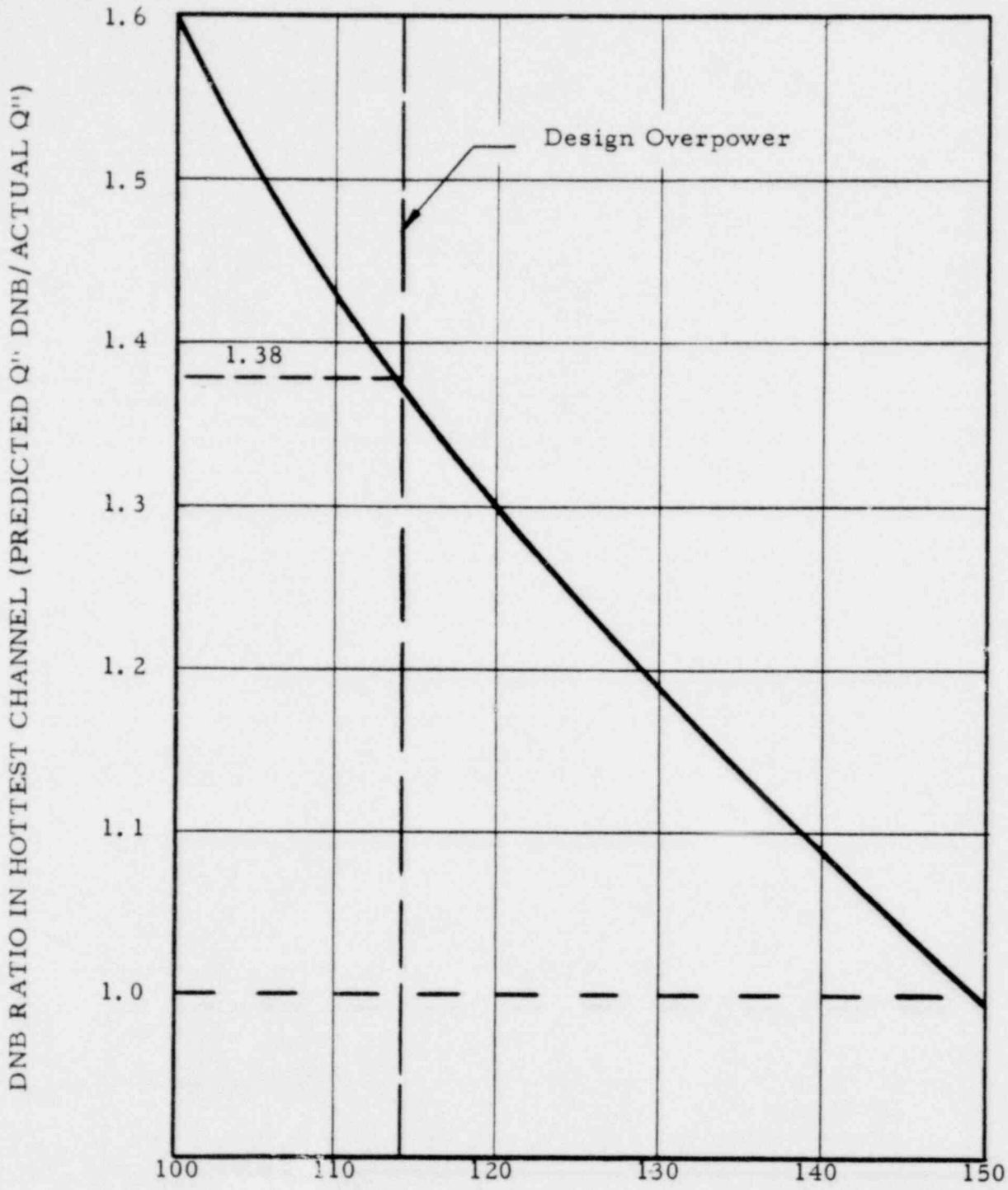

DNB RATIOS (BAW-168) VERSUS REACTOR POWER

OCONEE NUCLEAR STATION

FIGURE 3-14

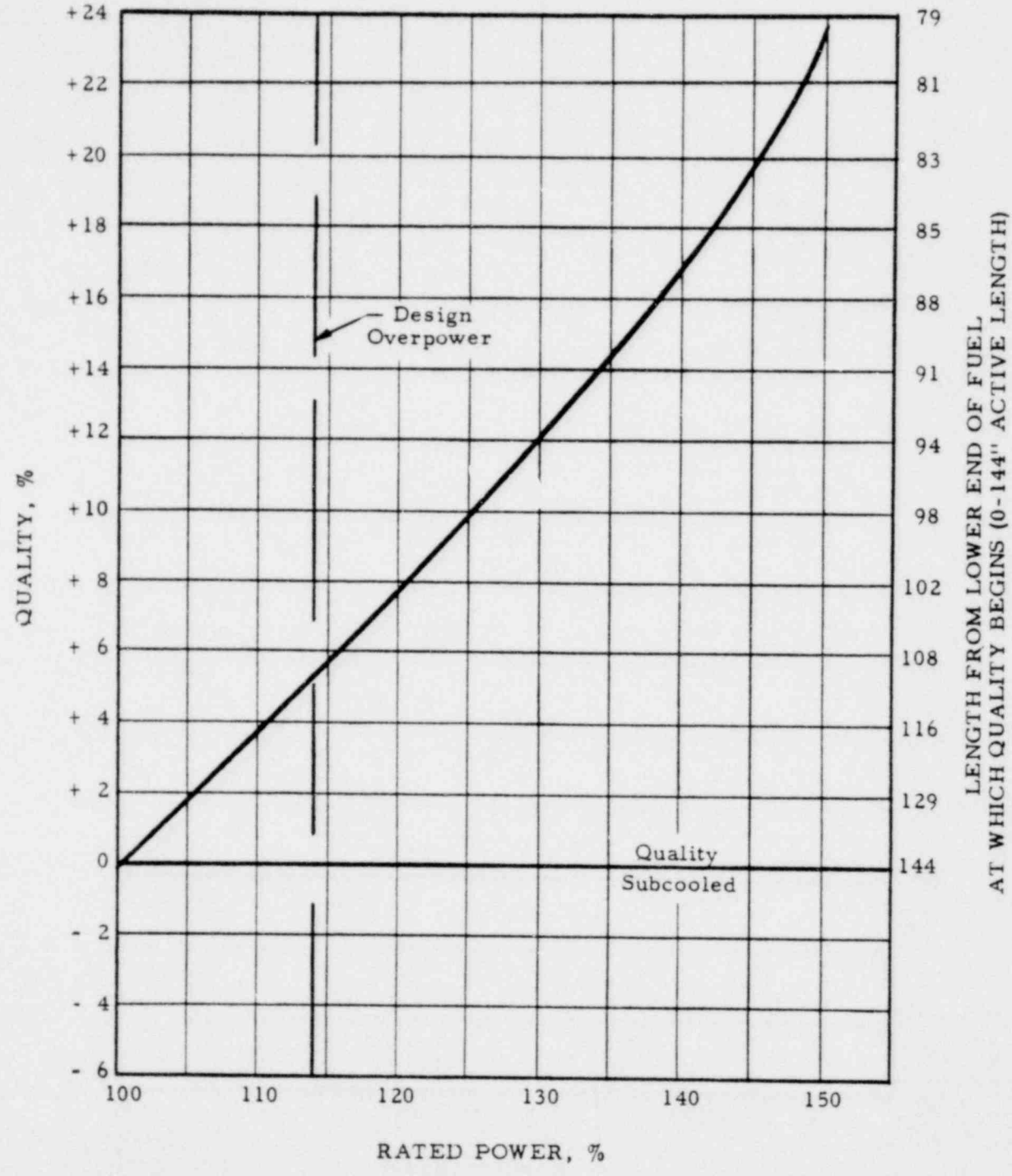

MAXIMUM HOT CHANNEL EXIT QUALITY
VERSUS REACTOR OVERPOWER

OCONEE NUCLEAR STATION
FIGURE 3-15

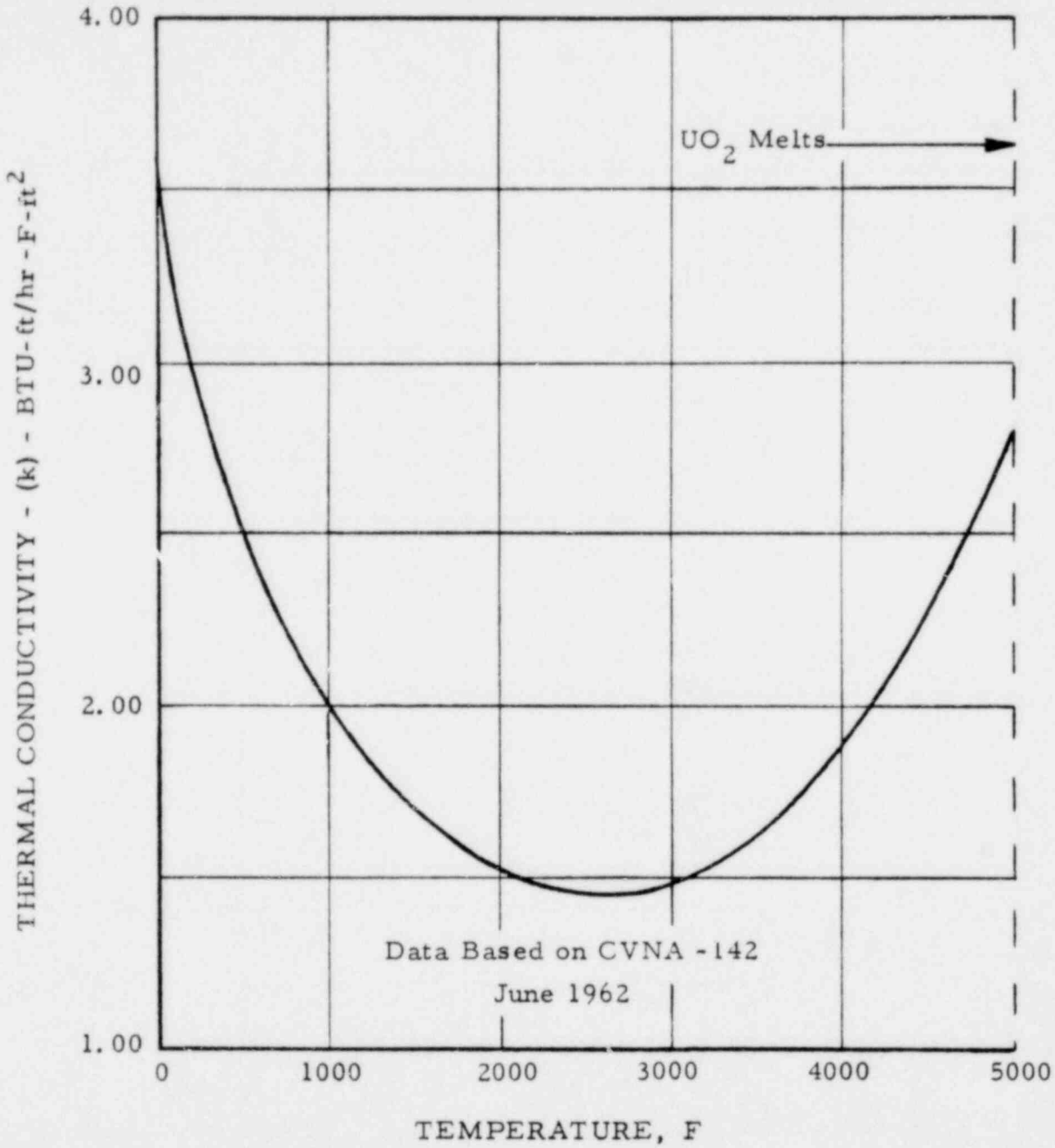

THERMAL CONDUCTIVITY OF UO_2

OCONEE NUCLEAR STATION
FIGURE 3-16

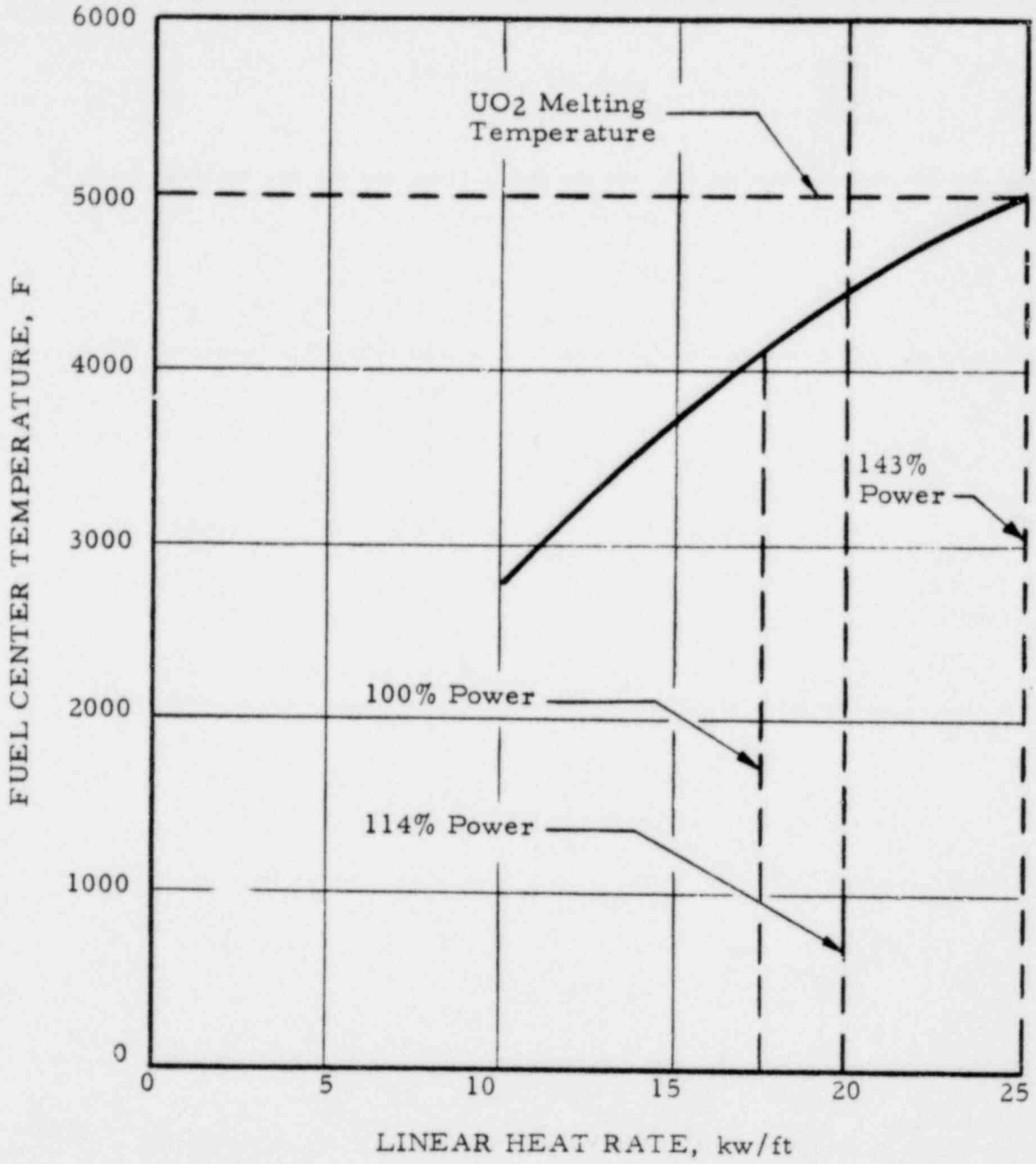

FIGURE 3-17

FUEL CENTER TEMPERATURE AT THE HOT SPOT VERSUS LINEAR POWER

OCONEE NUCLEAR STATION
FIGURE 3-17

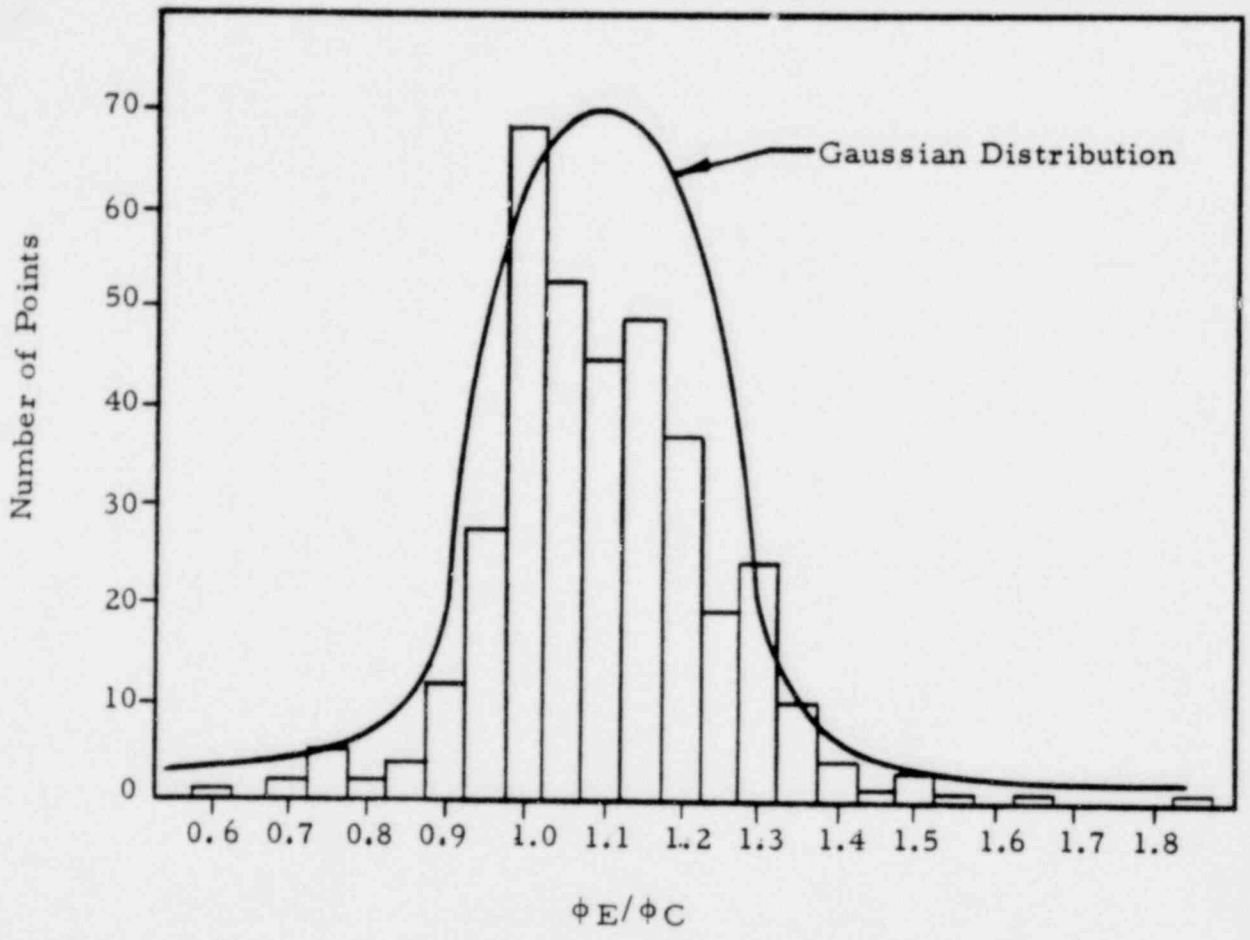

NUMBER OF DATA POINTS VERSUS $\phi E/\phi C$

OCONEE NUCLEAR STATION

FIGURE 3-18

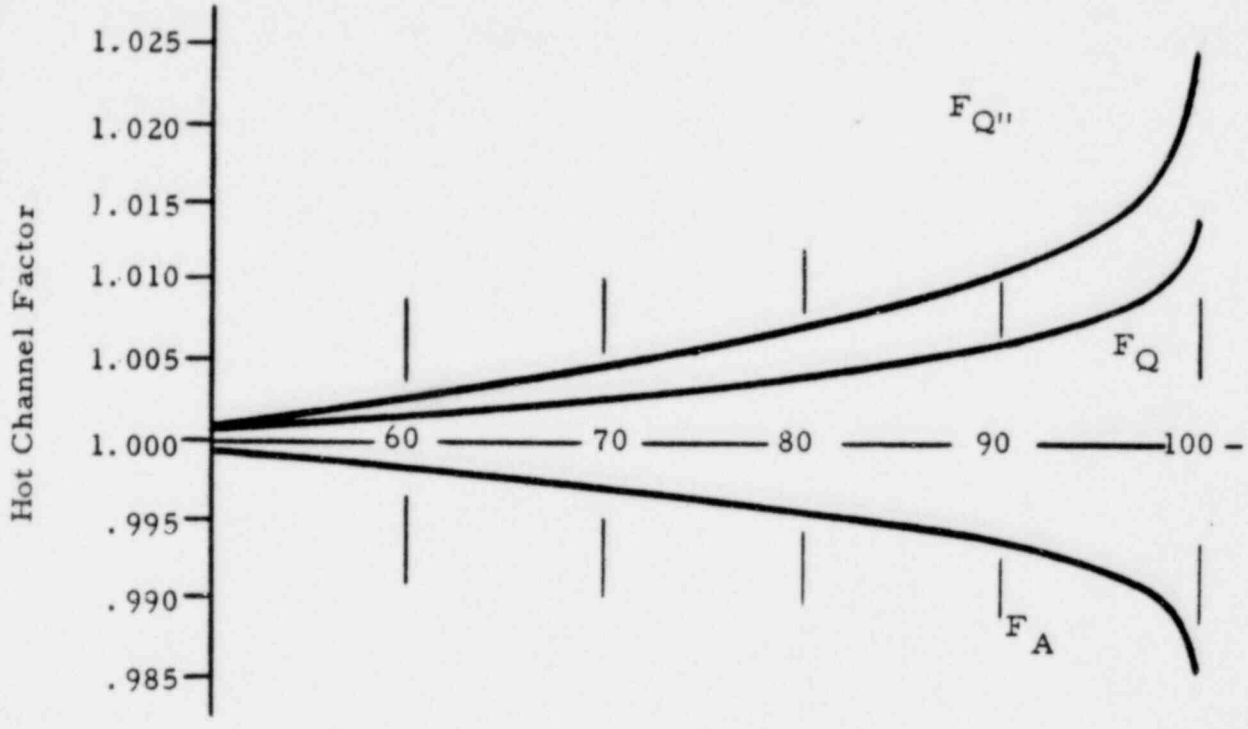

HOT CHANNEL FACTOR VERSUS PER CENT POPULATION PROTECTED

DUKE POWER COMPANY

OCONEE NUCLEAR STATION

FIGURE 3-19

00-00163

256

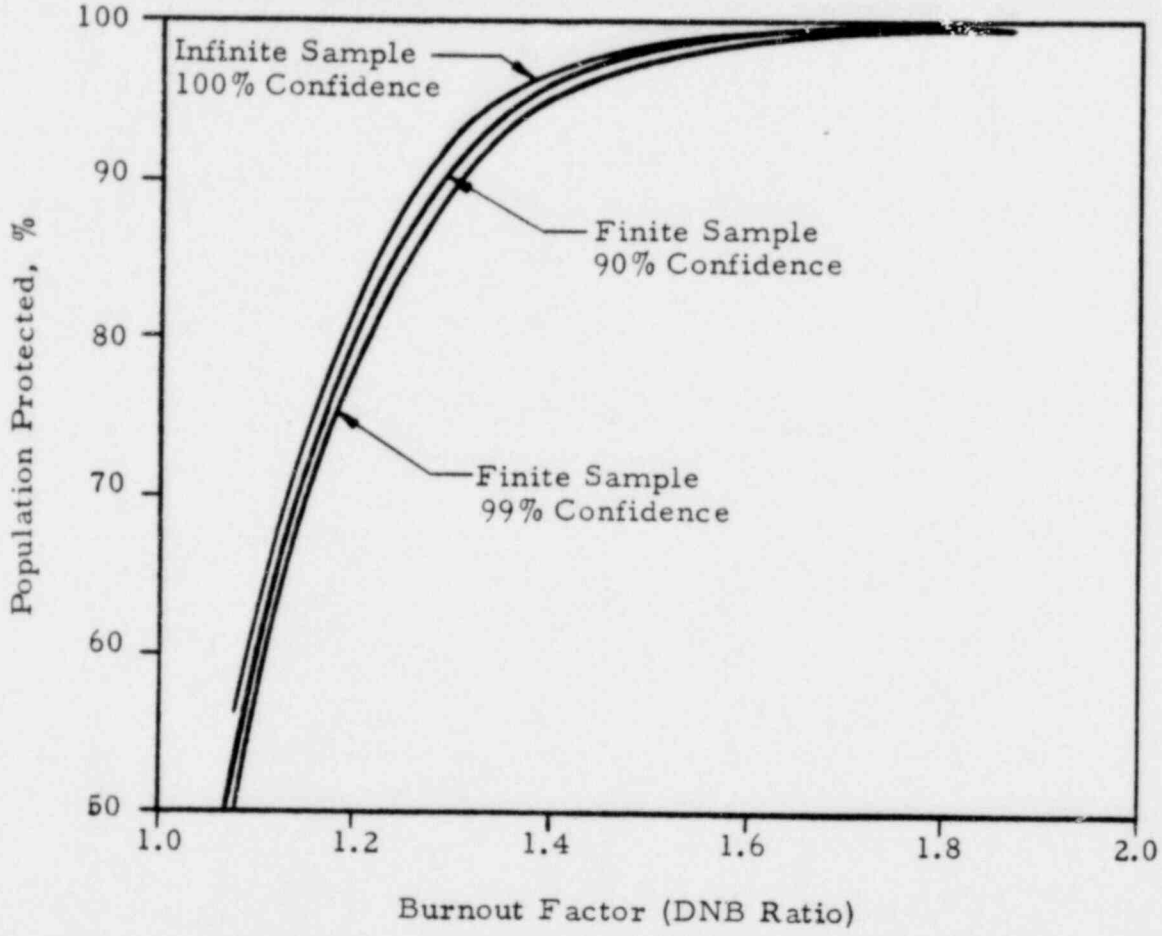

BURNOUT FACTOR VERSUS POPULATION
FOR VARIOUS CONFIDENCE LEVELS

OCONEE NUCLEAR STATION
FIGURE 3-20

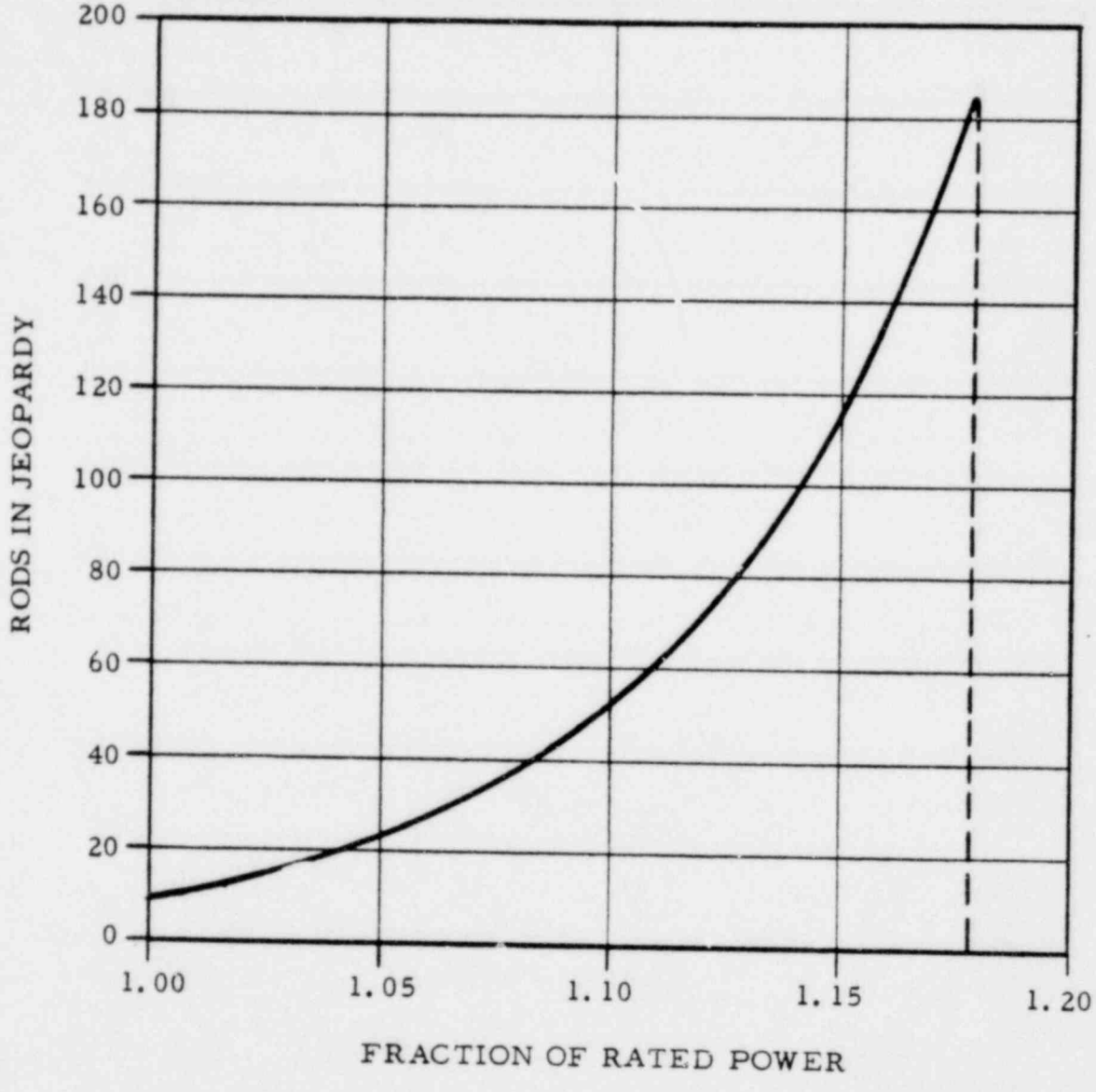

RODS IN JEOPARDY VERSUS POWER

OCONEE NUCLEAR STATION
FIGURE 3-21

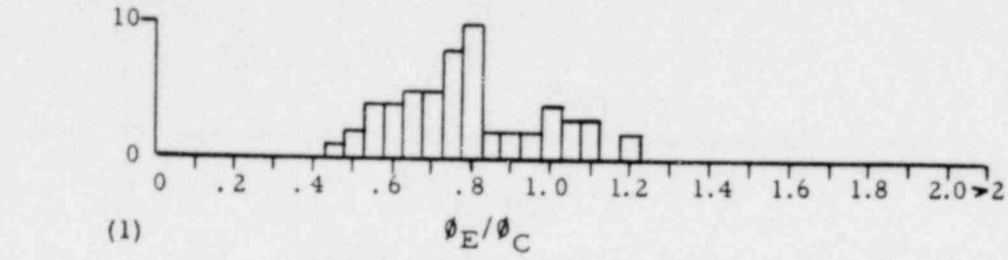

WAPD-188 500 psia Data and BAW-168

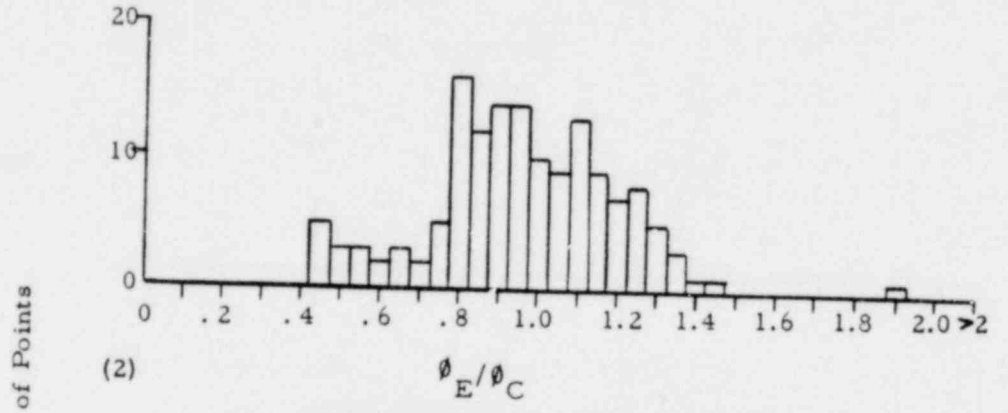

WAPD-188 600 psia Data and BAW-168

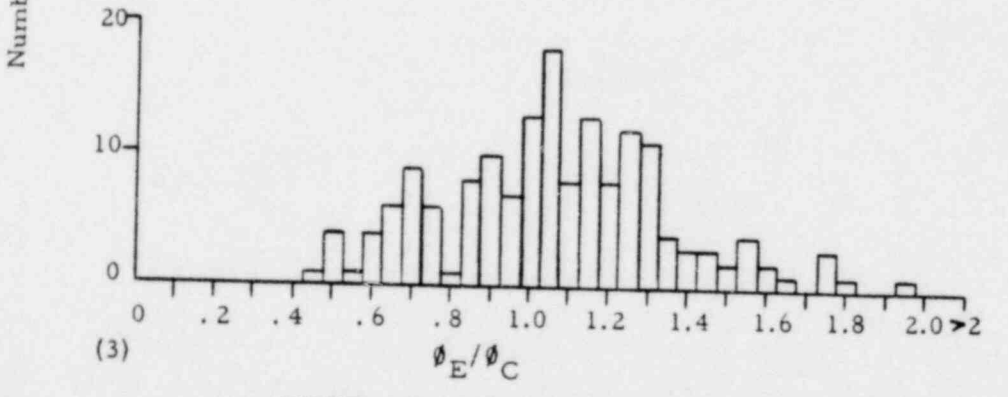

WAPD-188 1000 psia Data and BAW-168

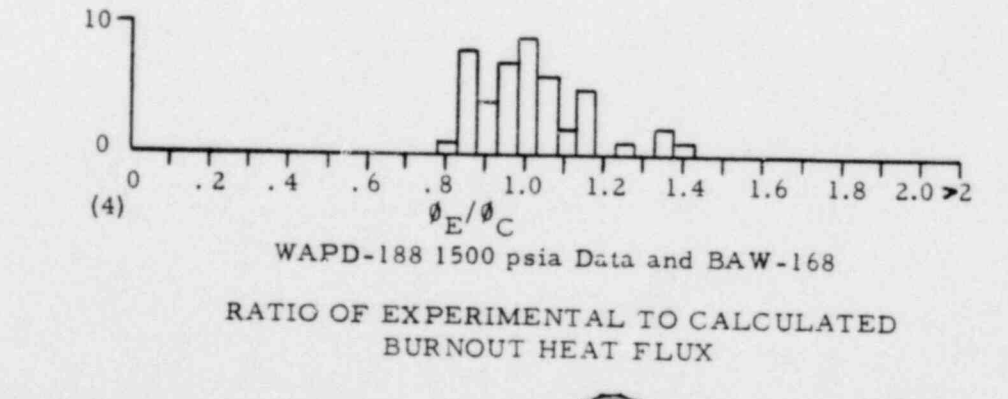

WAPD-188 1500 psia Data and BAW-168

Number of Points

RATIO OF EXPERIMENTAL TO CALCULATED
BURNOUT HEAT FLUX

OCONEE NUCLEAR STATION

FIGURE 3-22

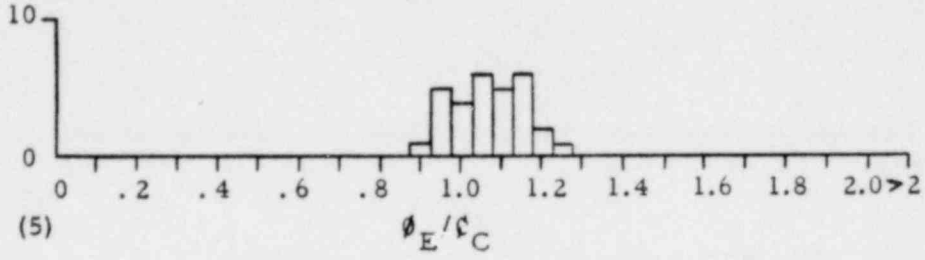

WAPD-188 1750 psia Data and BAW-168

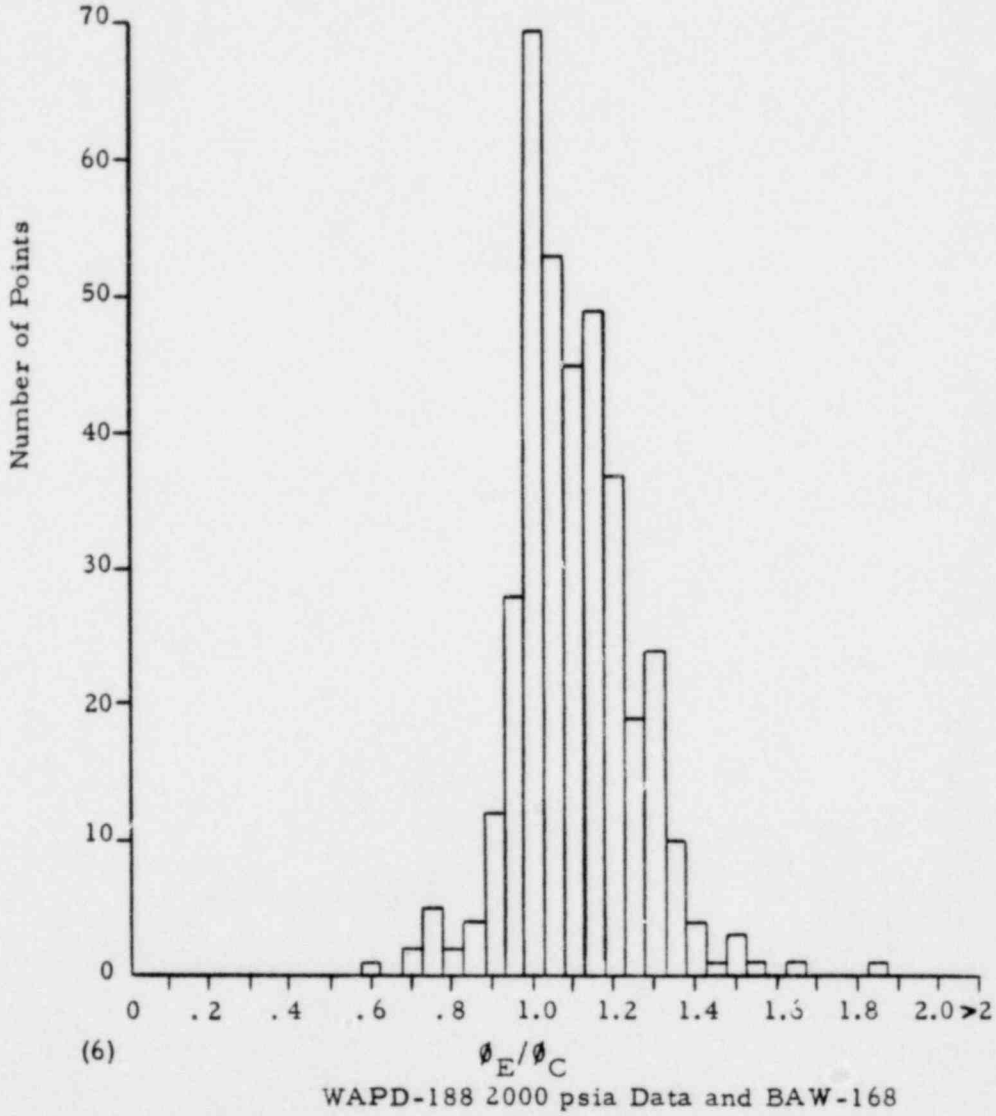

WAPD-188 2000 psia Data and BAW-168

RATIO OF EXPERIMENTAL TO CALCULATED
BURNOUT HEAT FLUX

OCONEE NUCLEAR STATION
FIGURE 3-23

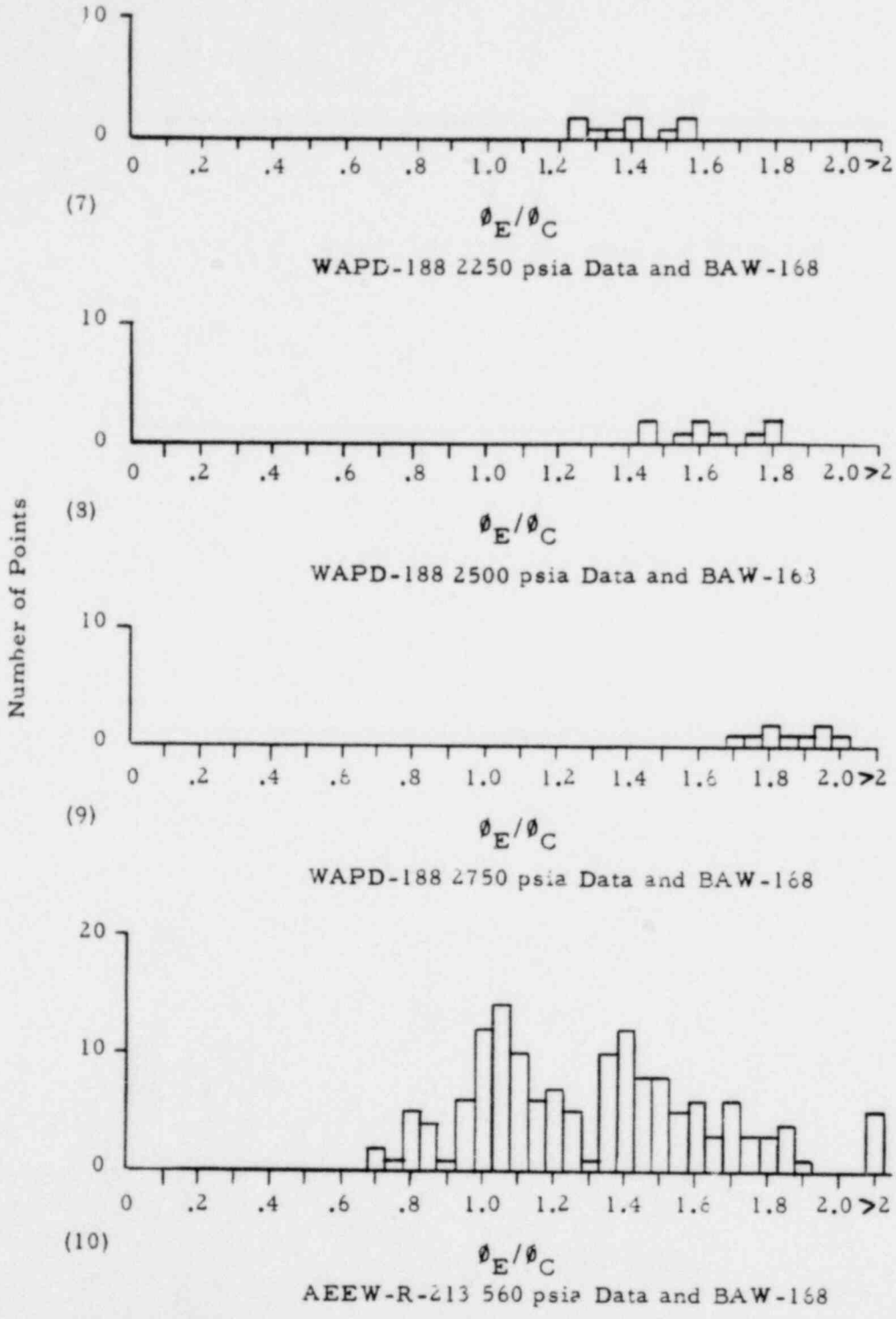

RATIO OF EXPERIMENTAL TO CALCULATED
BURNOUT HEAT FLUX

DUKE POWER COMPANY

OCONEE NUCLEAR STATION

FIGURE 3-24

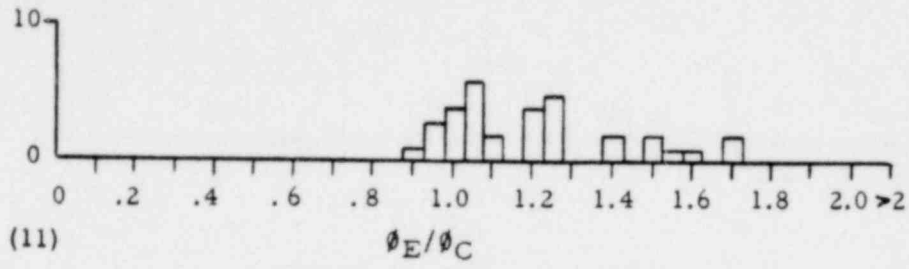

AEEW-R-213 720 psia Data and BAW-168

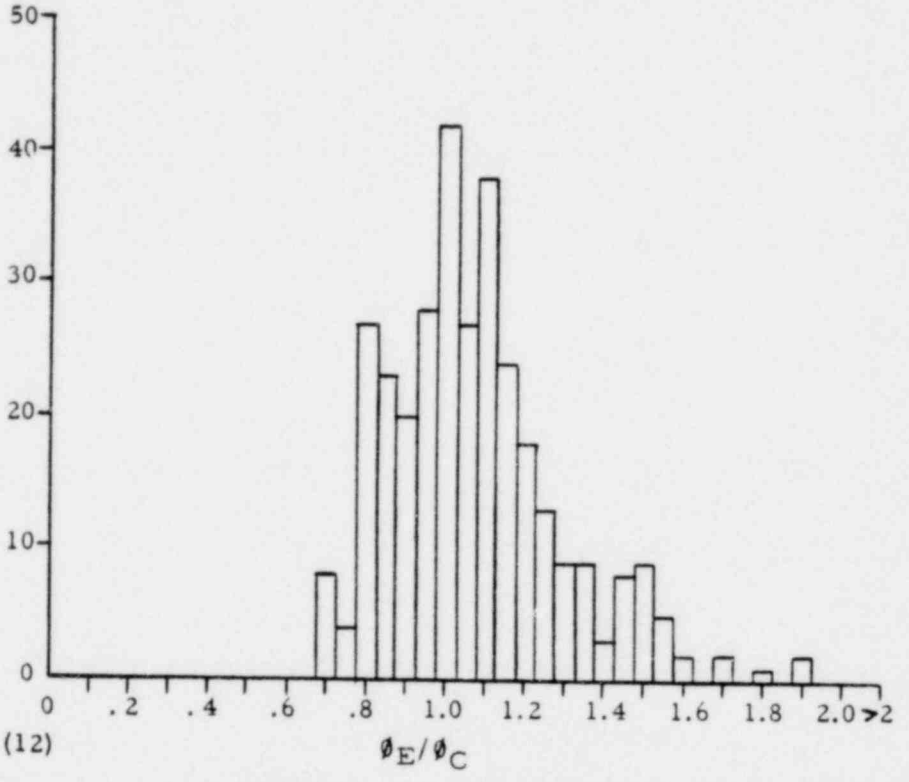

AEEW-R-213 1000 psia Data and BAW-168

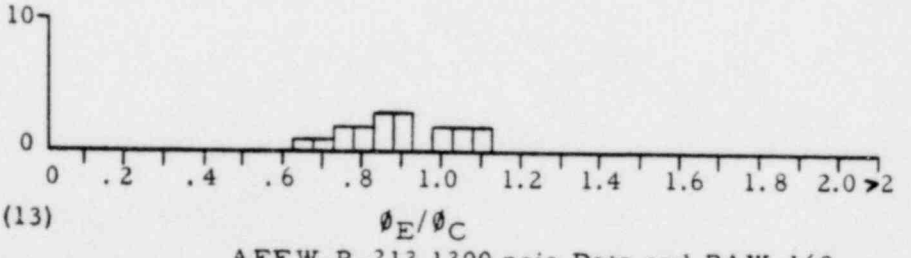

AEEW-R-213 1300 psia Data and BAW-168

RATIO OF EXPERIMENTAL TO CALCULATED
BURNOUT HEAT FLUX

OCONEE NUCLEAR STATION

FIGURE 3-25

00 00166267

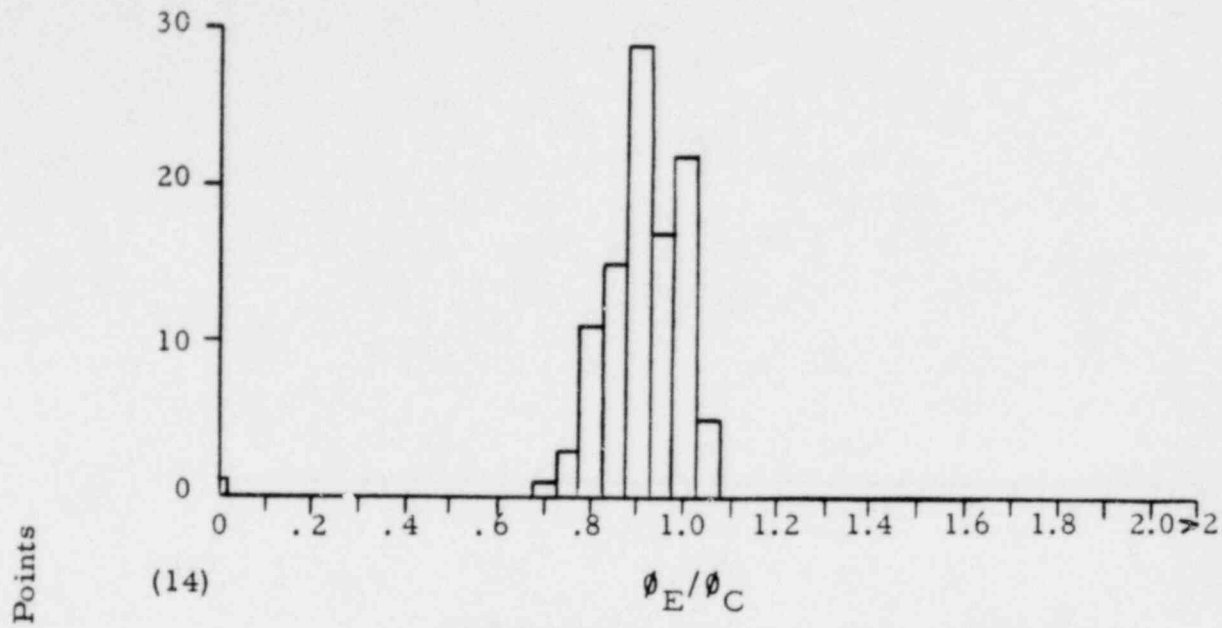

AEEW-R-213 1500 psia Data and BAW-168

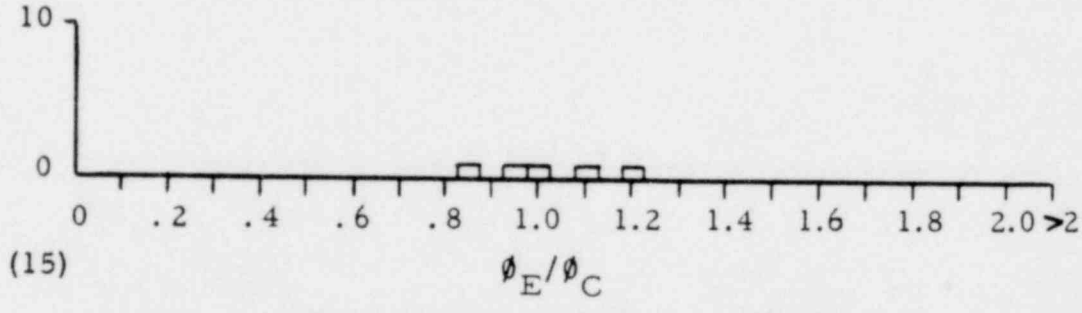

Columbia 500 psia Data and BAW-168

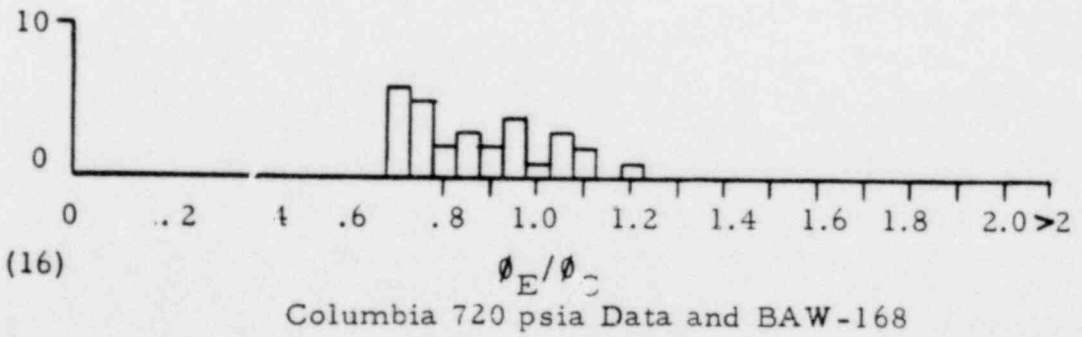

Columbia 720 psia Data and BAW-168

RATIO OF EXPERIMENTAL TO CALCULATED BURNOUT HEAT FLUX

DUKE POWER CITIZENSHIP SERVICE

OCONEE NUCLEAR STATION

FIGURE 3-26

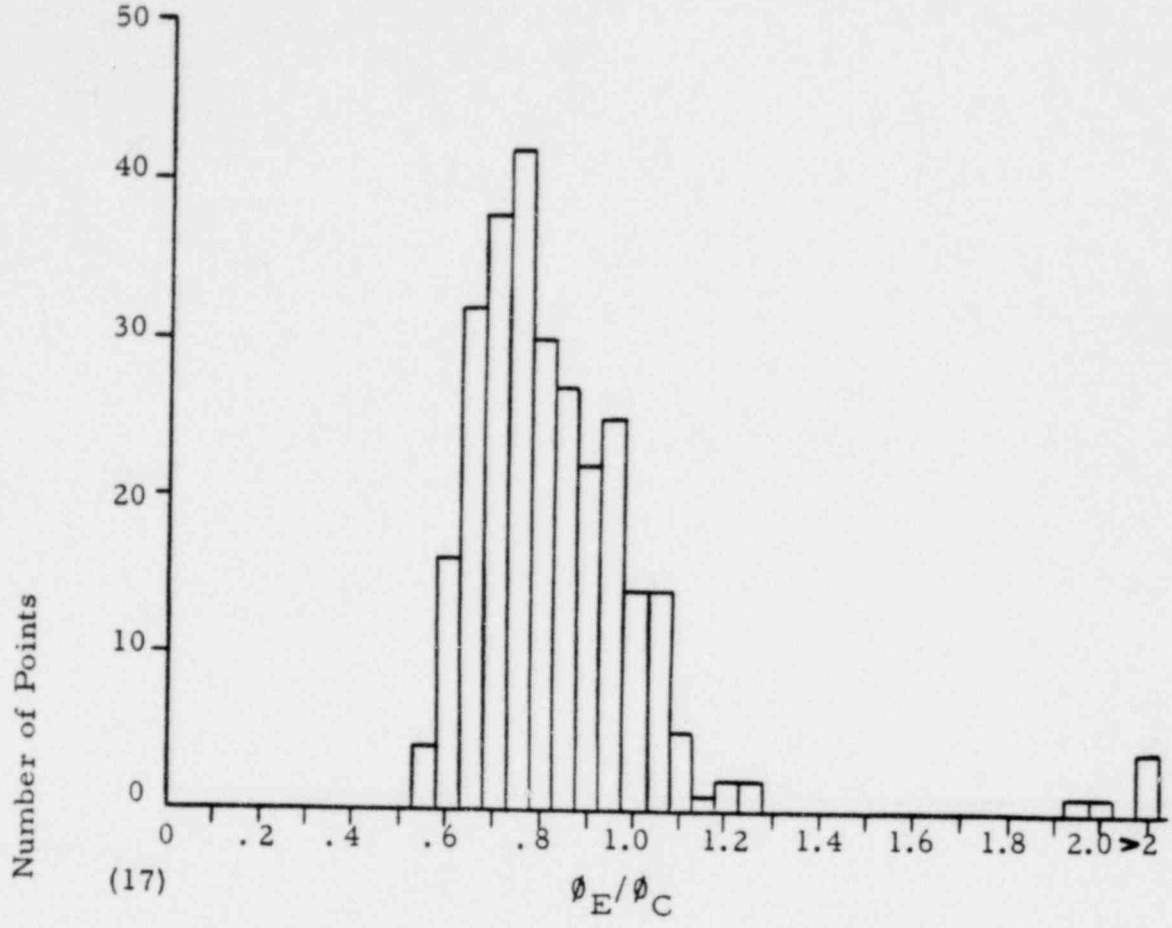

Columbia 1000 psia Data and BAW-168

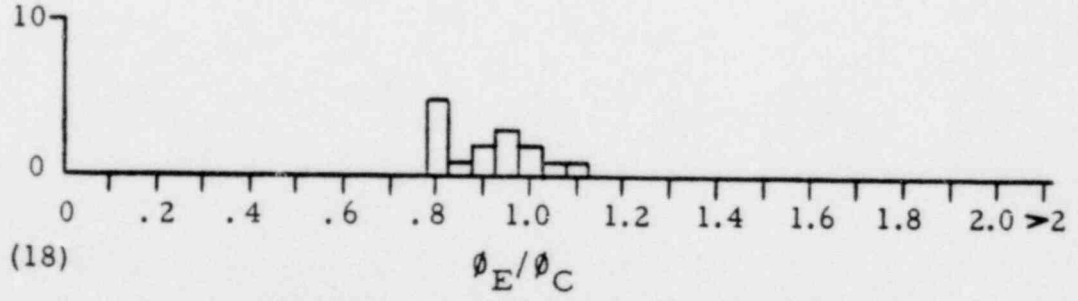

Columbia 1200 psia Data and BAW-168

RATIO OF EXPERIMENTAL TO
CALCULATED BURNOUT HEAT FLUX

OCONEE NUCLEAR STATION

FIGURE 3-27

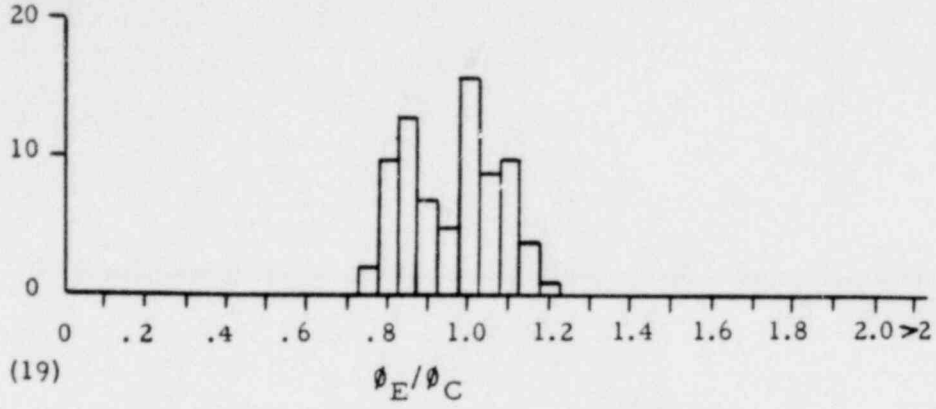

Columbia 1500 psia Data and BAW-168

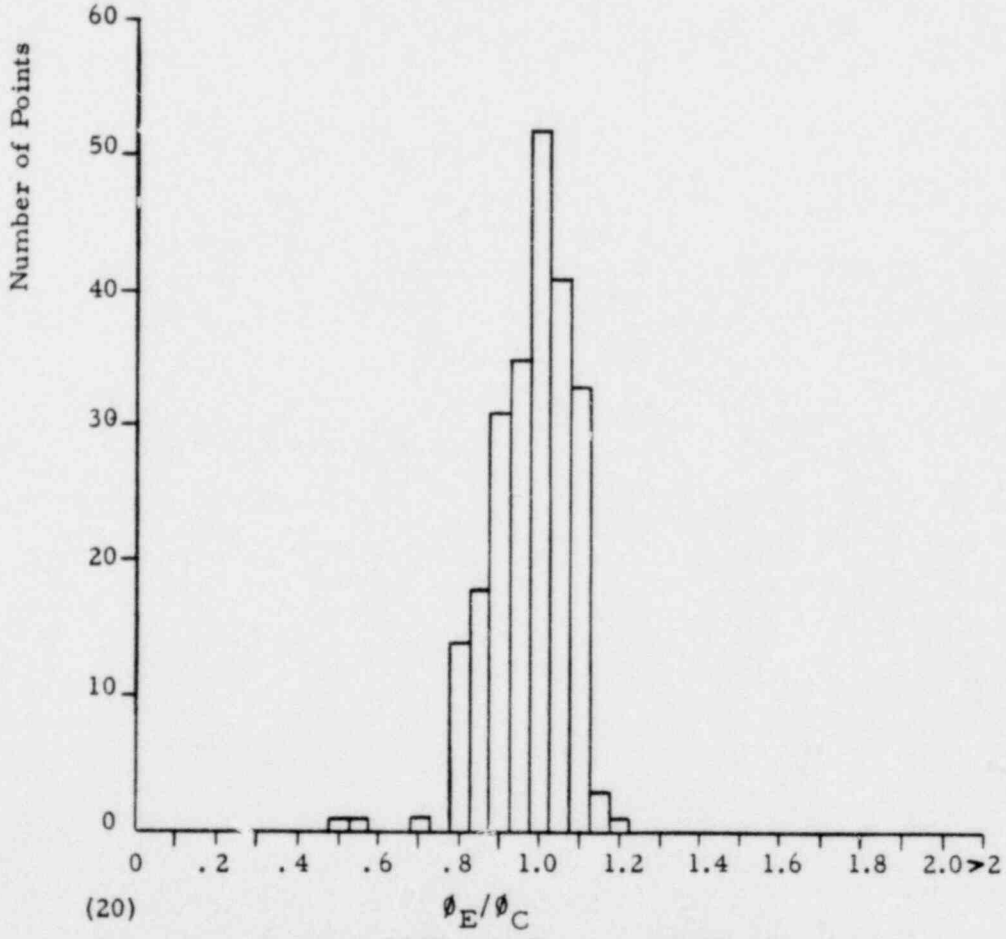

Argonne 2000 psia Data and BAW-168

RATIO OF EXPERIMENTAL TO CALCULATED
BURNOUT HEAT FLUX

OCONEE NUCLEAR STATION
FIGURE 3-28

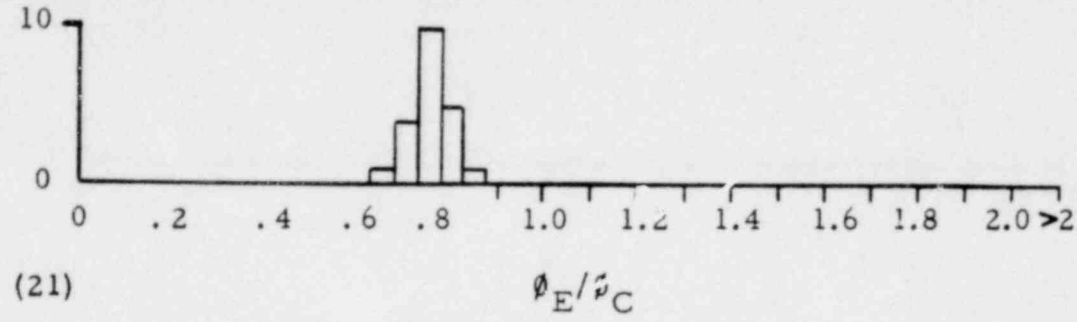

B&W 2000 psia Data and BAW-168

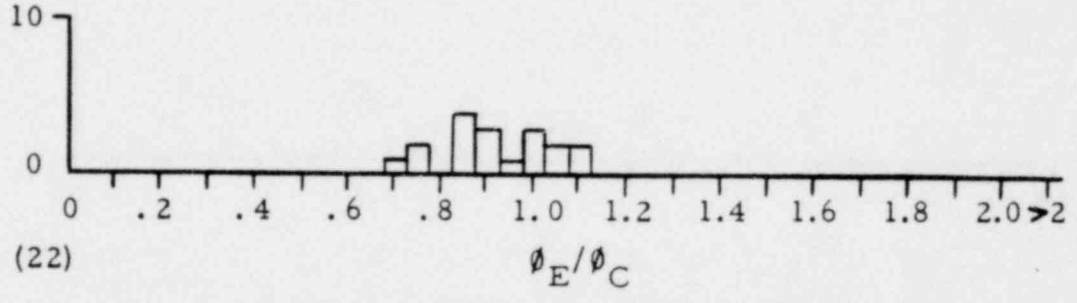

Euratom 1000 psia Data and BAW-168

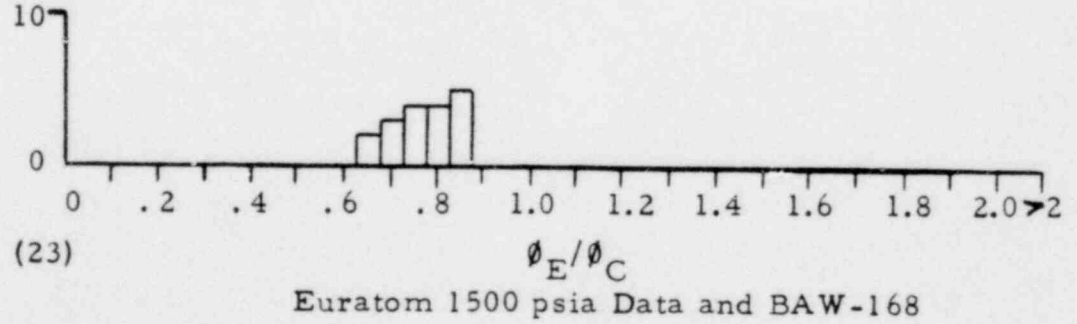

Euratom 1500 psia Data and BAW-168

RATIO OF EXPERIMENTAL TO CALCULATED BURNOUT HEAT FLUX

DUKE POWER SERVICE

OCONEE NUCLEAR STATION

FIGURE 3-29

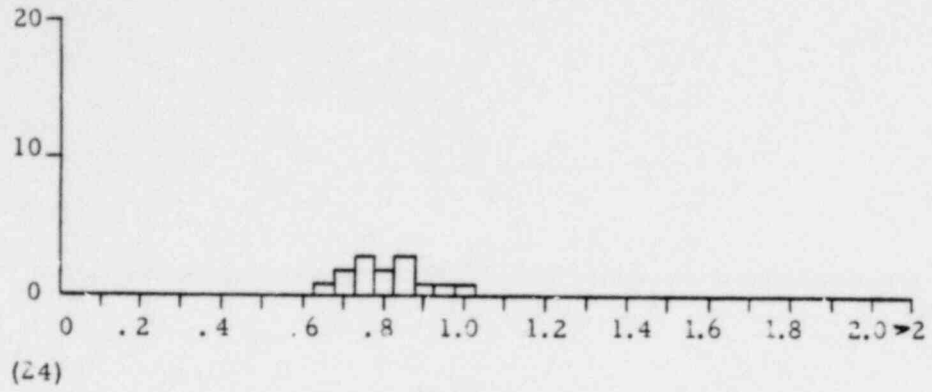

(24)

ϕ_E/ϕ_C

Euratom 2000 psia Data and BAW-168

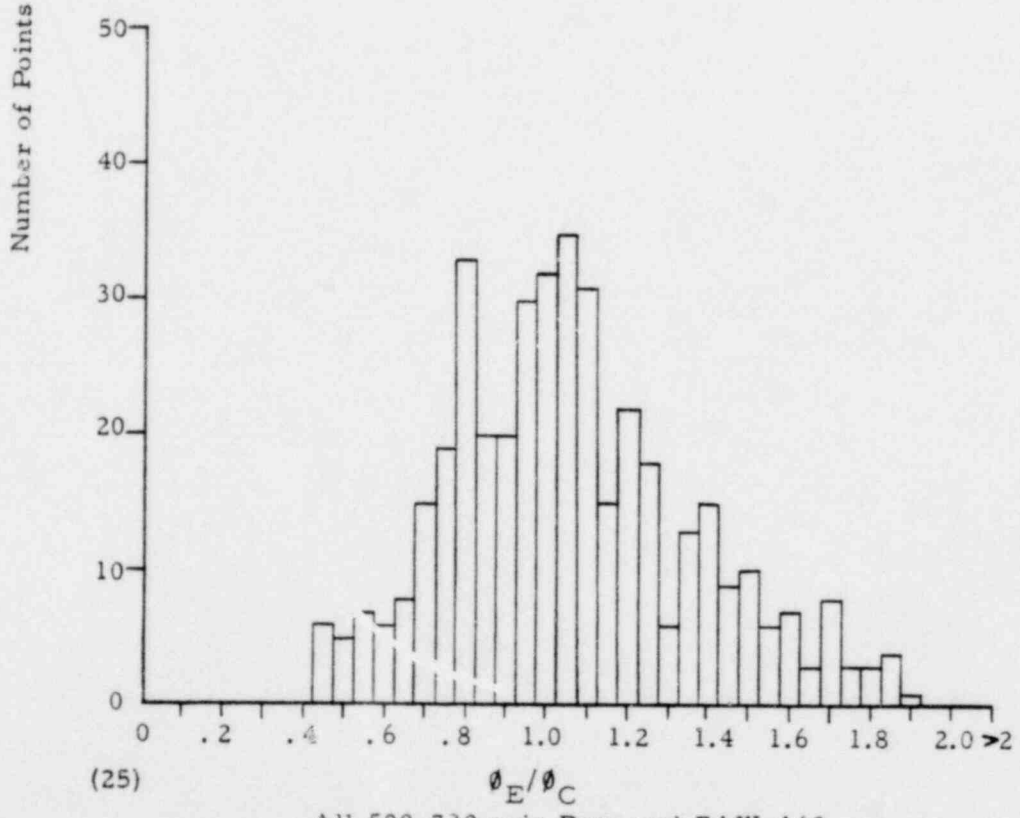

(25)

ϕ_E/ϕ_C

All 500-720 psia Data and BAW-168

RATIO OF EXPERIMENTAL TO CALCULATED
BURNOUT HEAT FLUX

DUKE POWER

OCONEE NUCLEAR STATION
FIGURE 3-30

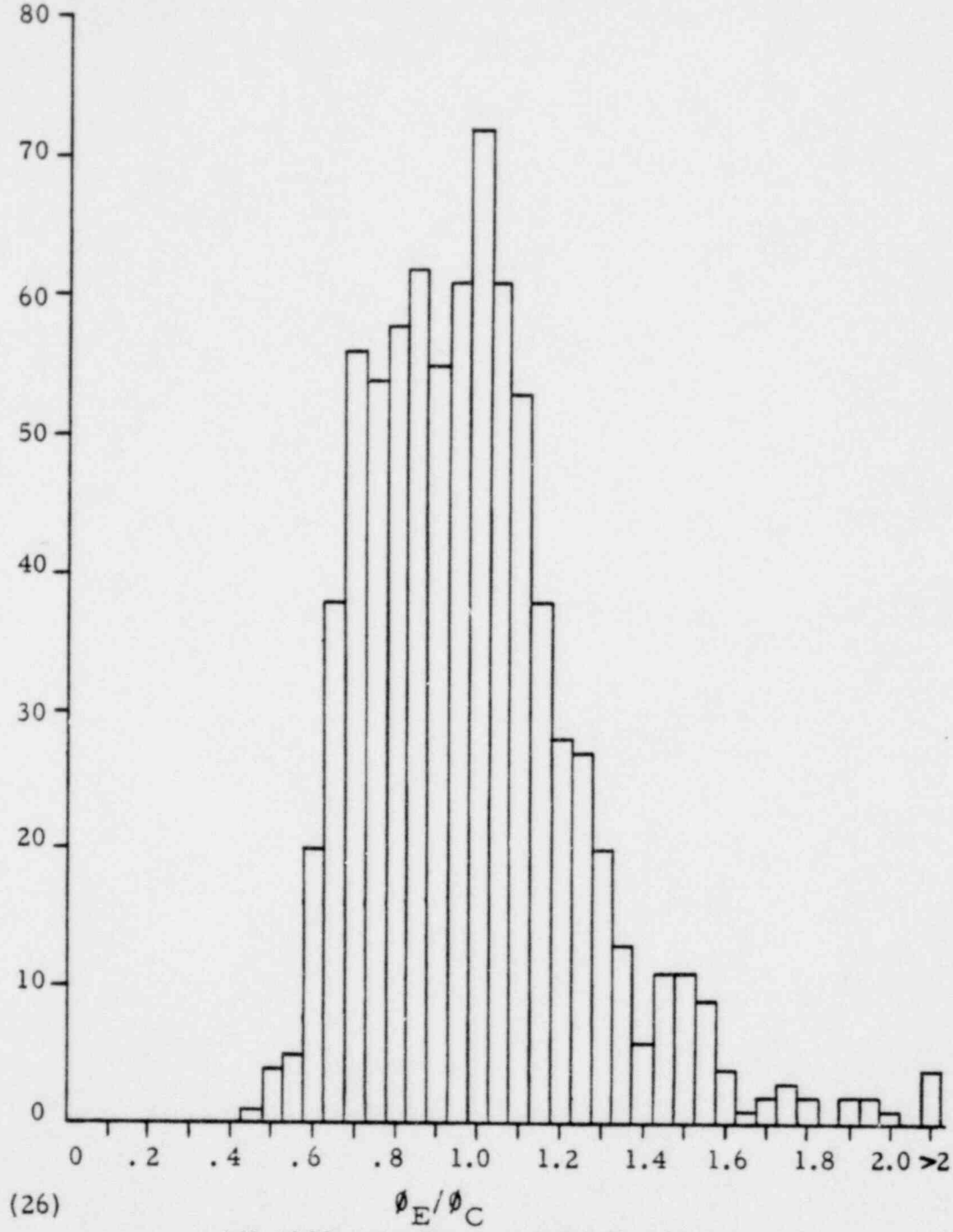

All 1000 psia Data and BAW-168

RATIO OF EXPERIMENTAL TO CALCULATED
BURNOUT HEAT FLUX

OCONEE NUCLEAR STATION

FIGURE 3-31

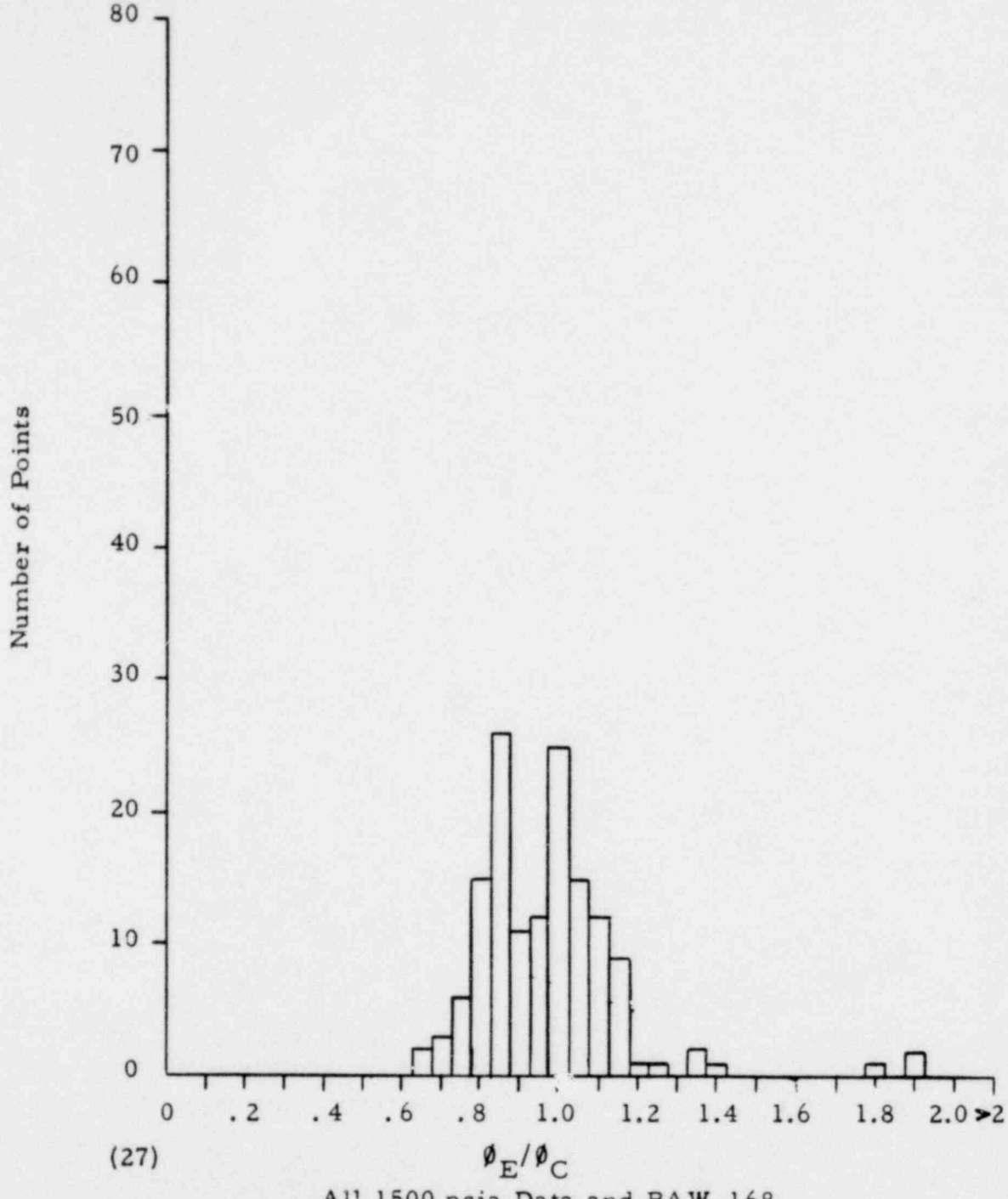

All 1500 psia Data and BAW-168

RATIO OF EXPERIMENTAL TO CALCULATED BURNOUT HEAT FLUX

DUKE POWER CITIZENSHIP SERVICE

OCONEE NUCLEAR STATION

FIGURE 3-32

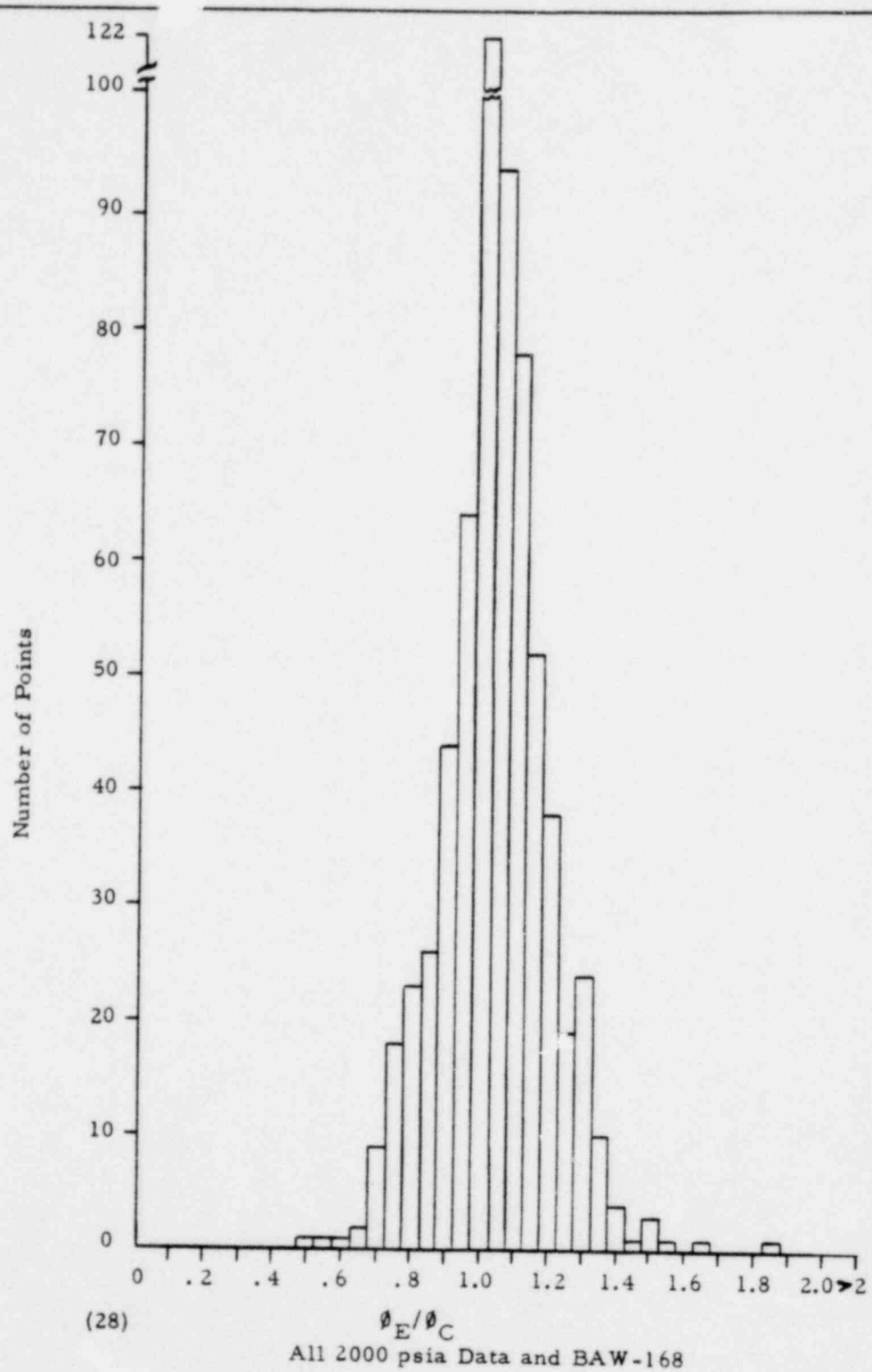

All 2000 psia Data and BAW-168

RATIO OF EXPERIMENTAL TO CALCULATED
BURNOUT HEAT FLUX

DUKE POWER COMPANY

OCONEE NUCLEAR STATION

FIGURE 3-33

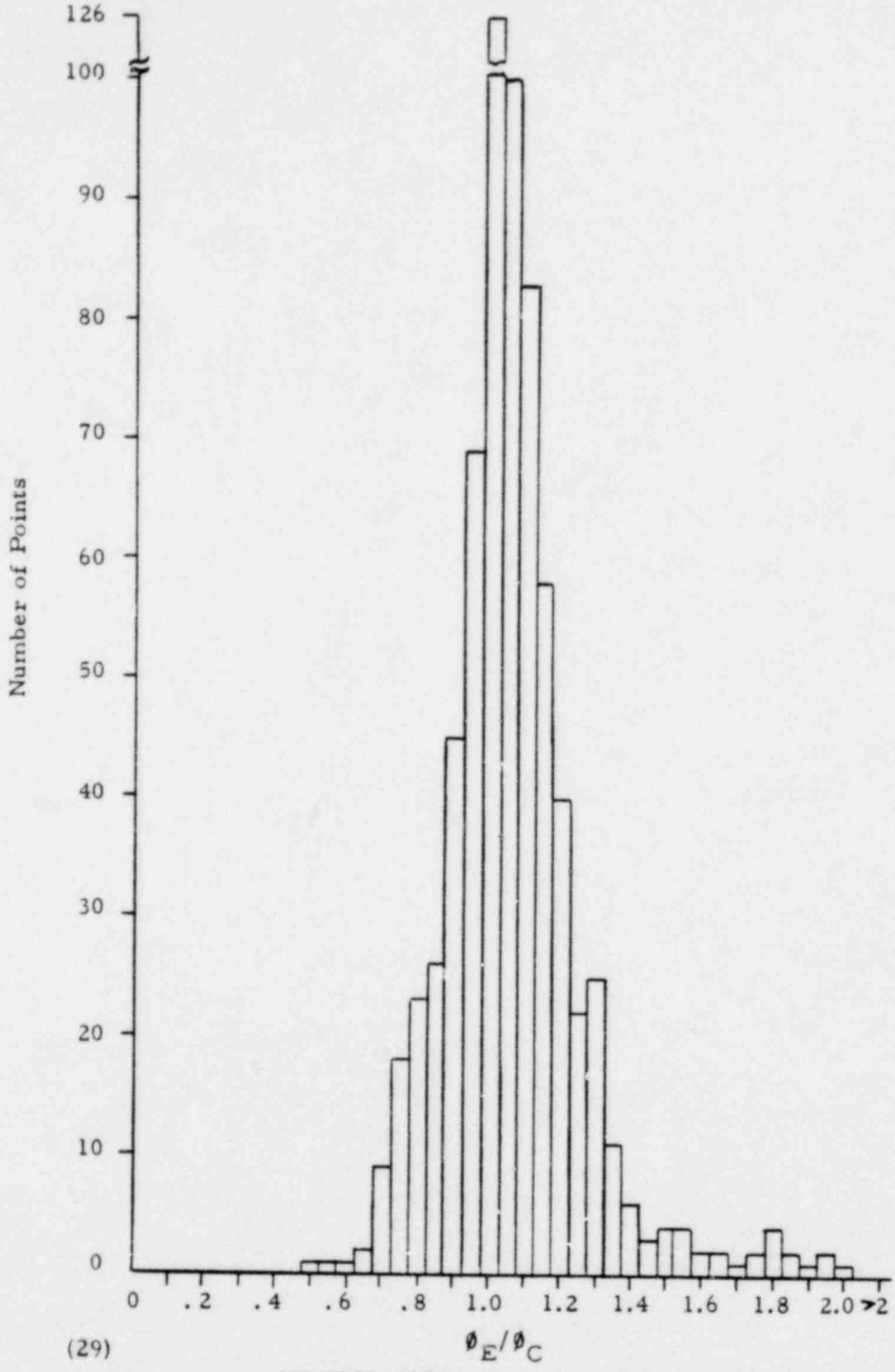

(29)

All 1750-2750 psia Data and BAW-168

RATIO OF EXPERIMENTAL TO CALCULATED BURNOUT HEAT FLUX

DUKE POWER SERVICE

OCONEE NUCLEAR STATION

FIGURE 3-34

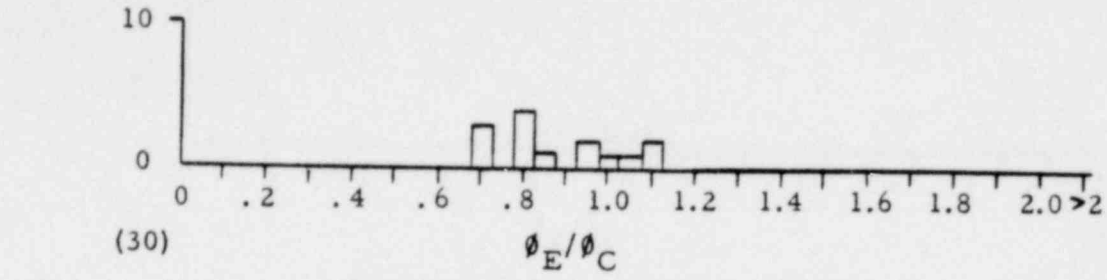

Euratom Chopped-Cosine 1000 psia Data and BAW-168

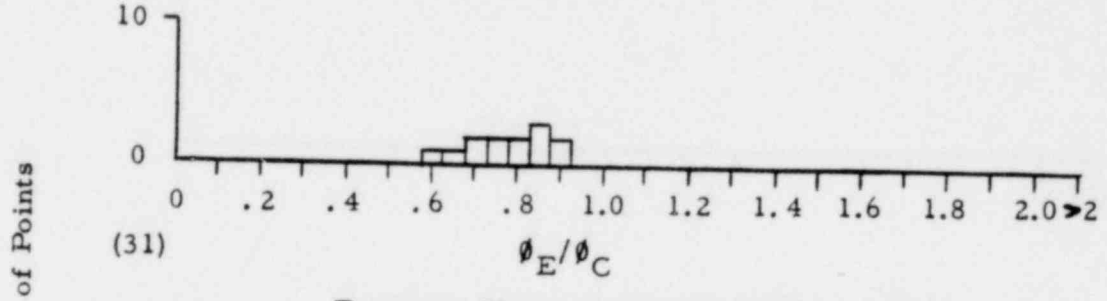

Euratom Chopped-Cosine 1500 psia Data and BAW-168

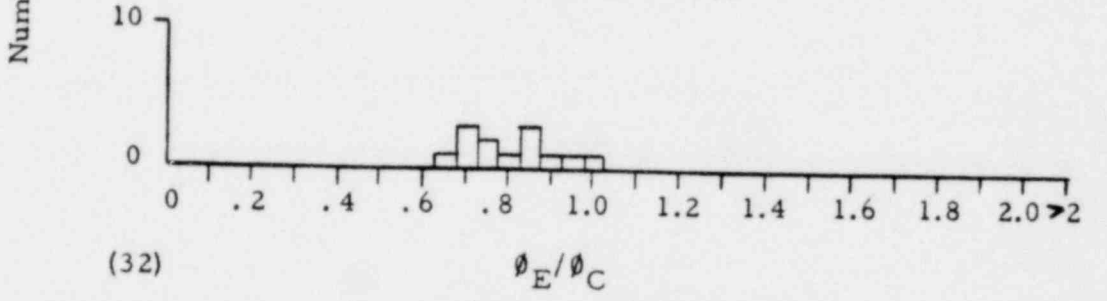

Euratom Chopped-Cosine 2000 psia Data and BAW-168

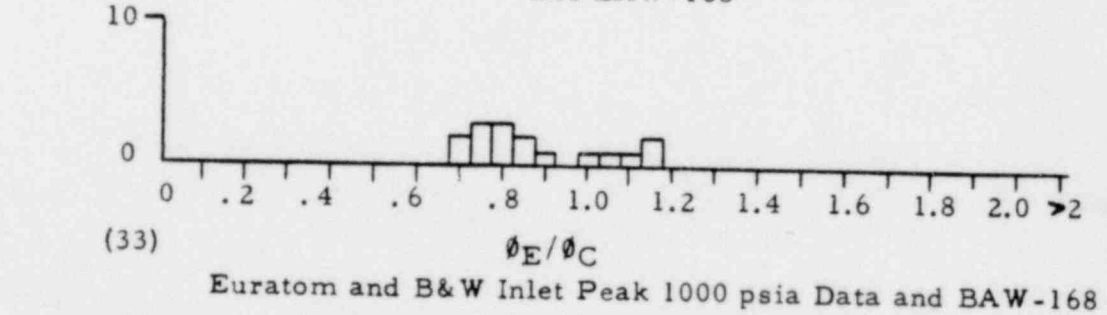

Euratom and B&W Inlet Peak 1000 psia Data and BAW-168

Number of Points

RATIO OF EXPERIMENTAL TO CALCULATED BURNOUT HEAT FLUX

DUKE POWER

OCONEE NUCLEAR STATION

FIGURE 3-35

00 00272

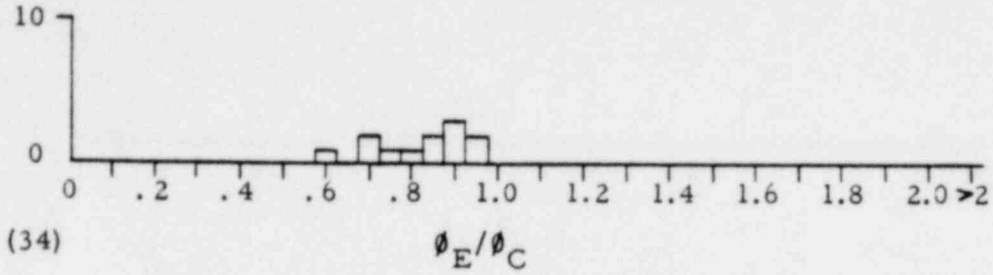

Euratom and B&W Inlet Peak 1500 psia Data and BAW-168

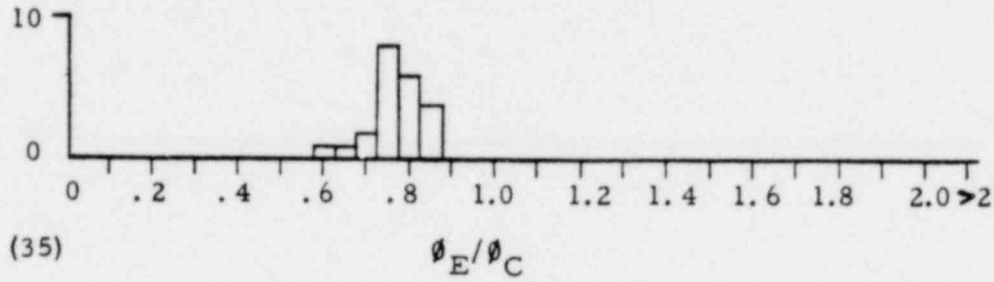

Number of Points

Euratom and B&W Inlet Peak 2000 psia Data and BAW-168

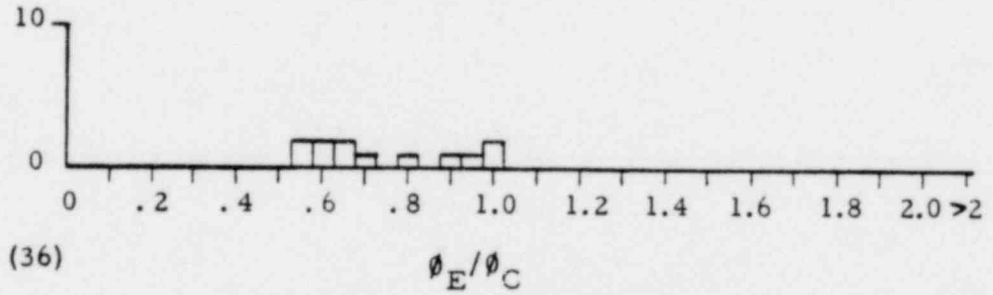

Euratom and B&W Outlet Peak 1000 psia Data and BAW-168

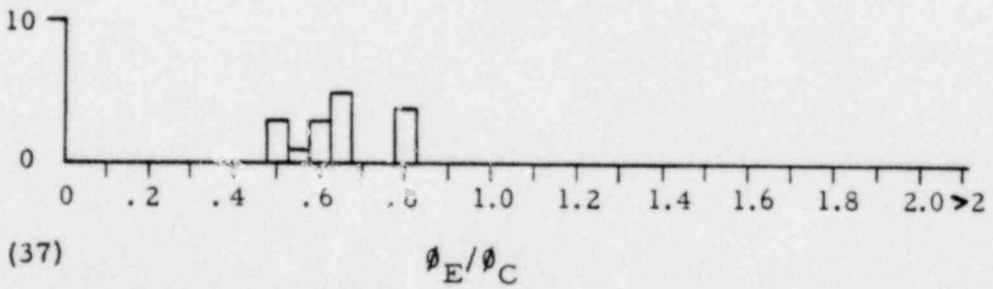

Euratom and B&W Outlet Peak 1500 psia Data and BAW-168

RATIO OF EXPERIMENTAL TO CALCULATED BURNOUT HEAT FLUX

OCONEE NUCLEAR STATION
FIGURE 3-36

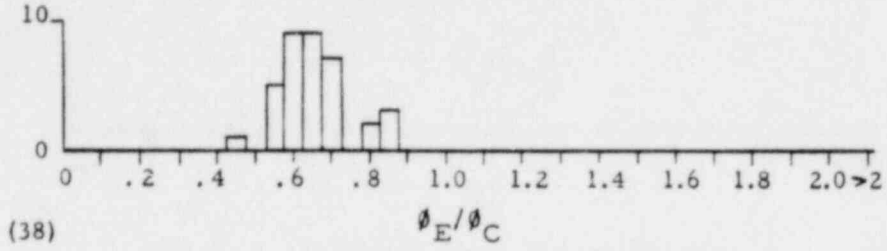

Euratom and B&W Outlet Peak 2000 psia Data and BAW-168

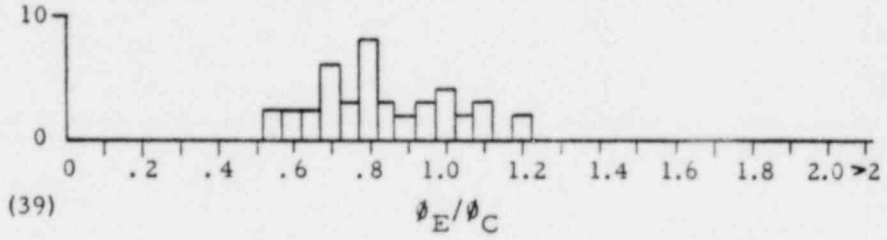

All 1000 psia Non-Uniform Data and BAW-168

Number of Points

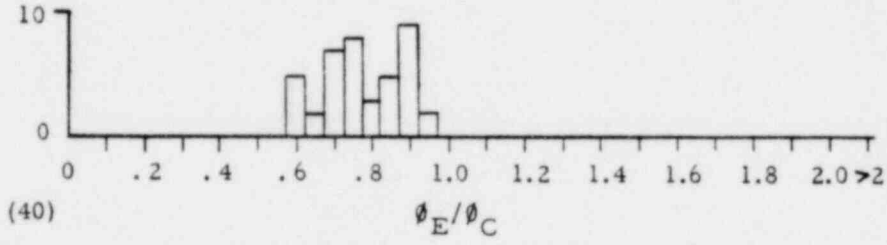

All 1500 psia Non-Uniform Data and BAW-168

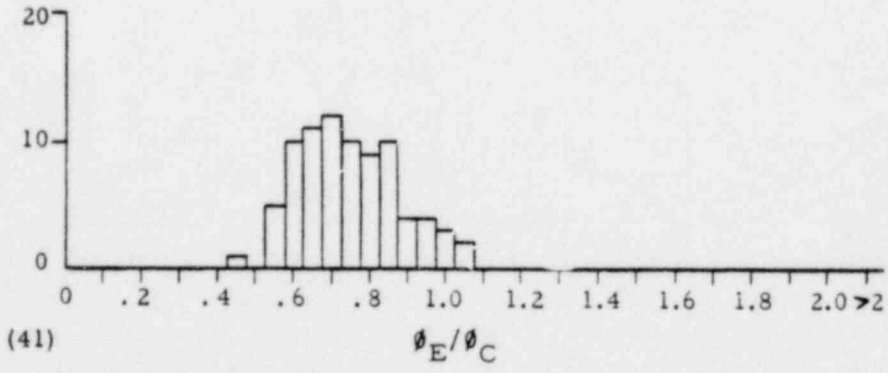

All 2000 psia Non-Uniform Data and BAW-168

RATIO OF EXPERIMENTAL TO CALCULATED BURNOUT HEAT FLUX

DUKE POWER

OCONEE NUCLEAR STATION

FIGURE 3-37

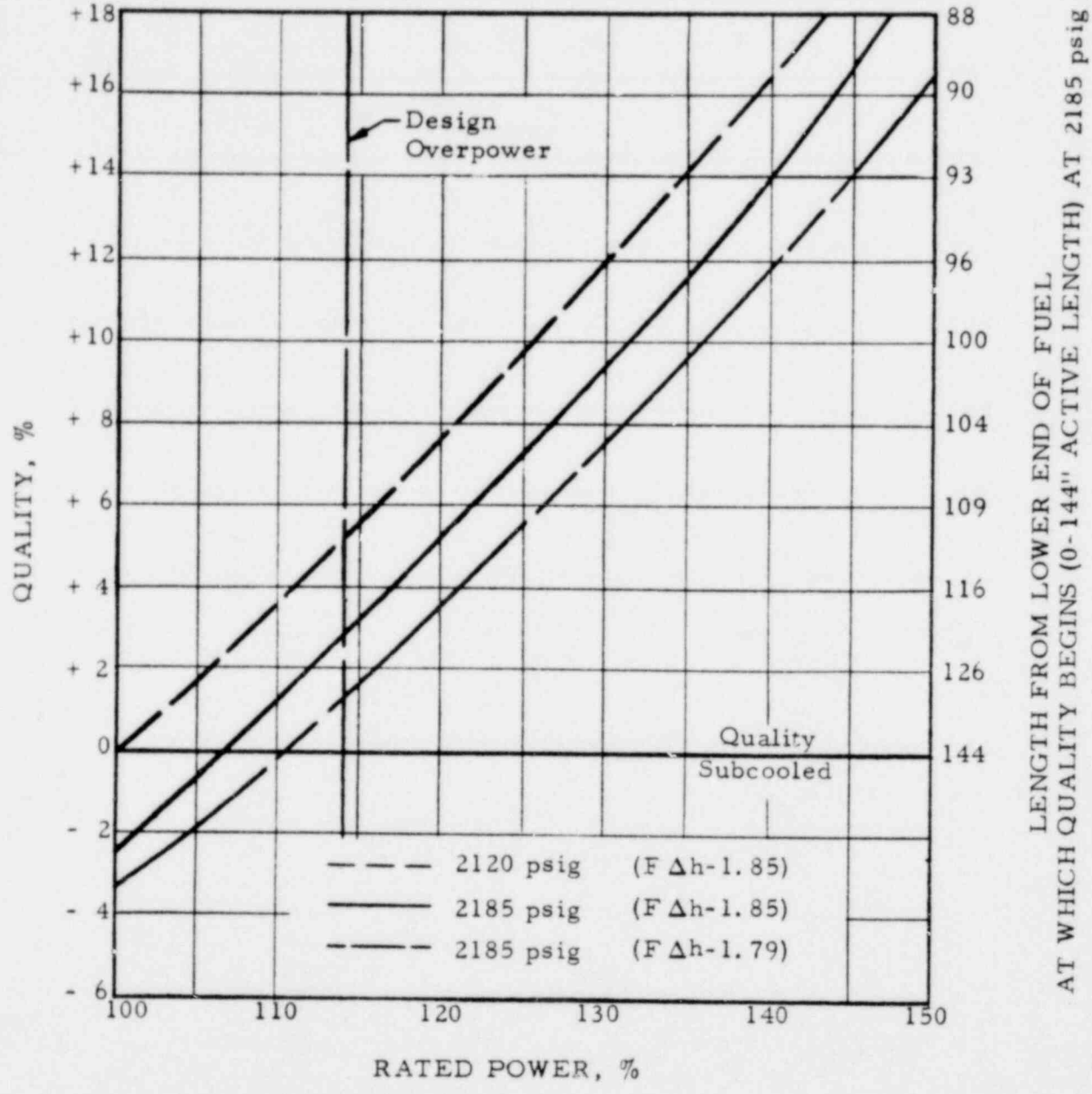

MAXIMUM HOT CHANNEL
EXIT QUALITY VERSUS REACTOR POWER

DUKE POWER

OCONEE NUCLEAR STATION
FIGURE 3-38

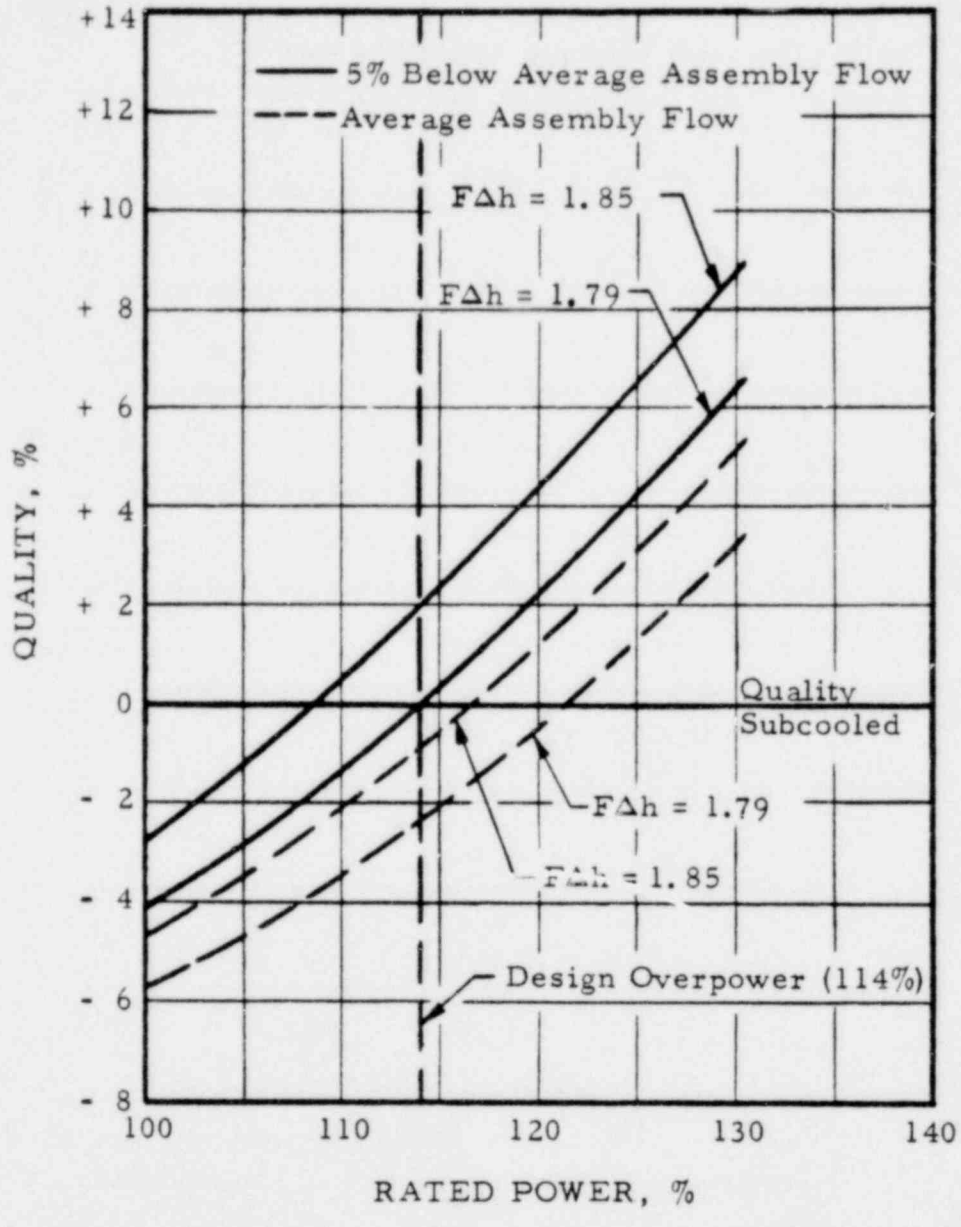

HOTTEST DESIGN AND NOMINAL CHANNEL
EXIT QUALITY VERSUS REACTOR POWER
(WITHOUT ENGINEERING HOT CHANNEL FACTORS)

OCONEE NUCLEAR STATION

FIGURE 3-39

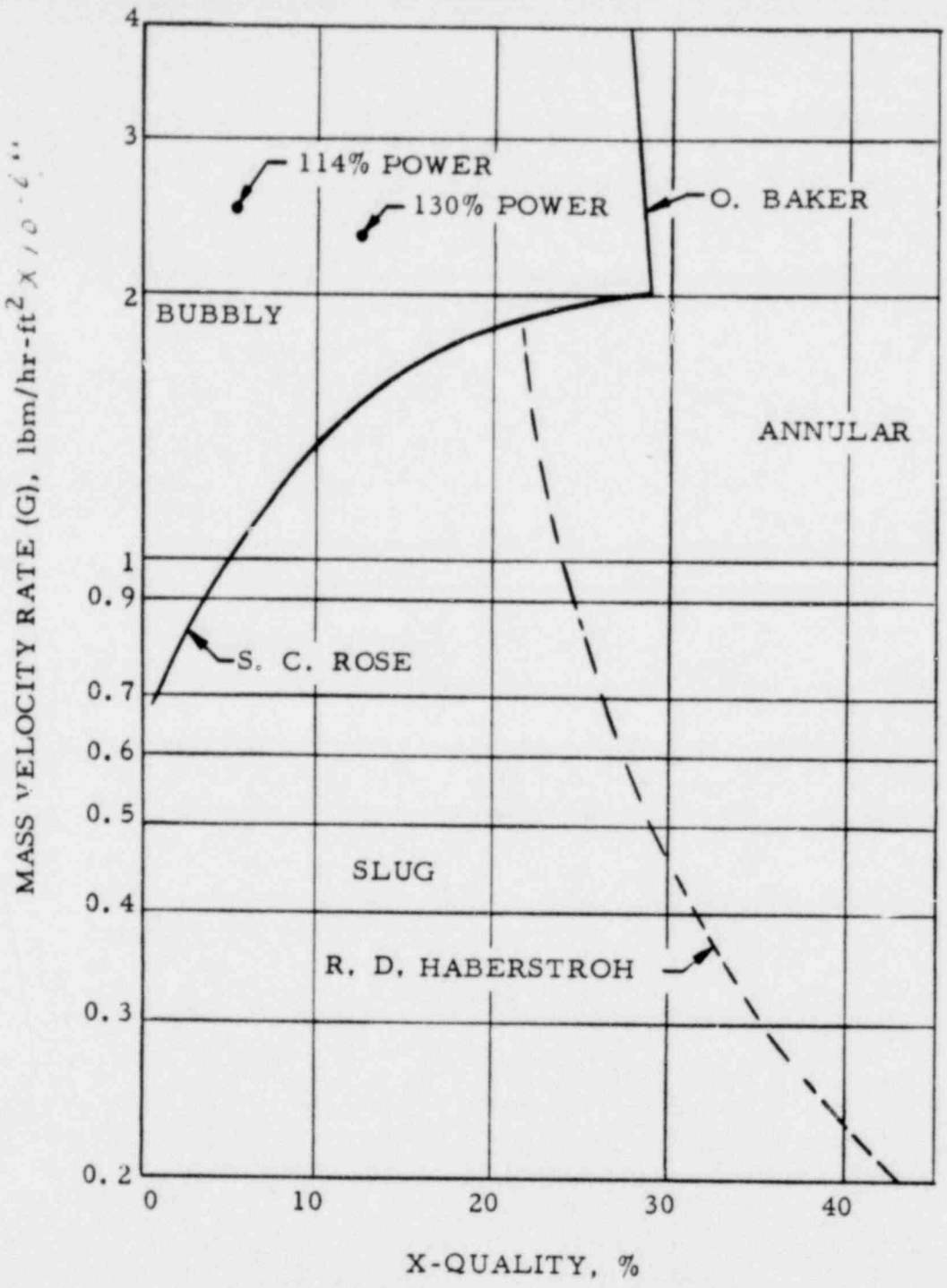

FLOW REGIME MAP AT 2185 PSIG

DUKE POWER

OCONEE NUCLEAR STATION

FIGURE 3-40

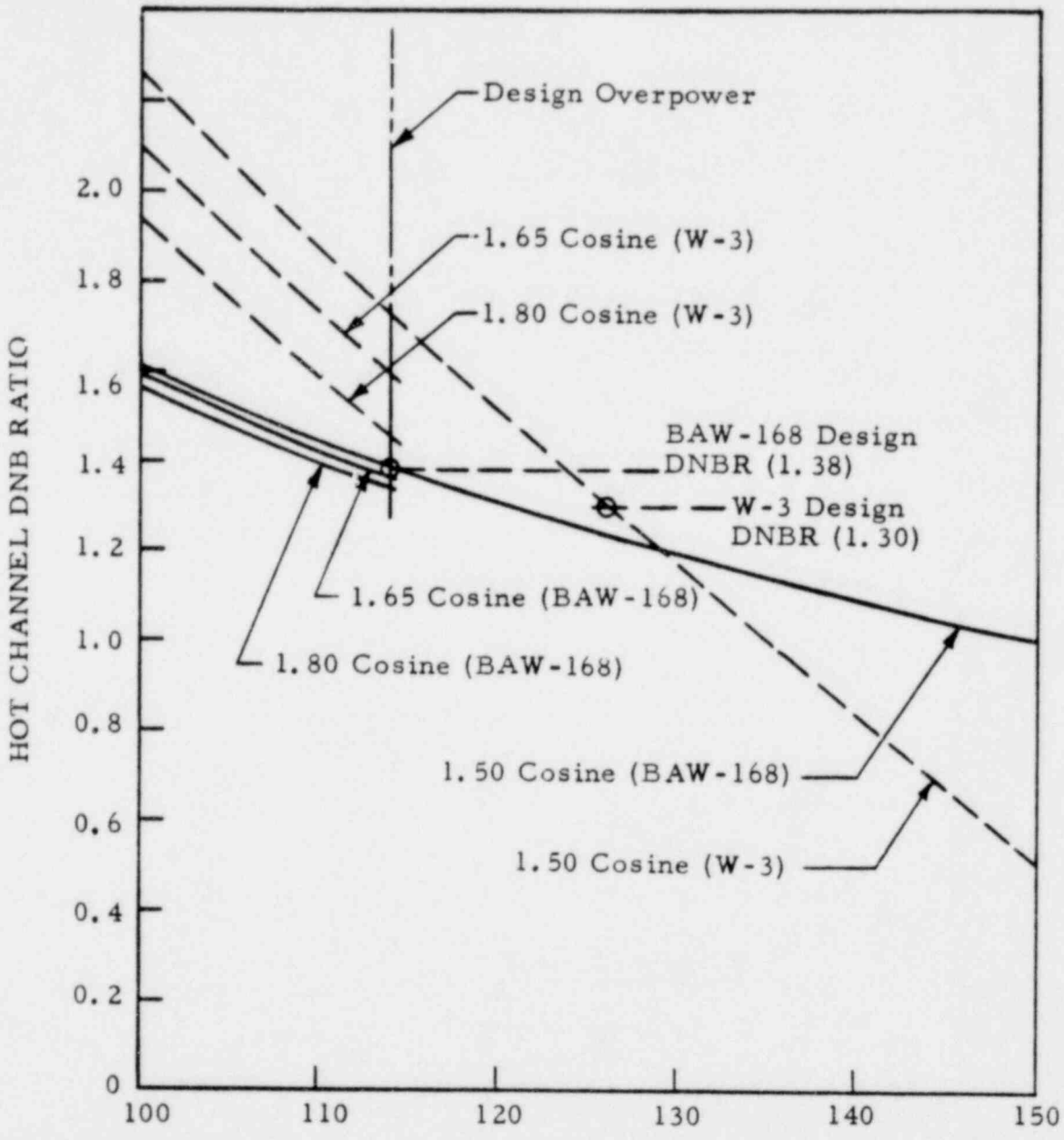

HOT CHANNEL DNB RATIO COMPARISON

OCONEE NUCLEAR STATION
FIGURE 3-41

00 00278

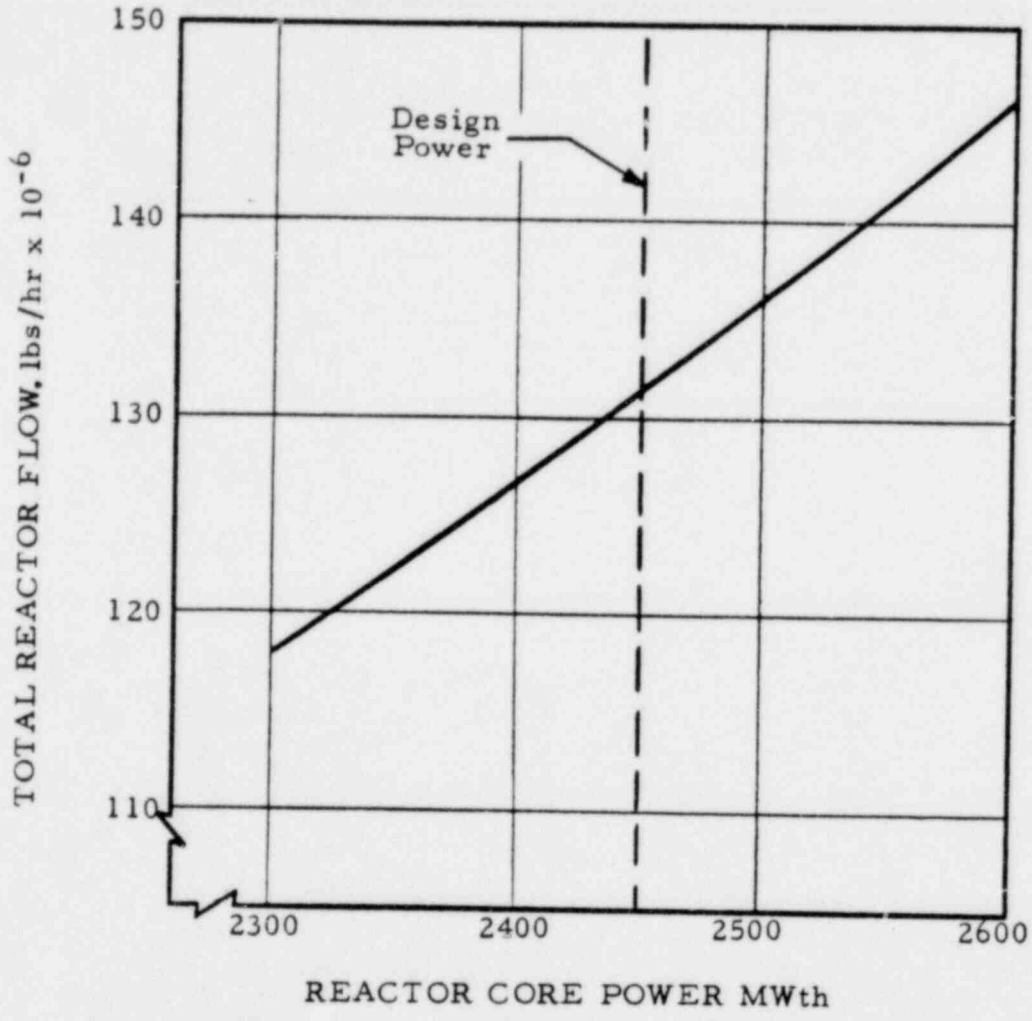

REACTOR COOLANT FLOW VERSUS POWER

OCONEE NUCLEAR STATION

FIGURE 3-42

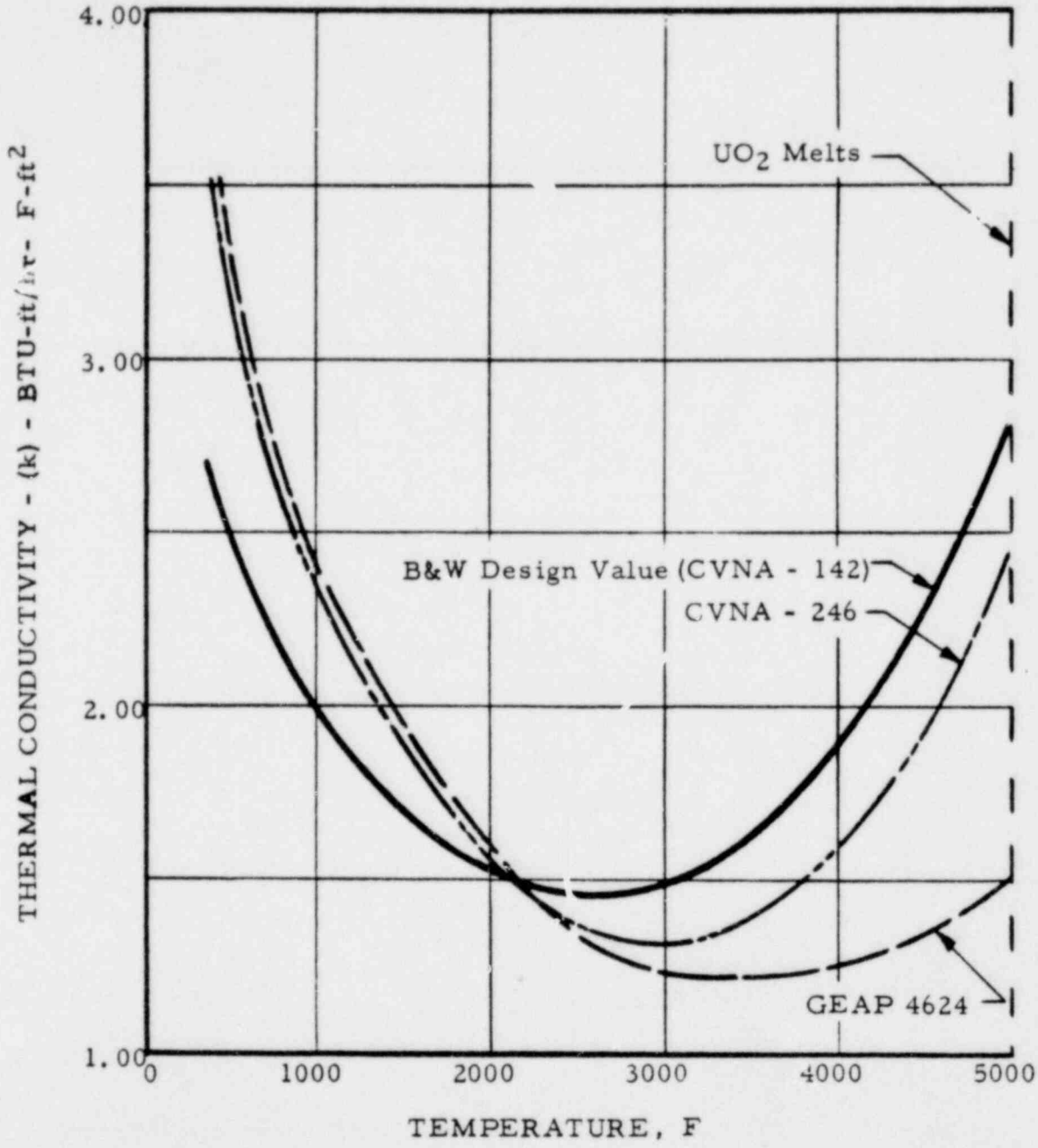

THERMAL CONDUCTIVITY OF 95%
DENSE SINTERED UO_2 PELLETS

OCONEE NUCLEAR STATION

FIGURE 3-43

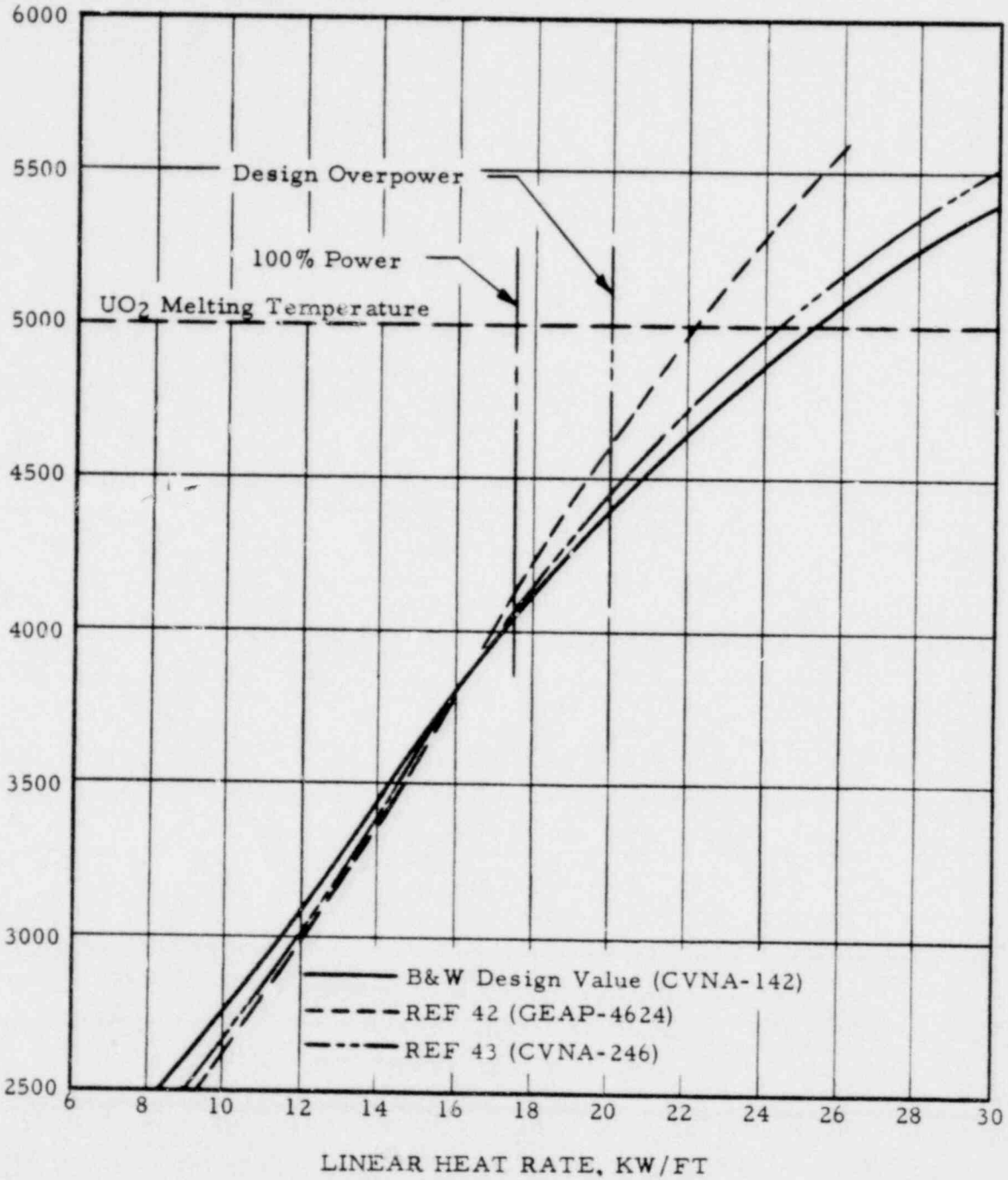

FUEL CENTER TEMPERATURE FOR
BEGINNING-OF-LIFE CONDITIONS

OCONEE NUCLEAR STATION

FIGURE 3-44

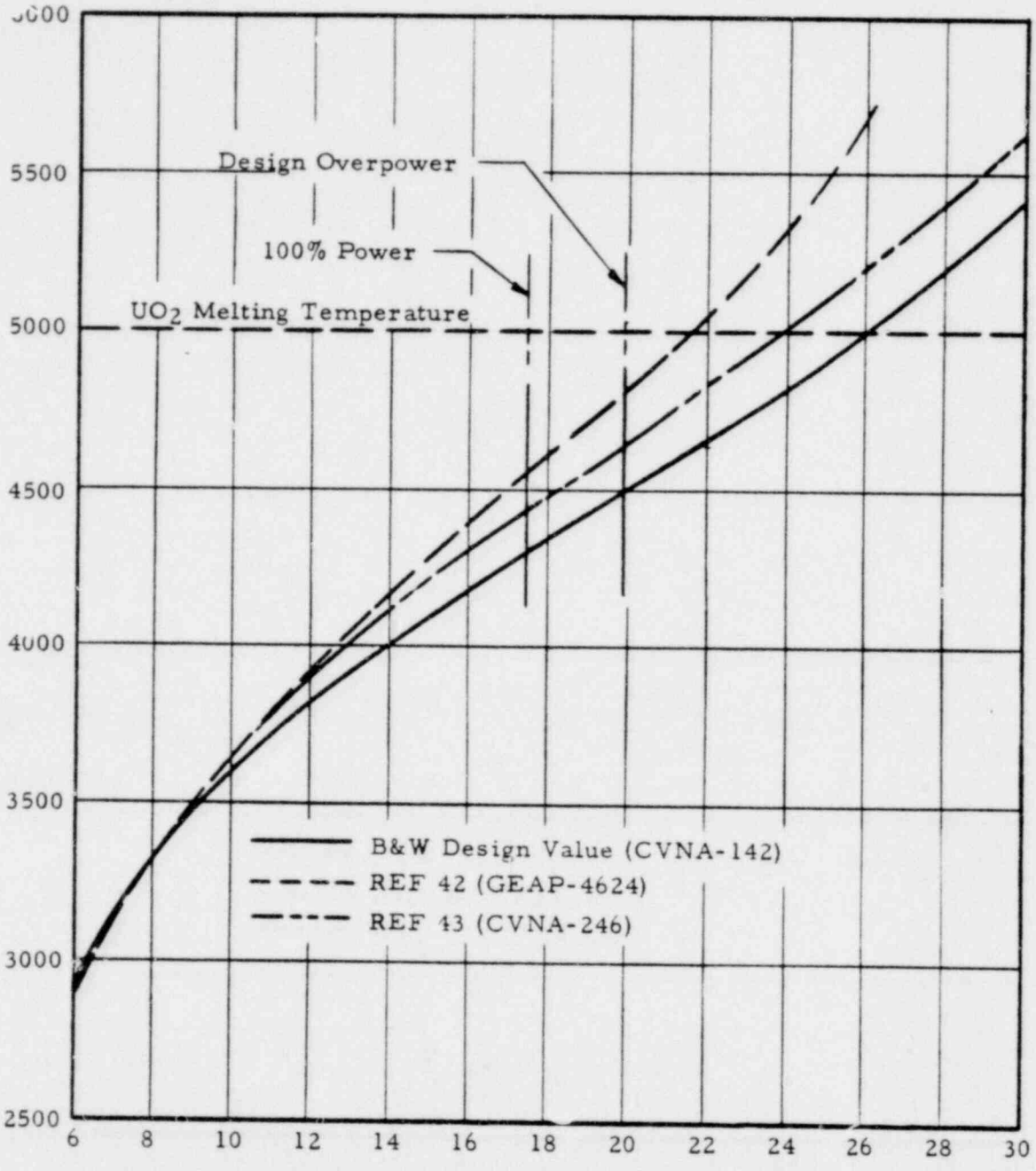

FUEL CENTER TEMPERATURE FOR
END-OF-LIFE CONDITIONS

DUKE POWER

OCONEE NUCLEAR STATION
FIGURE 3-45

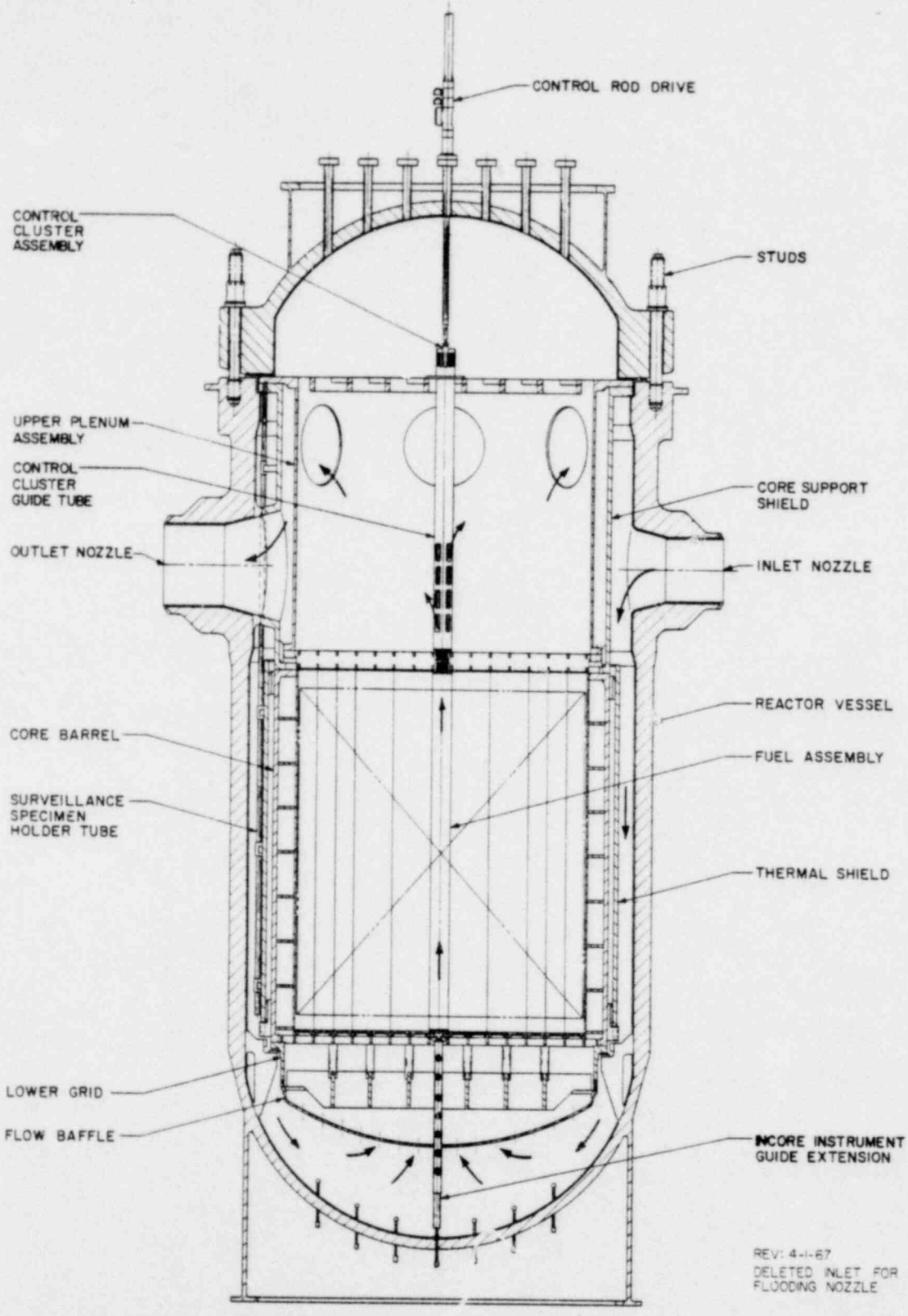

REACTOR VESSEL AND INTERNALS
GENERAL ARRANGEMENT

OCONEE NUCLEAR STATION
FIGURE 3-46

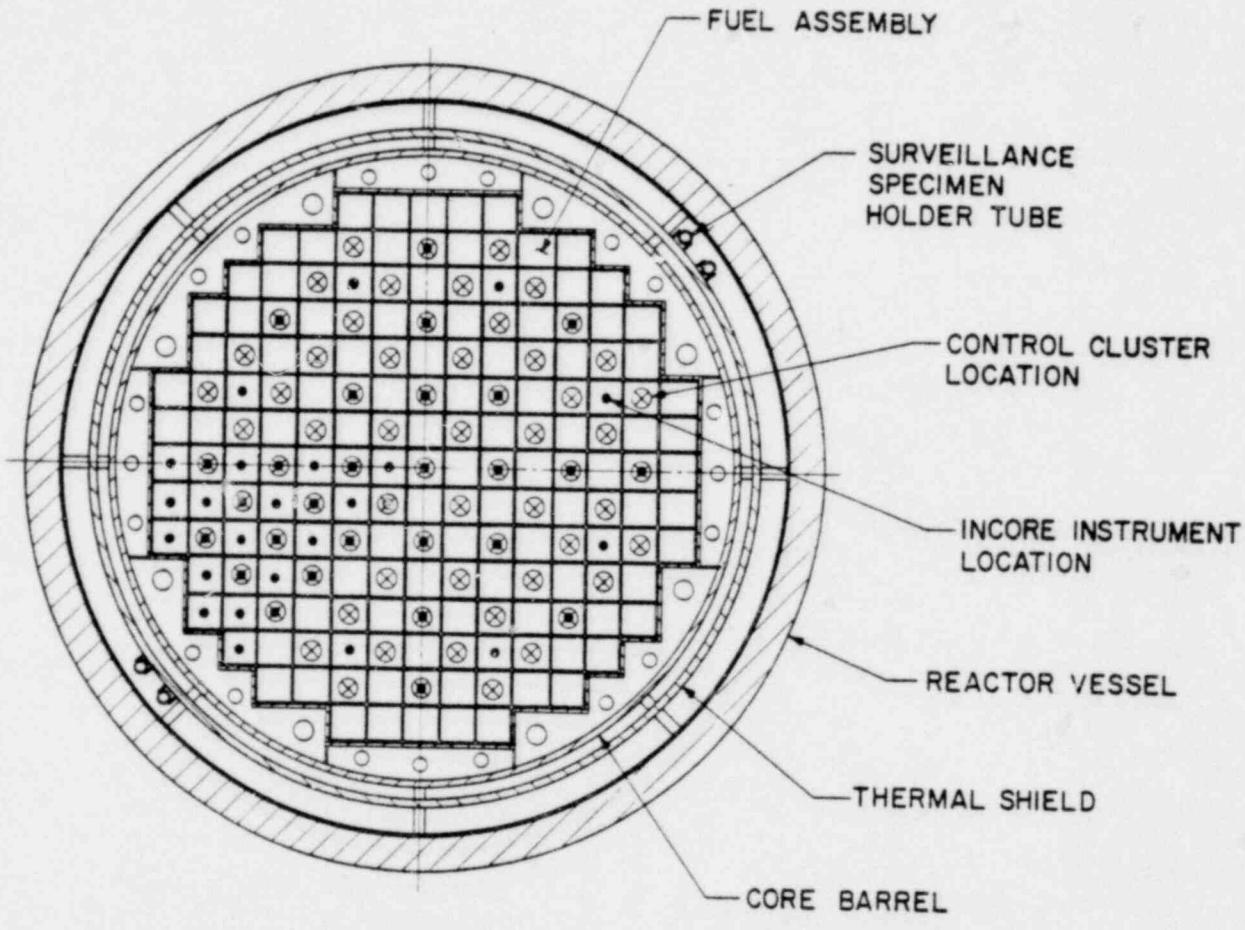

REACTOR VESSEL AND INTERNALS
GENERAL ARRANGEMENT
CROSS SECTION

OCONEE NUCLEAR STATION

FIGURE 3-47

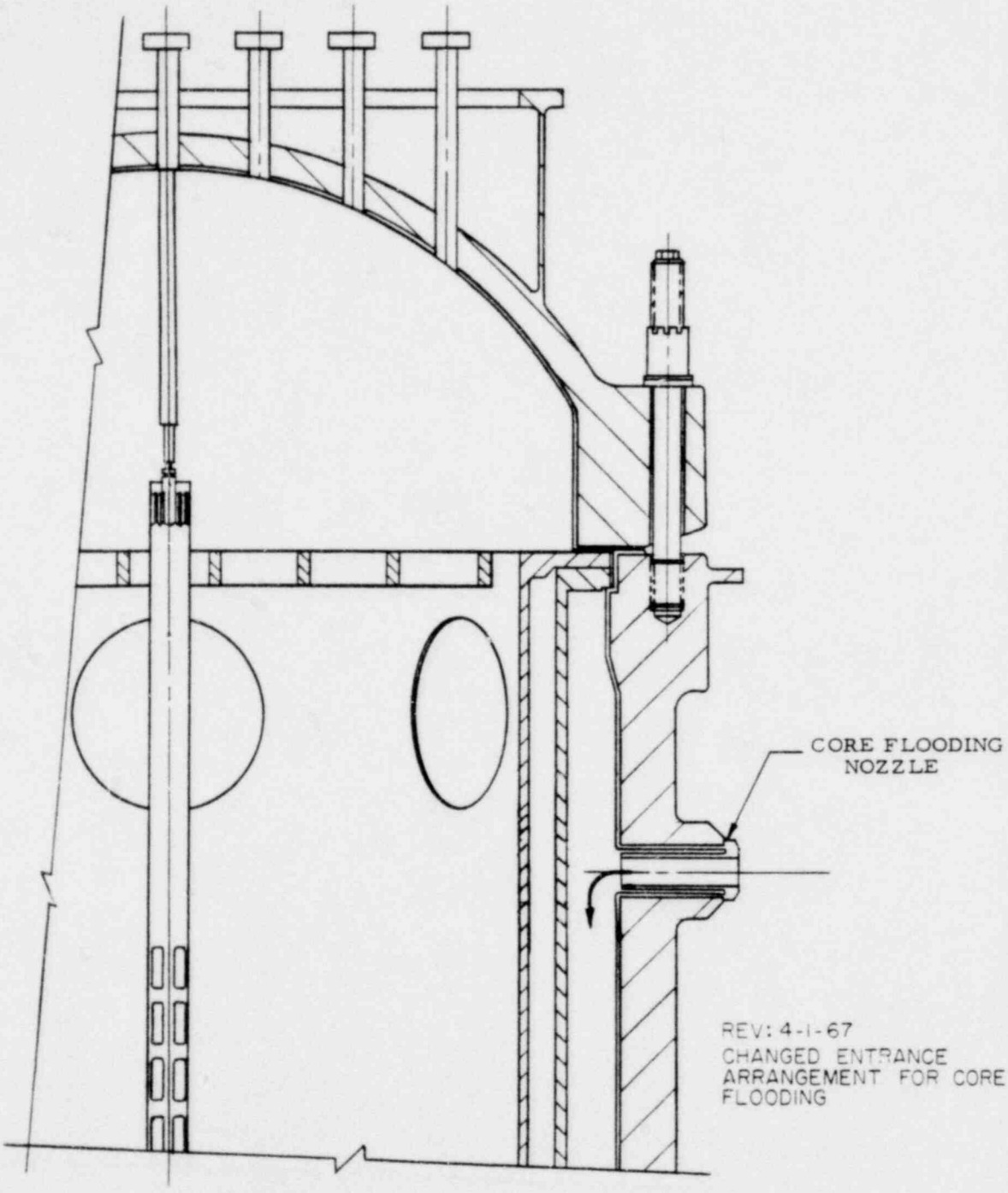

CORE FLOODING ARRANGEMENT

DUKE POWER SERVICE

OCONEE NUCLEAR STATION

FIGURE 3-48

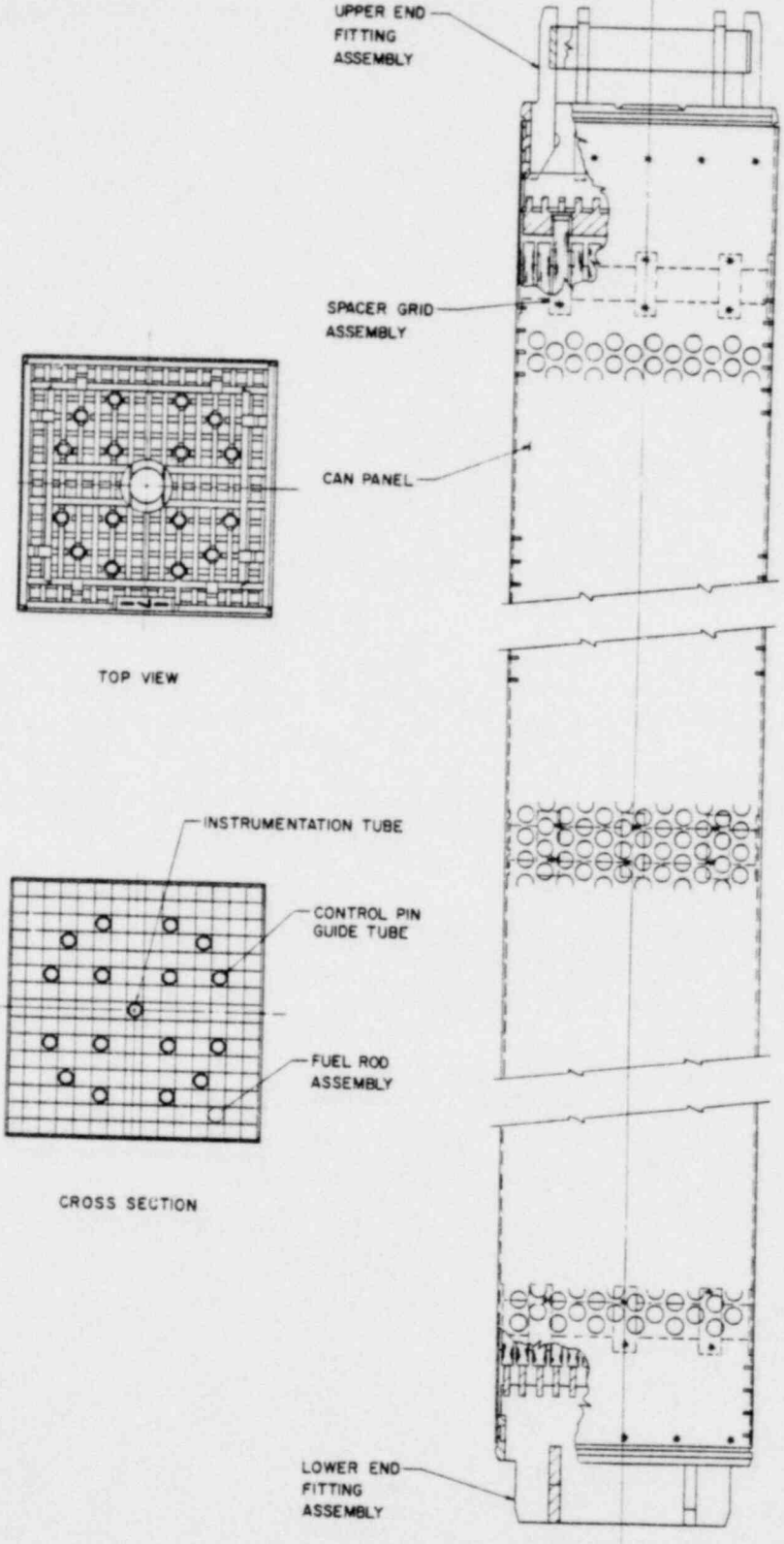

FUEL ASSEMBLY

OCONEE NUCLEAR STATION

FIGURE 3-49

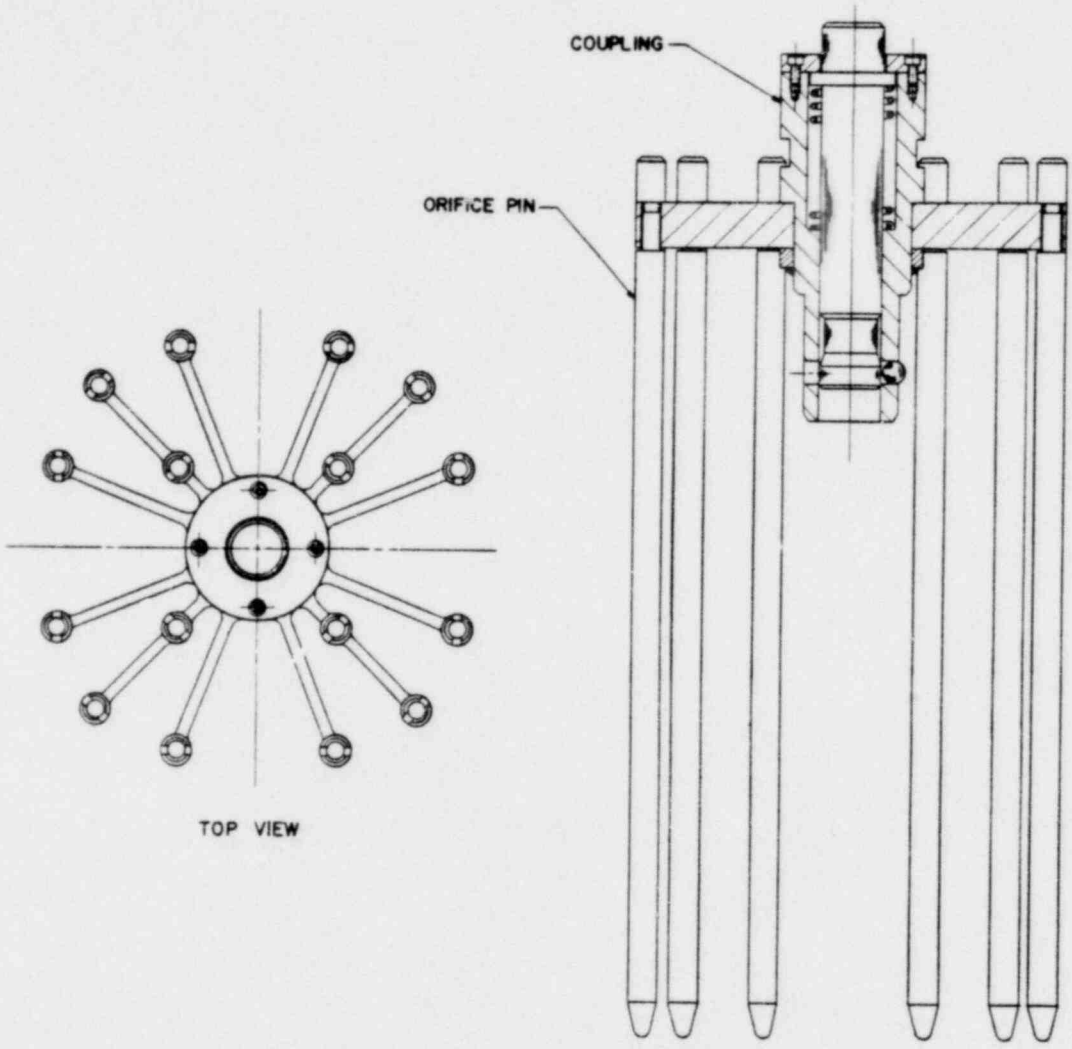

ORIFICE CLUSTER ASSEMBLY

OCONEE NUCLEAR STATION
FIGURE 3-50

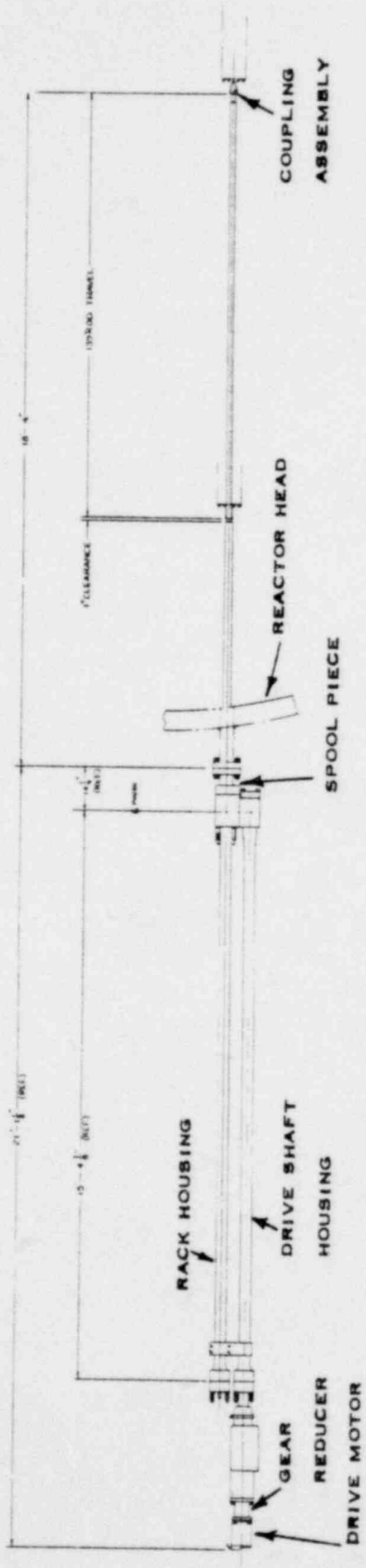

CONTROL ROD DRIVE

GENERAL ARRANGEMENT

OCONEE NUCLEAR STATION

FIGURE 3-51

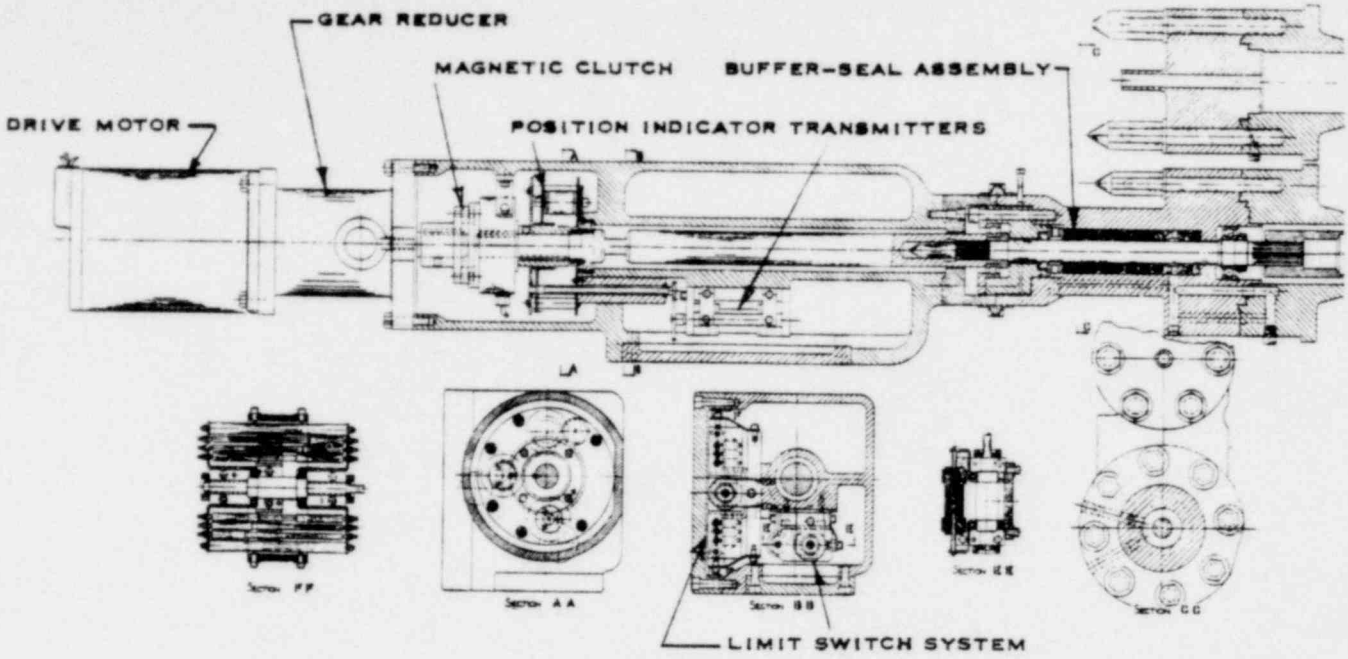

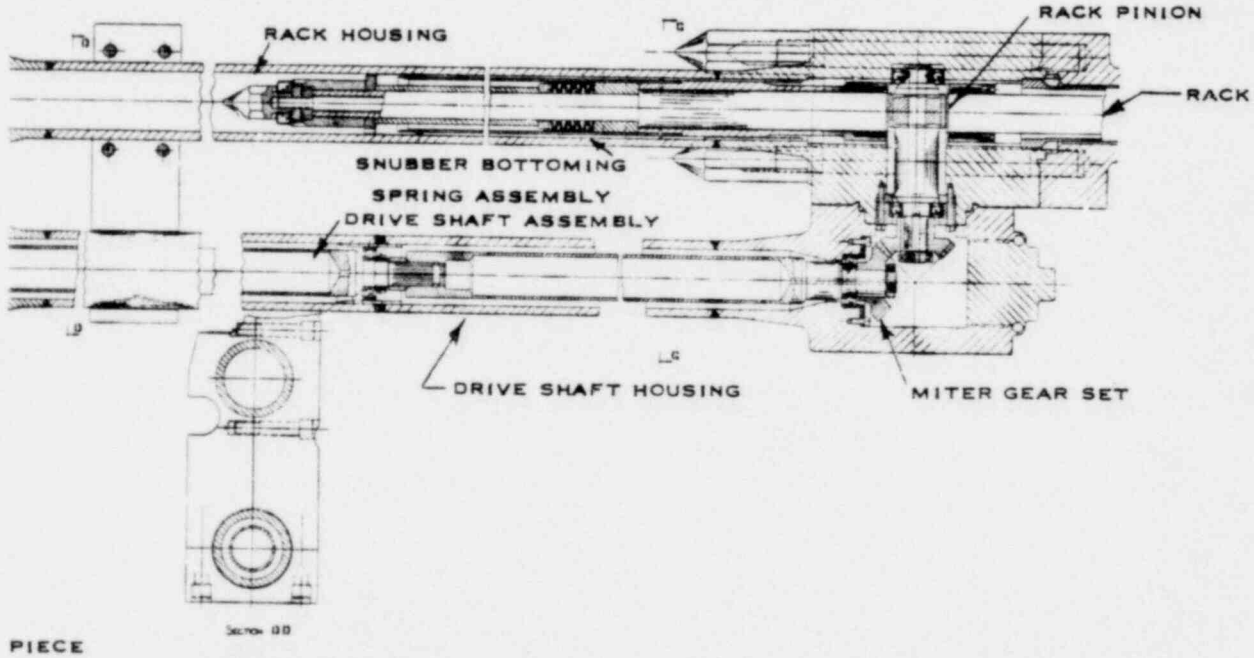

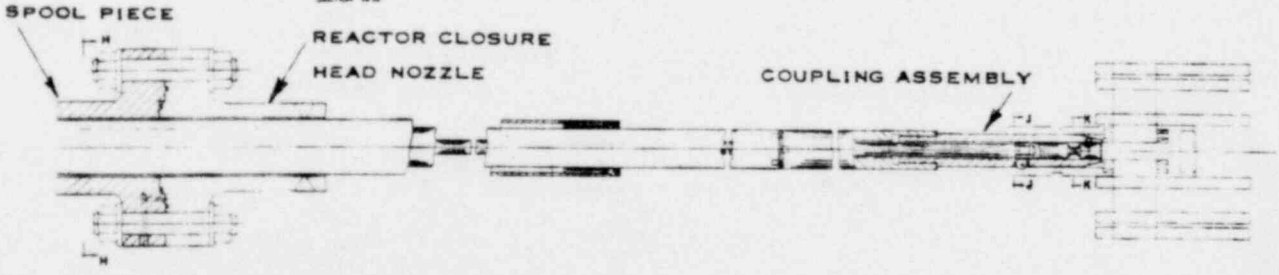

CONTROL ROD DRIVE - VERTICAL SECTION

OCONEE NUCLEAR STATION

FIGURE 3-52

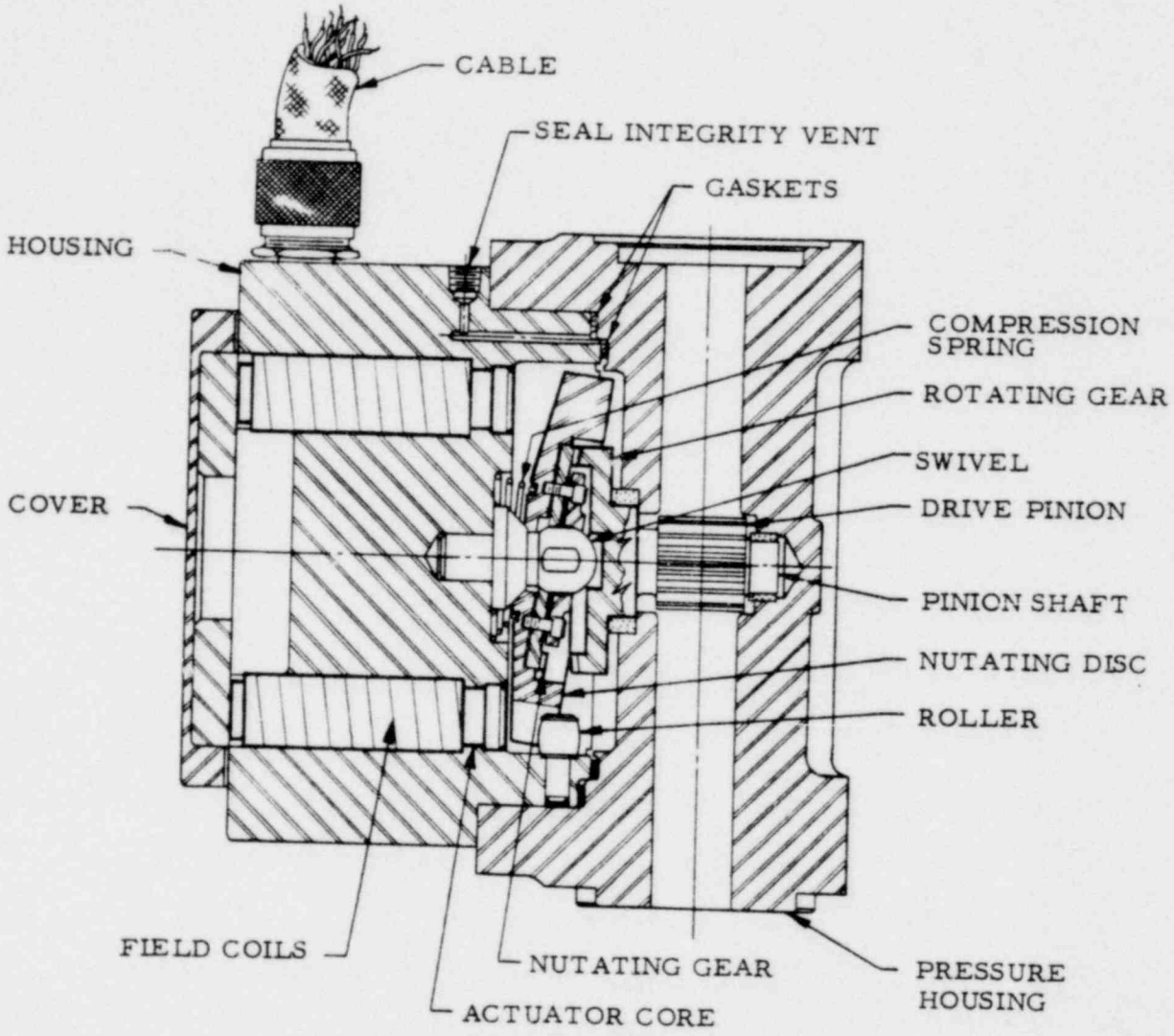

NUTATING DISC ACTUATOR

DUKE POWER CITIZENSHIP SERVICE

OCONEE NUCLEAR STATION

FIGURE 3-53

00 00290

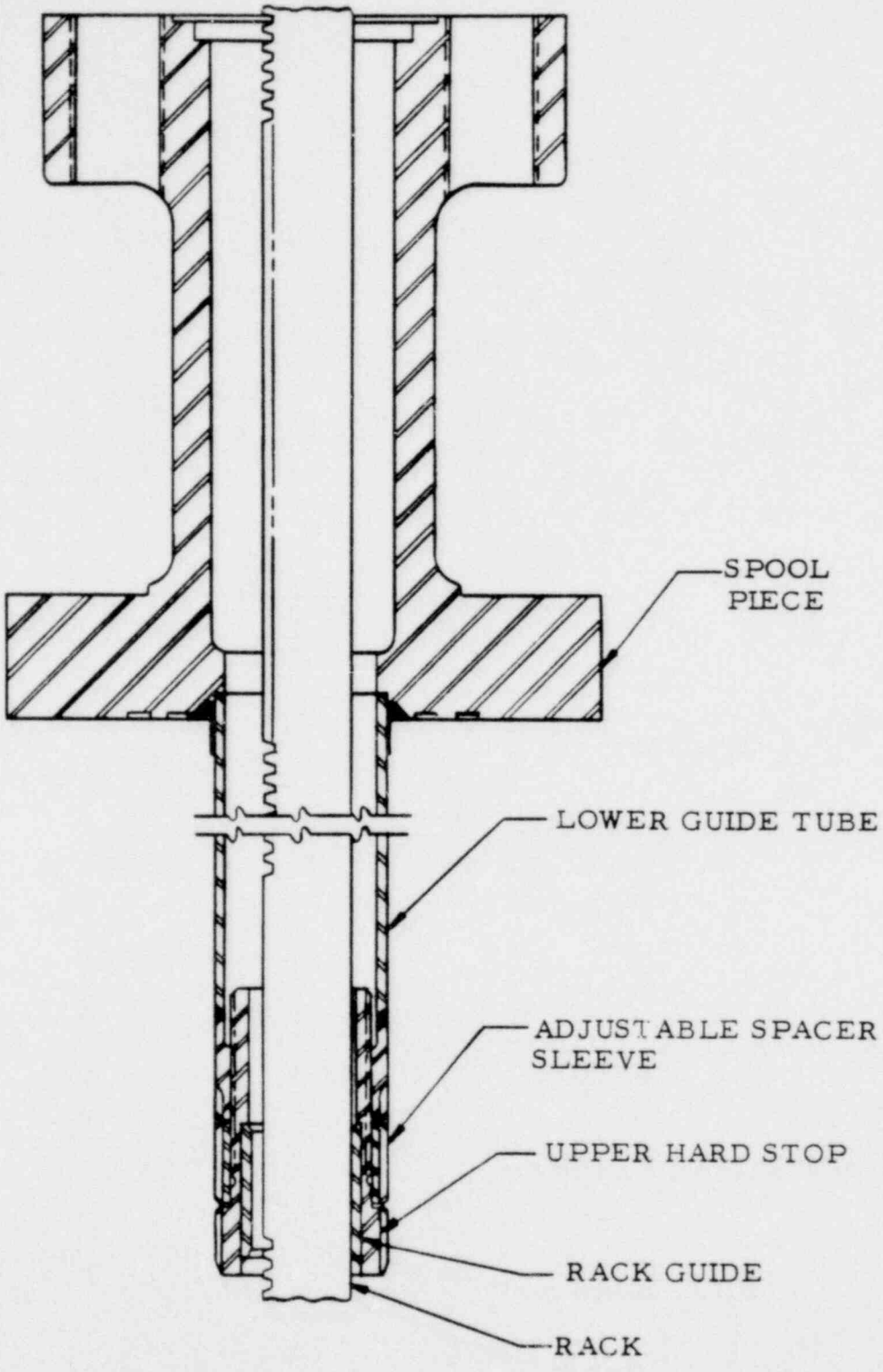

SPOOL PIECE AND LOWER GUIDE TUBE ASSEMBLY

DUKE POWER CITIZENSHIP SERVICE

OCONEE NUCLEAR STATION

FIGURE 3-54

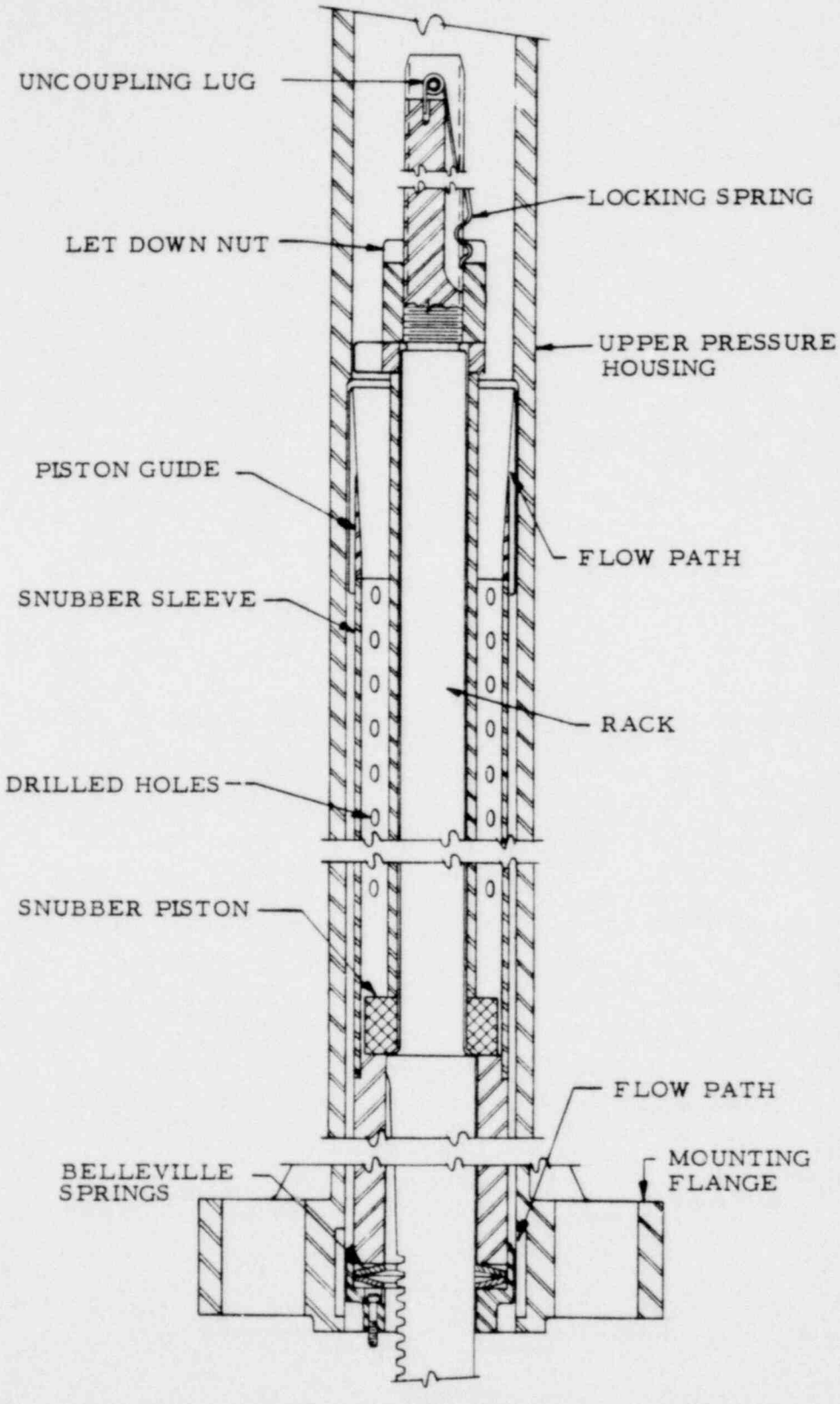

SNUBBER

OCONEE NUCLEAR STATION

FIGURE 3-55

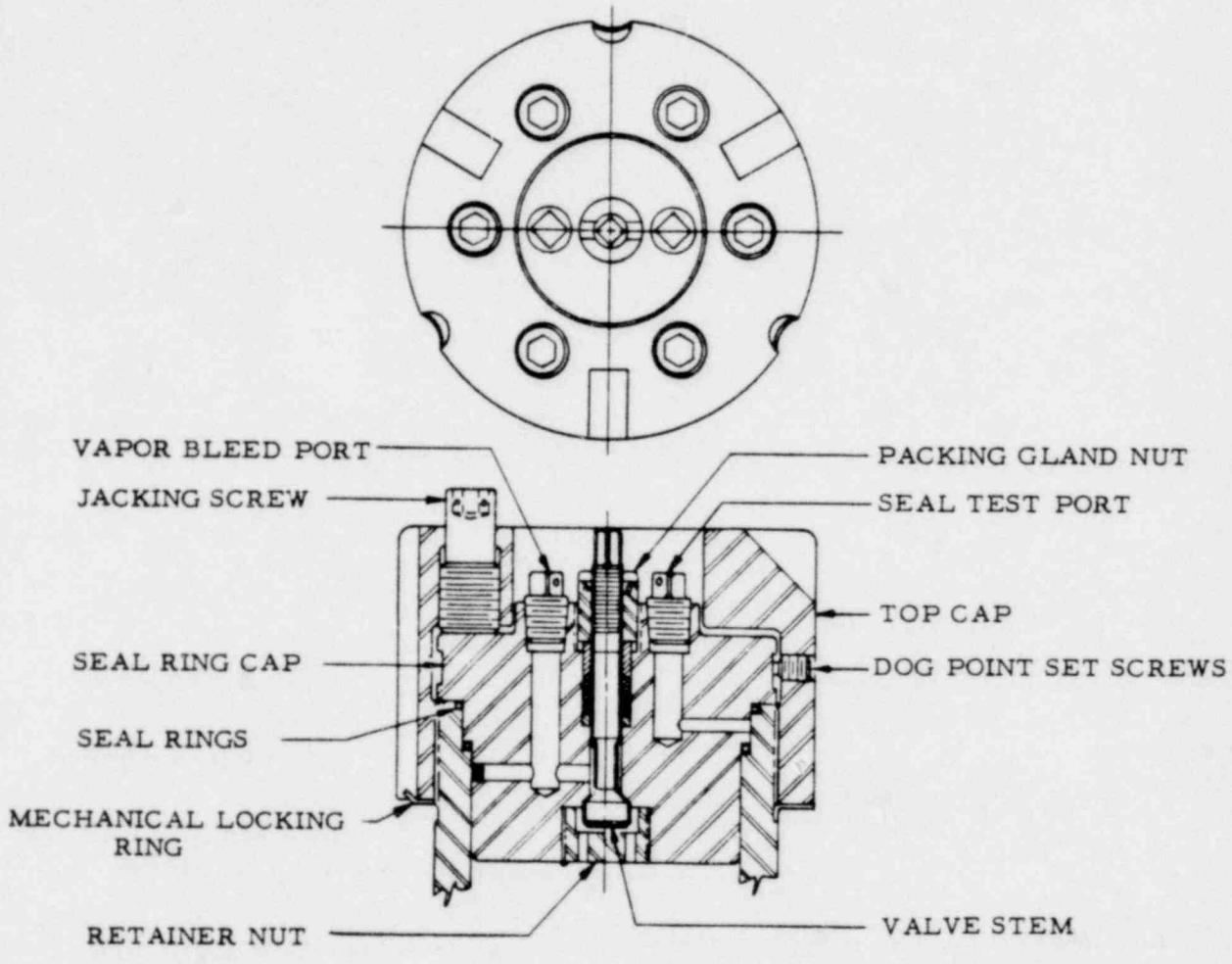

CAP AND DRIVE LINE VENT ASSEMBLY

OCONEE NUCLEAR STATION

FIGURE 3-56

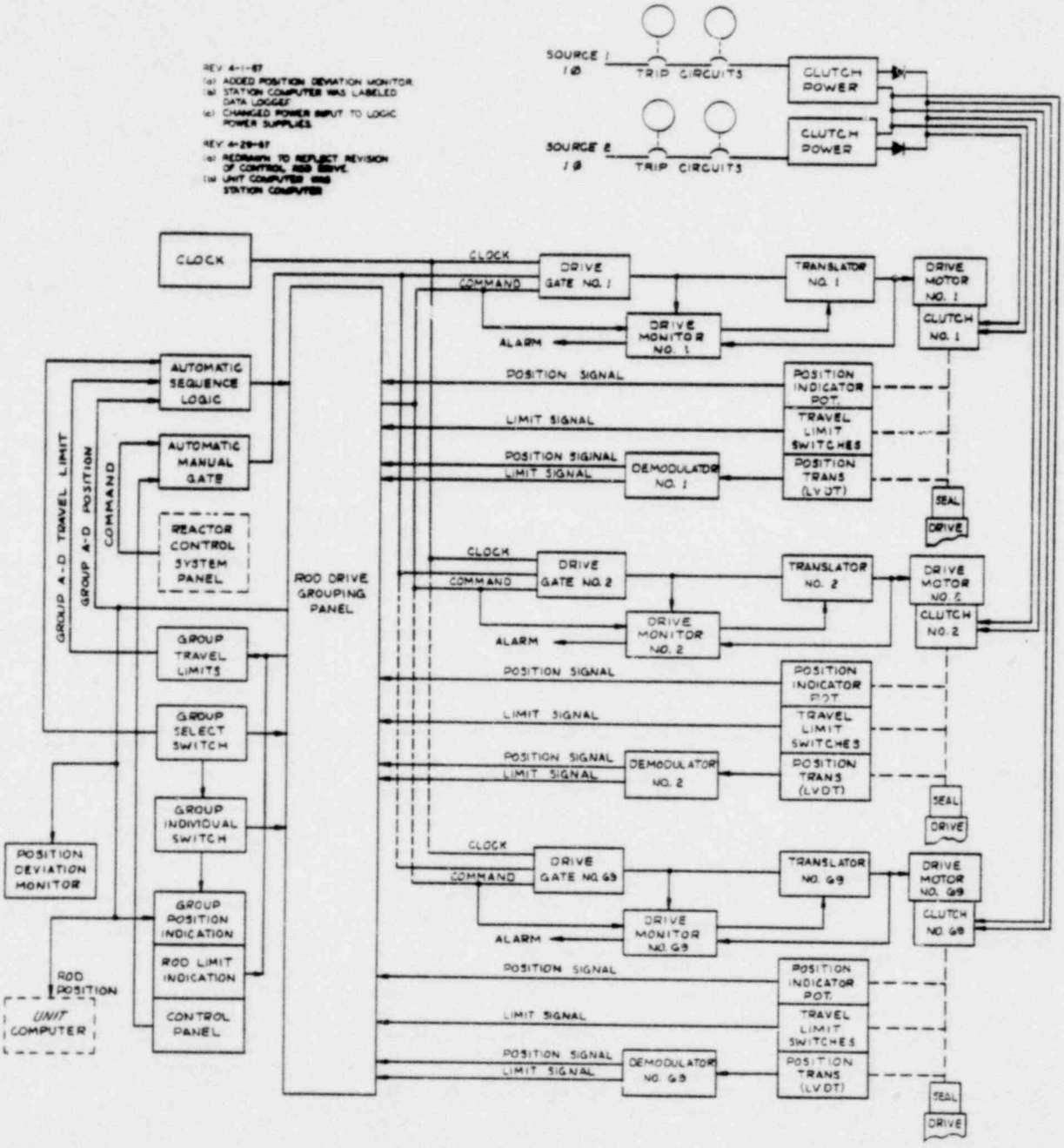

DRIVE MECHANISM
CONTROL BLOCK DIAGRAM

DUKE POWER CITIZENSHIP SERVICE

OCONEE NUCLEAR STATION

FIGURE 3-57

00 00294

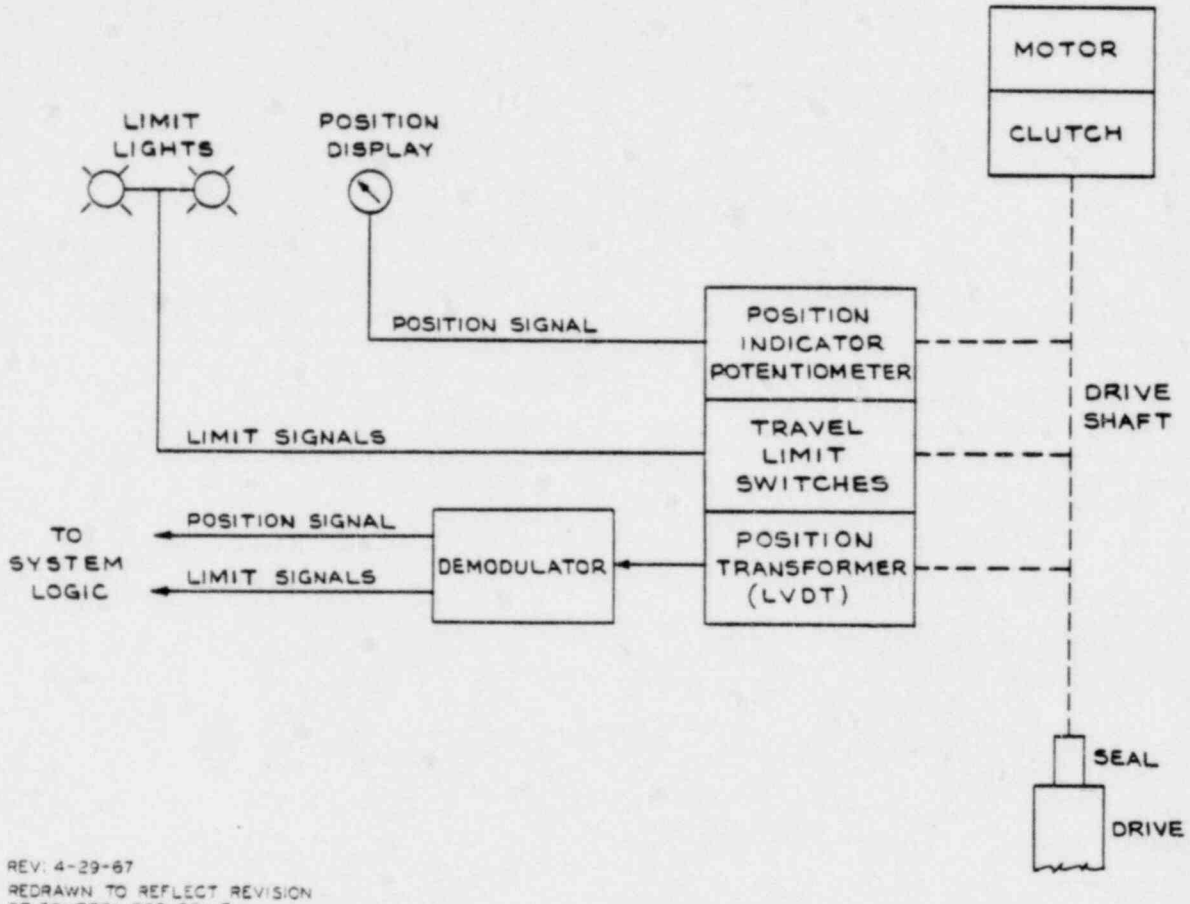

REV: 4-29-67
REDRAWN TO REFLECT REVISION OF CONTROL ROD DRIVE.

LIMIT SIGNAL AND
POSITION INDICATION SYSTEM

OCONEE NUCLEAR STATION
FIGURE 3-58

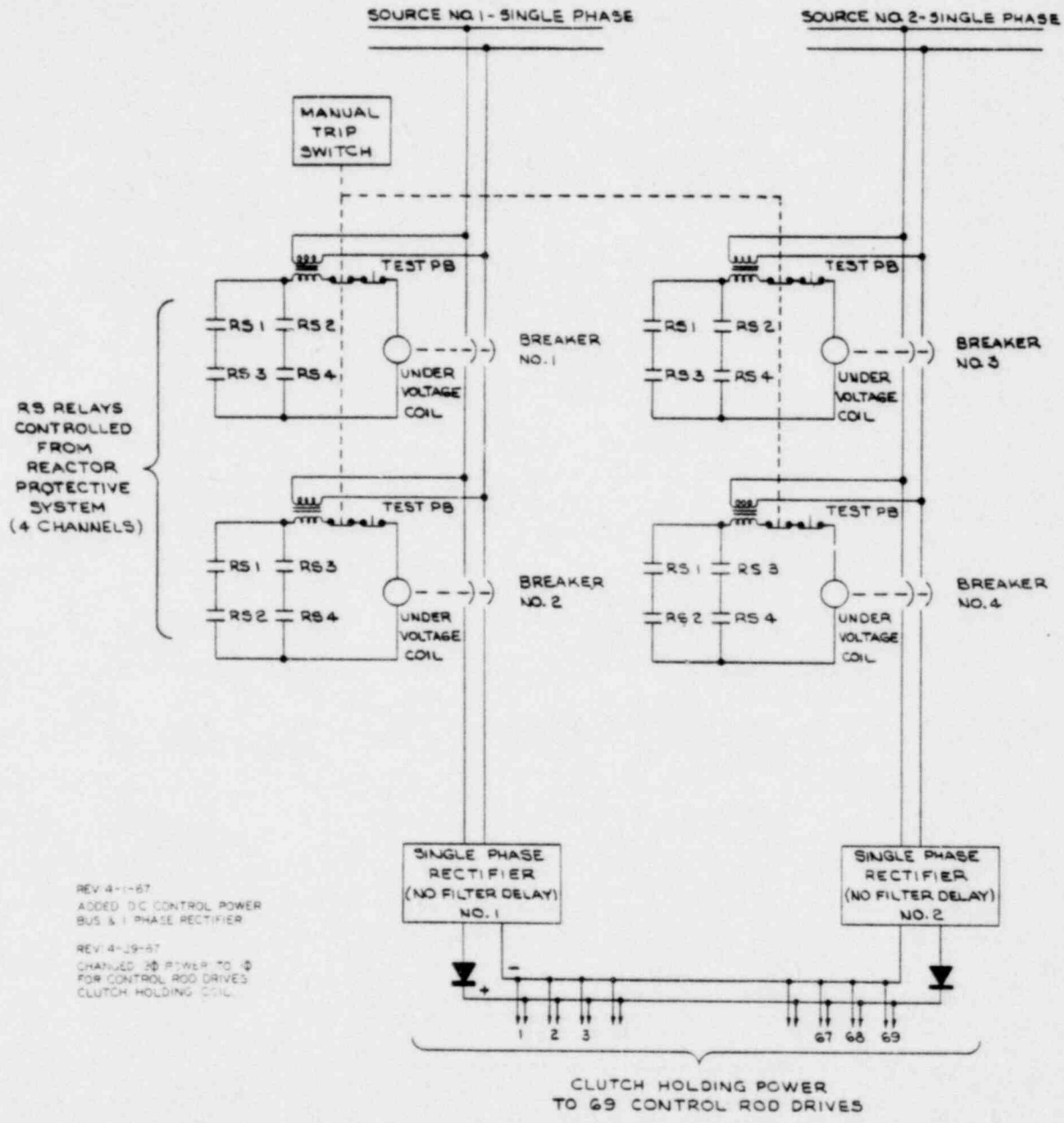

REV. 4-1-67
ADDED D.C. CONTROL POWER BUS & 1 PHASE RECTIFIER

REV. 4-19-67
CHANGED 3Ø POWER TO 1Ø FOR CONTROL ROD DRIVES CLUTCH HOLDING COIL

REACTOR TRIP CIRCUIT

OCONEE NUCLEAR STATION

FIGURE 3-59

00 00296

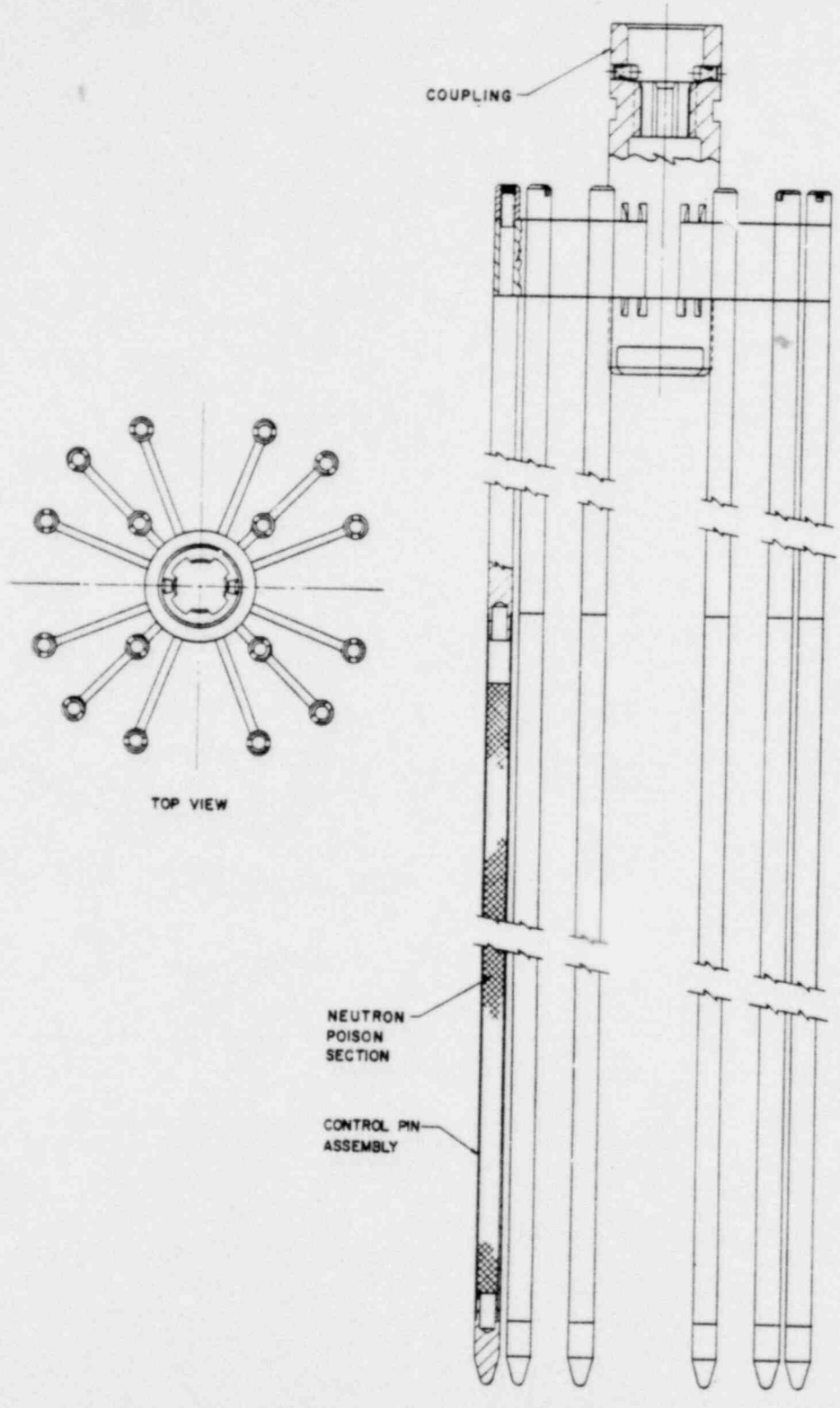

CONTROL CLUSTER ASSEMBLY

OCONEE NUCLEAR STATION

FIGURE 3-60